الجمهورية الجزائرية الديمقراطية الشعبية

PEOPLE'S DEMOCRATIC REPUBLIC OF ALGERIA

وزارة التعليم العالي و البحث العلمي

MINISTRY OF HIGHER EDUCATION AND SCIENTIFIC RESEARCH

UNIVERSITY OF KASDI MERBAH OUARGLA

Faculty of Hydrocarbons, Renewable Energies, Earth and Universe Sciences

Department of Renewable energy

N° Order:……
Series:……….

WITH A VIEW TO OBTAINING THE DOCTORAL DIPLOMA

IN RENEWABLE ENERGIES

OPTION: Geothermal applications

By Sabrin Korichi

The title of thesis

Etude du gisement géothermique et l'exploitation de la géothermie pour les diverses applications dans les régions arides et semi-arides

Study of the geothermal field and the exploitation of geothermal energy for the various applications in arid and semi-arid regions

Sustained on 17/02/2021

In front of the jury consists of:

Abdelmadjid DOBBI	President	Professor	Kasdi Merbeh University Ouargla
Bachir BOUCHEKIMA	Thesis director	Professor	Kasdi Merbeh University Ouargla
Khaled TOUAFEK	Examiner	Research Director	URAER/CDER Ghardaia
Sidi Mohammed El Amine BEKKOUCHE	Examiner	Research Director	URAER/CDER Ghardaia
Hocine MOHCENE	Examiner	Assistant Professor	Kasdi Merbeh University Ouargla
Messaouda AZZOUZI	Co- Director	Professor	Ziane Achour University Djelfa
Nabiha NAILI	Guest member	Assistant Professor	LPT/CRTEn Tunisia

Academic year 2021-2022

Dedications

We dedicate this work to:

My mother;

My father;

My thesis director Bouchekima Bachir;

All my friends and colleagues;

All those who contributed to complete this work

SABRIN KORICHI

ACKNOWLEDGEMENTS

I would like to thank all those who contributed directly or indirectly to the accomplishment of this work, and in particular:

Mr. Bachir Bouchekima, thesis director, Professor at the Faculty of Hydrocarbons, Renewable Energy, Earth and Universe Sciences (FHREEUS), University of Kasdi Merbah-Ouargla, who proposed this thesis and who guided my reflections throughout these years.

Mrs. Nabiha Naili, Assistant Professor at Laboratory of Thermal Processes, Research and Technology Center of Energy, who first introduced me to the fields of ground source geothermal technology and building energy simulation, which i have benefited greatly ever since.

Mrs. Messaouda Azouzzi, Assistant Professor at the Faculty of Science and Technology, University Ziane Achour of Djelfa, who worked as co-director along the course of the research. Her expertise in writing articles was quite valuable in helping me to coordinate my writing.

Dr. Dobbi Abdelmadjid, Dr. Slimane Boughali, and Dr. Hocine Mahcene, the members of doctoral scientific committee.

Dr Khaled Touafek and Dr Sidi Mohammed El Amine Bekkouche, the members of Jury.

My parents, my sister and my brothers who constantly support my researches.

This research was partly supported by the basic research project by the “Laboratoire des Procédés Thermiques (LPT)”, “Centre de Recherches et des Technologies de l’Energie (CRTEn)”, Tunisia. And by the laboratory of new and renewable energy in arid and Saharan zones–LENREZA, Algeria.

Abstract

This paper presents a feasibility and performance study of ground source heat pump (GSHP) coupled with horizontal ground heat exchanger (HGHX) used for cooling and heating a residential unit equipped with radiant floor system (RFs) under the meteorological conditions of Saharan environment in Ouargla, city located in Southeast Algeria. A dynamic simulation system is developed using TRNSYS software for modeling the performance of the GSHP system. To verify the reliability of GSHP including HGHX system programs, the modeling procedure was validated against experimental data from a horizontal ground source heat pump system (HGSHPs) installed at the Research and Technology Center of Energy (CRTEn), Tunisia, and a good agreement was obtained. Then, to obtain an acceptable balance between system efficiency and total cost of HGSHPs an economic analysis was carried out to determine the optimum design parameters of the HGHX. The simulation results obtained from this study indicated that the HGSHPs could effectively solve cooling and heating problems and reduce traditional energy consumption in the Saharan areas; it is possible to lower the mean indoor air temperature below 26 °C in cooling season and raise the mean indoor air temperature to reach 24.5 °C in heating season. By concentrating principally on the thermal-economic optimization, the optimized COP of the GSHPs that combines the reliability and economy of cooling and heating in long term were found to be 3.89 and 4.36, respectively.

Keywords: Ground source heat pump, Horizontal ground heat exchanger, TRNSYS software, Optimization, Thermal-economic modeling, Saharan environment.

Résume

Le travail présenté dans cette thèse vise à évaluer le potentiel de la géothermie pour le refroidissement et le chauffage dans les conditions climatiques du milieu saharien par l'exploitation d'une pompe à chaleur géothermique (PACG). Par conséquent, une étude de faisabilité et de performance a été réalisée d'une pompe à chaleur géothermique (PACG) couplée à un échangeur de chaleur au sol horizontal (ECH) utilisé pour refroidir et chauffer une unité résidentielle équipée d'un système de plancher radiant (PR) dans les conditions météorologiques de Ouargla, ville situé dans le sud-est de l'Algérie. Un système de simulation dynamique est développé à l'aide du logiciel TRNSYS pour modéliser les performances du système PACG. Pour vérifier la fiabilité des programmes du PAC , y compris ECH, la procédure de modélisation a été validée par rapport aux données expérimentales d'un système de pompe à chaleur géothermique horizontale (PACGH) installé au Centre de recherche et de technologie de l'énergie (CRTEn), Tunisie, et un bon accord a été obtenu. Ensuite, pour obtenir un équilibre acceptable entre l'efficacité du système et le coût total des PACGH, une analyse économique a été effectuée pour déterminer les paramètres de conception optimaux de l'ECH. Les résultats de simulation obtenus à partir de cette étude ont indiqué que les PACGH pourraient résoudre efficacement les problèmes de refroidissement et de chauffage et réduire la consommation d'énergie traditionnelle dans les zones sahariennes; il est possible d'abaisser la température moyenne de l'air intérieur au-dessous de 26 °C pendant la saison de refroidissement et d'augmenter la température moyenne de l'air intérieur pour atteindre 24.5°C pendant la saison de chauffage. En se concentrant principalement sur l'optimisation énergétique et économique, le COP optimisé du PACG qui combine la fiabilité et l'économie du refroidissement et du chauffage à long terme étaient respectivement de 3,89 et 4,36.

Mots clés: Pompe à chaleur géothermique, Échangeur de chaleur au sol horizontal, Logiciel TRNSYS, Optimisation, Modélisation thermo-économique, Environnement saharien.

List of papers

Parts of contents in this thesis are based on three conference papers and two journal articles listed below.

Journal articles

- Performance analysis of horizontal ground source heat pump for building cooling in arid Saharan climate: thermal-economic modeling and optimization on TRNSYS
- The thermal behavior of a novel wall radiator panel coupled with horizontal ground source heat pump heating system: improve indoor environment to reduce the airborne transmission of infectious diseases

Conference papers

- Performance analysis of horizontal ground source heat pump systems for cooling in southern climate
- Verification of a dynamic simulation model of ground source heat pump in cooling mode: optimization and modeling on TRNSYS
- Effect of soil type on vertical closed-loop geothermal heat exchangers sizing

Table of contents

List of figures

List of tables

Nomenclature

T_{in-con}	Condenser entering water temperature (°C)
$T_{out-con}$	Condenser leaving water temperature (°C)
$\dot{m}_{w-Con}$	Condenser water mass flow rate (kg/s)
COP	Coefficient of performance in cooling mode
$\dot{m}_{w-Evp}$	Evaporator water mass flow rate (kg/s)
T_{in-Evp}	Evaporator entering water temperature (°C)
$T_{out-Evp}$	Evaporator leaving water temperature (°C)
T_{in-GHX}	GHX entering water temperature (°C)
$T_{out-GHX}$	GHX leaving water temperature (°C)
$\dot{m}_{w-GHX}$	GHX water mass flow rate (kg/s)
T_g	Ground temperature (°C)
W	Power consumption (kW)
T_{in-RF}	RF entering water temperature (°C)
T_{out-RF}	RF Leaving water temperature (°C)
$\dot{m}_{w-RF}$	RF water mass flow rate (kg/s)
Q_b	The heat transfer rate in the building (W)
Q_g	The heat transfer rate in the ground (W)
Q_{Evp}	The heat transfer rate in the evaporator (W)
Q_{Con}	The heat transfer rate in the condenser (W)
C_{p-H_2O}	The fluid specific heat of the fluid (kJ/kgK)
E	The annual power consumption kWh/y
T_w	The average water temperature in the GHX (°C)

C_{inv}	The investment cost of GSHPs ($/y)
C_{elec}	The annual cost of power consumption ($/y)
$C_{heatpump}$	The cost of heat pump ($)
C_{pump}	The cost of circulation pump ($)
$c_{earthworks}$	The regional price of the drilling and refilling ($/$m^2$)
c_{Pipe}	The regional cost of polyethylene pipe per meter ($/m)
i	The interest rate (%)
n	The number of operation years (y)
E_{tariff}	The tariff of unit electricity consumption ($/kWh)
L_{GHX}	The pipe length of heat exchanger (m)
$D_{i,GHX}$	The inner pipe diamete of the GHX (m)
$D_{o,GHX}$	The outer pipe diameter of GHX (m)
NPT	The number of parallel pipe
Z	The depth of the ground (m)
K_{GHX}	The thermal conductivity of GHX pipe (kW/m K)
R_{total}	The total thermal resistance of the GHX (K/kW)
H_{pump}	The total pumping head in the GHX
$\overline{T_g}$	The mean value of the ground surface temperature (°C)
A_s	The amplitude of surface temperature
TAC	Total annual cost ($/y)

Subscripts

b	Building
C	Cooling mode
Con	Condenser

Comp	Compressor
Pump	Circulating pump
elec	Electricity
evp	Evaporator
g	Ground
h	Heating mode
inv	Investment
i	Inner
RF	Radiant floor
Min	Minimum
Max	Maximum
O	Outlet
s	System
W	Water
Re	The reynolds number

Abbreviation

EER	Energy efficiency ratio
GSHP	Ground source heat pump
GHX	Ground heat exchangers
GHP	Ground heat pump
HDPE	High-density polyethylene
HGSHP	Horizontal ground source heat pump
HGHX	Horizontal ground heat exchangers
OF	Objective function

RF	Radiant floor
SEER	Seasonal energy efficiency ratio
TAC	Total annual cost
CRF	Capital recovery factor

Greek letters

α_g	Ground diffusivity (m^2/day)

GENERAL INTRODUCTION

1 Context

The energy consumption in urban buildings has gained an increasing demand recently due to the high comfort standards [1]. This energy reaches about 40% of the world's energy use, e.g. in Algeria, the residential sector is the largest consumer of energy, accounting about 43% of the total national energy consumption [2]. This value will increase to reach 179.78 TWh in 2040 with the increasing of population and because of urbanization and improvement of the living standards [2]. Indeed, these values indicate that the residential sector represents the largest source of greenhouse gas emissions (GHG) and ecological problems in the world.

In recent years, global warming has become a major threat to the environment, especially in arid and semi-arid areas where the desert regions in southern Algeria recorded a significant increase in ambient temperature that exceeded the normal rate, which constituted a burden on conventional air conditioners to provide the cooling needs for the buildings during the summer. Therefore, it is necessary to highlight the use of new technologies based on renewable energies, which still represents only 0.1% of Algerian energy consumption [3].

The renewable energy that appears to be very well adapted in the building sector is geothermal energy; it represents the solution for reducing the large energy consumption and minimizing the environmental problems of the building sector.

The shallow geothermal energy is a clean, sustainable and low carbon solution for the heating and cooling of buildings by pumping heat from or to the shallow subsurface to provide the thermal loads. Compared with other renewable sources, the shallow geothermal energy has important advantage, it can be used everywhere in the world especially in residential sector areas where the quantity of exploitable geothermal energy stored in the shallow subsurface is greater than its annual requirements for cooling and heating.

In the last decades, shallow geothermal systems such as ground source heat pump systems have been gradually gaining attention and it is expected to have wide application in the future of geothermal technology that can provide heating and/or cooling to residential buildings and infrastructures. Among the different types of GSHPs, the closed ground source heat pump system (GCHPs) is one of the best configurations in terms of practicability and independent installation. It has attracted the most attention due to its relatively high efficiency and reliability. Despite its advantages, the high installation cost is one of the main challenges limiting the market spread of GSHP technology. The high overall initial cost of the GSHPs is mainly due to the installation of the GHX which is the essential part of the system. Since the thermal performance of the GHX and the feasibility of using GSHPs are strongly influenced by many factors such as geological and climate conditions which varies with places, it is important to design the system properly according to the wells properties and the actual thermal needs of buildings. A regional-scale spatial analysis is necessary to evaluate the energy-economic feasibility of using the GSHPs for each region which is to be subsidized.

2 Research aim

The main aim of this study was to pre-investigate the exploitation of horizontal ground source heat pump systems for cooling and heating in arid Saharan environment. The specific objectives of the work were as follows:

- To develop optimal design for HGHXs including ground heat pump system (GHPs) in both heating and cooling cases.
- To evaluate the economic feasibility of using HGSHPs within the Saharan climate zones in Algeria.

- To control long term HGSHPs operation in order to maximize their overall energy efficiency without violating the operating constraints.

3 Research methodology

The thesis objectives were achieved through combined simulation investigation and experimental tests. A TRNSYS simulation model of HGSHPs equipped with RFs is proposed to provide cooling and heating for residential building of about 95 m^2 area located in Ouargla, South-East of Algeria. The model was validated using experimental data collected from a HGSHPs conducted in the Research and Technology Center of Energy at Borj Cédria, northern Tunisia. For optimal system design, a thermal-economic optimization was carried out to estimate the optimum HGHX design parameters for the case study region. The effect of the pipe length, burial depth, pipe diameter and mass flow rate on the thermal performance and the system total cost were investigated. Then to ensure the reliability of optimization results in the long run, the simulation inlet and outlet temperatures of the HGHX were calibrated using ASHRAE guideline constraints.

4 Thesis outline

This thesis consists of 9 parts organized as follows:

- Firstly, the general introduction presents the context, research aim, research methodology and organization of this thesis.
- Chapter 1 provides a general overview on geothermal energy and presents its technologies as well as its developments and future perspectives in Algeria and the world.
- Chapter 2 presents a general literature review regarding the GSHPs, with a key focus on design methods, optimization process and operation control of the systems. Factors

affecting the energy performance and financial feasibility of the GSHPs are also presented.

- Chapter 3 presents the theoretical process undertaken in the multi-objective optimization. A general description of the vapor-compression theoretical cycle of the heat pump was also provided.
- Chapter 4 presents the dynamic characterization of HGSHPs. The operation conditions of the system were also analyzed through a developed TRNSYS simulation model.
- Chapter 5 presents the development of experimental test and the validation of the HGSHPs simulation model.
- Chapter 6 presents energy-economic feasibility study of using GSHPs under desert climatic conditions. A parametric analysis was performed in order to select the optimal values of the most-cost effective design parameters of GHXs including GHPs.
- Chapter 7 provides a general calibration for the designed HGSHPs. The effects of the long-term operation of the optimized system on both the thermal behavior of the GHXs and the soil temperature were also assessed.
- Finally, the general conclusion summaries the key findings from chapters and provides some recommendations for future work.

CHAPTER 1

GEOTHERMAL ENERGY OVERVIEW

1.1 Introduction

The geothermal energy is one of the most important renewable energy sources that can be generated and stored in the ground. It is local, inexhaustible, limitless, clean, sustainable, efficiency and environment-friendly. This kind of thermal energy has different applications, such as generating electricity; heating/cooling of buildings, Streets and greenhouses; providing warm/cold air/water for agricultural products and balneological use.

This chapter introduces a general overview of geothermal energy, it is organised as follows. Section 1.2 provides a general review regarding the global geothermal resources. A detailed description of geothermal energy exploitation is presented in section 1.3. Section 1.4 reviews the historical development, the current state and the future prospects of the exploitation of geothermal energy around the world. Section 1.5 summaries the potential of geothermal energy and reviews the current state of its exploitation in Algeria. The future development and policy are also discussed.

1.2 Geothermal basics

1.2.1 The geothermal resources

In general, the pressure and temperature increase with increasing depth into the Earth's crust, reaching hundreds of degrees Celsius near the upper mantle (see Fig 1.1). This heterogeneous distribution of temperature and pressure across the Earth's crust creates a big collections of geothermal resources that can be existed into three main forms: low-temperature forms (corresponding to temperatures below 90 °C), Moderate-temperature forms (corresponding to temperatures ranging between 90 °C and 150 °C) and high-temperature forms (corresponding to a temperatures higher than 150 °C) [4].

This part describes a database of the global geothermal resources that includes information on heat flow map and geothermal reservoirs distribution.

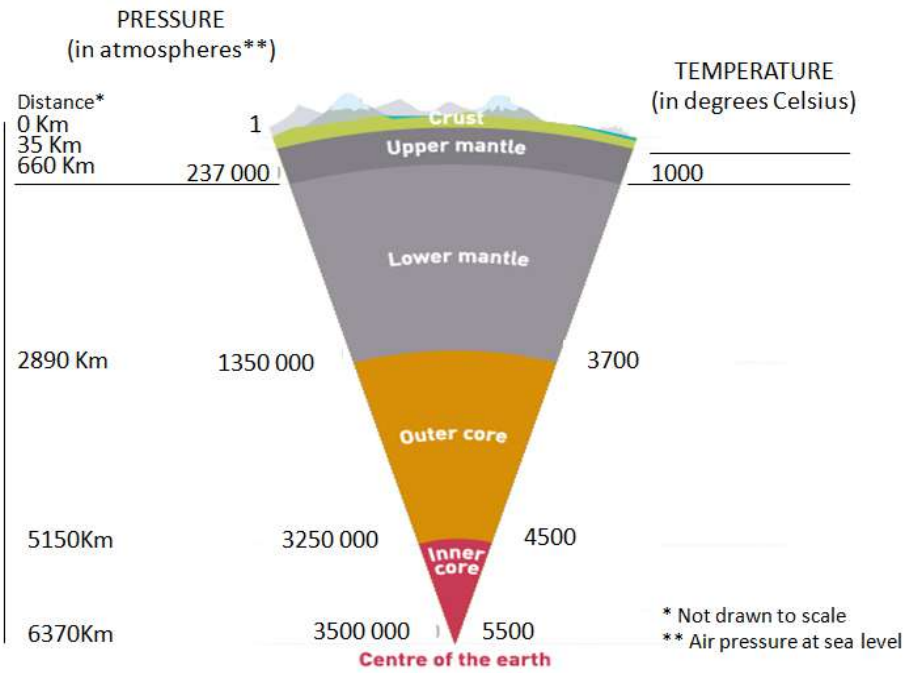

Fig 1.1 Cross section of the earth, the pressure and temperature of the earth's interior [5]

1.2.1.1 The geothermal heat flow

The geothermal heat is mainly produced by the radioactive decay of potassium, thorium, and uranium in Earth's interior [6]. Indeed, it is estimated that 99% of the earth's volume is at temperatures above 1000 °C, with only 0.1% of its volume at less than 100 °C [7]. The total heat content of the Earth is estimated to be equivalent to 1031 J and is expected to remain so for billions of years before exhaust it via the global heat flux, which continuously emanating from the earth's interior with a capacity of 40 million MW [8]. The distribution of global surface heat flow in all continents and oceans are presented in Fig 1.2. The mean global heat flow for all continents and oceans yields a value of 83 mW/m with a standard deviation of 60 mW/m [9].

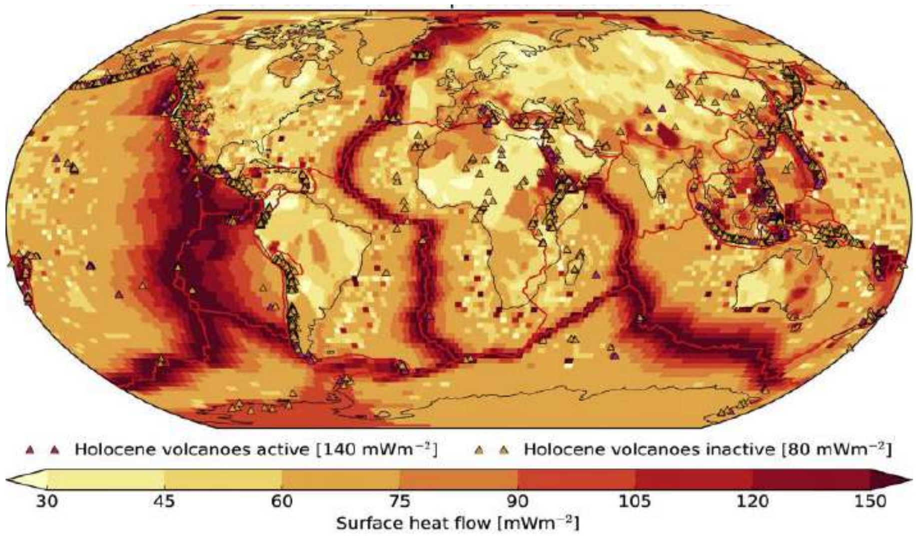

Fig 1.2 Global surface heat flow [9]

1.2.1.2 The geothermal reservoirs

The high temperature and pressure in Earth's interior resulting in portions of the mantle and molten rocks convecting upward since they are lighter than the surrounding rock. Sometimes the magma reaches the surface as lava, but it usually remains below the Earth's crust, heating nearby rocks and ground water. The hot water and steam can manifest itself on the crust surface as hot springs or geysers or can be trapped in cracks and porous rock underground. These natural collections of hot water, steam or mixtures of both are called geothermal reservoirs. The maximum deep aquifer temperatures computed according to the geothermal gradient and maximum aquifer thickness (computed for only maximum depth of 3 km) are presented in Fig 1.3.

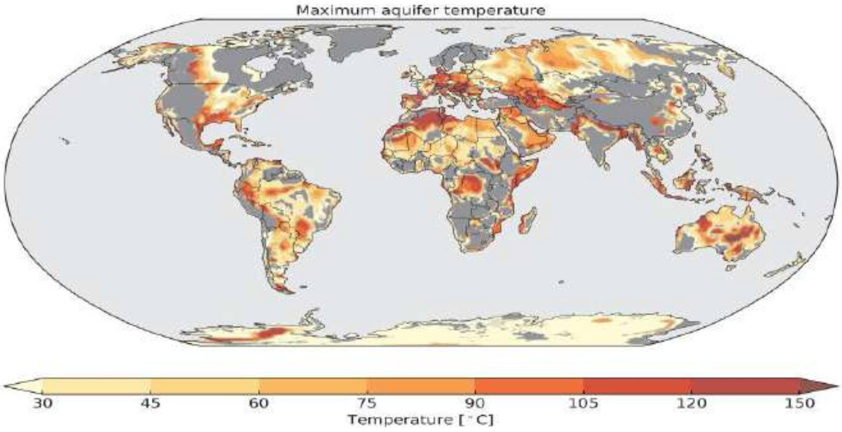

Fig 1.3 The maximum aquifer temperature. Grey areas on the land surface indicate a sediment thickness less than 100 m and are not considered in this map [9]

1.2.2 The exploitation of geothermal energy resources

The exploitation of the huge geothermal potential depends on extraction method and it can be divided into three categories: direct use applications, geothermal heat pumps and electric power generation.

1.2.2.1 Direct-use applications

Direct or non-electric use of geothermal energy is one of the oldest, most versatile and common form of utilizing geothermal energy [10]. It refers to the immediate use of the heat energy rather than to its conversion to some other form such as electrical energy. Most direct use applications are confined to the low-moderate temperature resources that are more wide-spread than the higher temperature resources used for electricity generation. In general, the major areas of direct utilization are: aquaculture(mainly fish farming and raceway heating), agriculture(mainly greenhouse heating, crop drying and some heating of buildings housing livestock in order to increase growth rates), some industrial processes, swimming, bathing and balneology (therapeutic use), space heating and cooling including district heating, and crop drying etc [11].

The global resource assessments for geothermal energy within deep aquifers for direct heat utilization were performed in literatures. The reviews show that there is a large global geothermal resource base in sedimentary aquifers for direct heat use. The global technical potential for generalized direct heat is presented in the Appendix A.

1.2.2.2 Electric power generation

Electric generation from geothermal sources has a long history of more than one hundred years [12]. It refers to the electrical conversion of thermal energy coming from high enthalpy geothermal resources using geothermal power plant technologies. Depending upon the state of the geothermal reservoir fluid and its temperature, geothermal power plants can produce electricity by different ways using three main technologies [12,13]: a. flash power plants, b. dry steam power plants and c. binary power plants.

a. **Dry steam power plants:** These plants directly use dry steam that is naturally produced in the geothermal reservoir [14], and no separation process is necessary because wells only produce steam. The steam from the production well passes to the surface and than through the turbine-generator unit, and after transferring its energy to electric energy via the turbine it condenses and is injected back into the ground (see Fig 1.4).

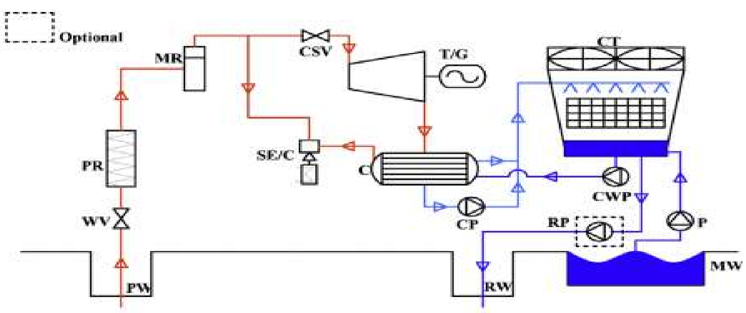

PW	Production well	WV	Wellhead valve	PR	Particulate remover
MR	Moisture remover	C	condenser	CP	Condensate pump
CSV	Control and stop valve	SE/C	Steam ejector/condenser	T/G	Turbine and generator
CT	Cooling tower	CWP	Cooling water pump	RP	Reinjection pump
RW	Reinjection well	P	Pump	MW	Make-up water

Fig 1.4 Simplified schematic of a dry steam plant [15]

b. **Flash power plants:** Flash steam power plants use the liquid-dominant mixture that is produced at the hydrothermal reservoir. Geothermal heated water over 180 °C is separated in a flash vessel (called a steam separator) into steam and hot water (called “brine”). The steam is sent to the turbine, and the turbine powers a generator. The remaining liquid is injected back into the reservoir, and also might be further flashed at lower pressure to generate additional steam, in which case the result is a double flash power plant [16] (see Fig 1.5). The cost of these systems is increased due to more complex parts; however they are still the most common due to the lack of vapor-dominant reservoirs.

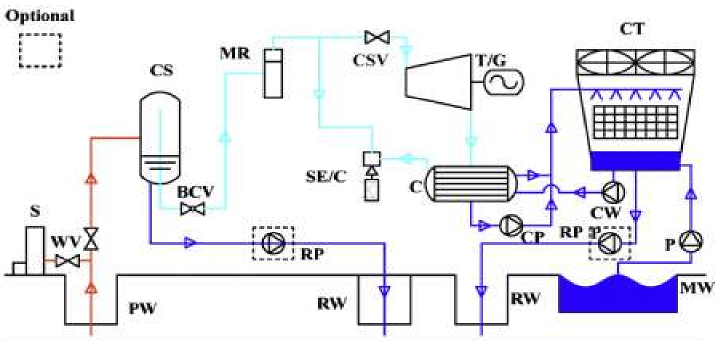

PW	Production well	WV	Wellhead valve	S	Silencer
CS	Cyclone separator	BCV	Ball check valve	MR	Moisture remover
CSV	Control / stop valve	T/G	Turbine / generator	SE/C	Steam ejector/condenser
C	condenser	CT	Cooling tower	CWP	Cooling water pump
CP	Condensate pump	RP	Reinjection pump	RW	Reinjection well
P	Pump	MW	Make-up water		

Fig 1.5 Simplified schematic for a single-flash plant [15]

c. **Binary power plants**

The binary power plants can make use of lower temperature water than the other two types of plants. These technologies have made possible the production of electricity from the low and medium temperature geothermal resources (in the temperature range 70-100 °C and 100-150 °C, respectively) [17]. They use a secondary loop (hence the name "binary") which contains an organic fluid that has a low boiling point and high vapor pressure when compared to water at a given temperature [18]. The working fluid receives heat energy from the geothermal fluid through a heat exchanger unit and evaporates due to its low boiling point. The force of the expanding vapor turns then the turbines that power the generators. All of the produced geothermal water is injected back into the reservoir (see Fig 1.6).

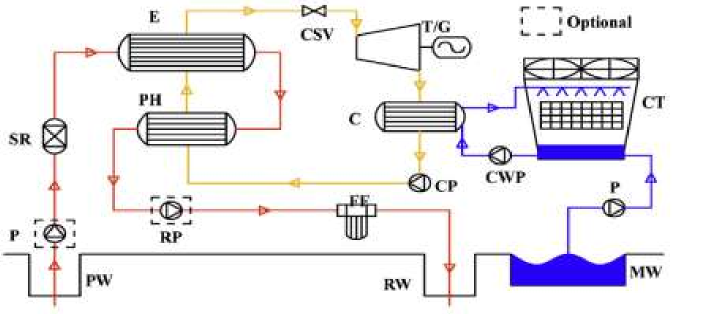

PW	Production well	P	Pump	SR	Sand remover
E	Evaporator	PH	Pre-heater	C	Condenser
CP	Condensate pump	RP	Reinjection pump	FF	Final filter
CSV	Control / stop valve	T/G	Turbine / generator	CWP	Cooling water pump
CT	Cooling tower	RW	Reinjection well	MW	Make-up water

Fig 1.6 Simplified schematic of a basic binary geothermal power plant [15]

1.2.2.3 Geothermal heat pumps

Geothermal heat pumps, also called ground source heat pumps, are proven renewable energy technology for space heating and cooling. These systems are combining heat pumps (Fig 1.7) with a geothermal field that uses the ground, groundwater, or surface water as a heat source and sink. The GSHPs can be subdivided according to the type of exterior heat exchange system into three main types: (i) groundwater heat pump systems (GWHPs), (ii) surface water heat pump systems (SWHPs), and (iii) ground-coupled heat pump systems (GCHPs). [20].

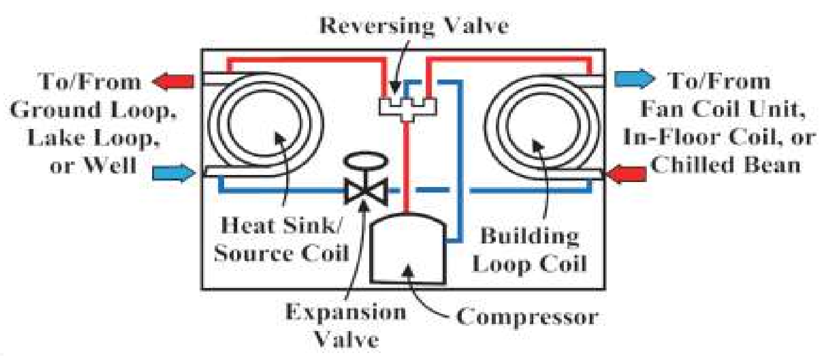

Fig 1.7 Ground heat pump [19]

1.2.2.3.1 Ground water heat pumps

Ground water heat pump systems (see Fig 1.8), also called open-loop systems, are the first type of geothermal heat pumps [21]. These heat pumps use the water as heat source and sink for heating and cooling. It removes ground water from wells via vertical open-loop and delivers it to a heat pump or to an intermediate heat exchanger to serve as a heat source or sink [22]. The GWHP systems have some marked advantages including their low cost and that they do not need a wide ground surface area compared to other GSHP systems [21]. The disadvantages of these systems are related to the lack in available groundwater, fouling precautions may be necessary if the well water is poor quality and pumping energy can be excessive if the circulating well pumps are oversized [19].

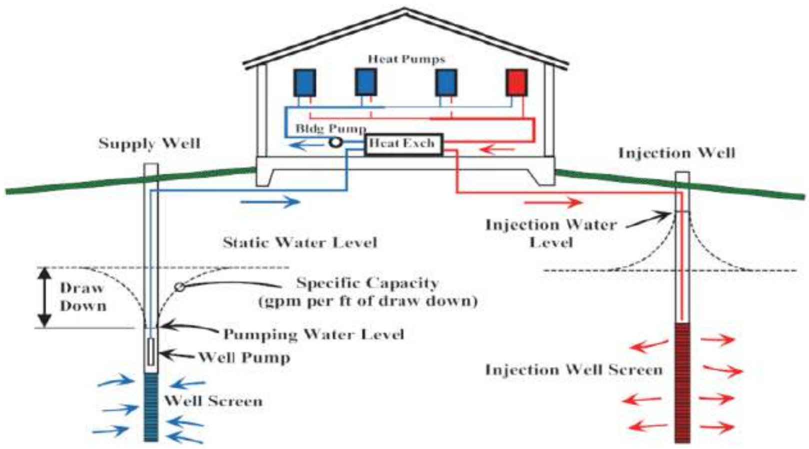

Fig 1.8 Open-loop groundwater heat pump [19]

1.2.2.3.2 Ground coupled heat pumps

The ground coupled heat pumps (see Fig 1.9), also called closed loop ground source heat pumps, consists of a reversible heat pump that is linked to a closed loop, i.e. ground heat exchanger. In these systems, the heat is extracted from or rejected to the ground via buried pipes, through which pure water or antifreeze fluid circulates.

The GCHPs are categorized according to ground heat exchanger types that include horizontal ground heat exchangers and vertical ground heat exchangers (VGHX) [22].

- **The horizontal GHX:** The HGHX means the heat exchangers that installed horizontally at a few meter below the ground surface. As with all the GHX types, the horizontal ground heat exchanger consists of HDPE (high-density polyethylene) pipes through which heat exchange fluid are circulated. It can be divided into three subgroups: linear [23, 24], slinky [25, 26] and spiral coil-type [27] (see the Appendix Appendix B).
- **The vertical GHX:** The U-tube heat exchangers installed vertically in the ground are called vertical ground heat exchangers. These types of heat exchangers have many configurations (configuration A, B, C; see the Appendix B) which can be installed in a one, tens, or even hundreds of boreholes according to the thermal loads. The design of vertical ground heat exchangers is complicated by many constraints that include the variety of geological formation at the installation site as well as the huge initial investment cost especially with the large projects**.**

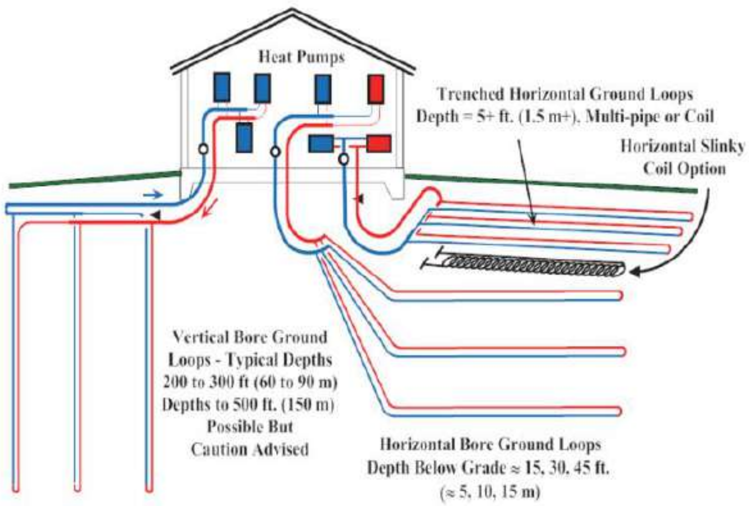

Fig 1.9 Closed-loop ground source heat pump with three ground-loop options [19]

1.2.2.3.3 Surface water heat pumps

These heat pumps use the surface water as heat source or sink (see Fig 1.10). In general, the surface water bodies including lakes, ponds, rivers, and oceans have ideal thermal characteristics as heat source [22]. The temperature profile over the year including the maximum and the minimum temperatures of the water body which is in direct contact with the atmosphere are very suitable for efficient operation of the heat pump, especially in cooling mode. The SWHPs can be either closed-loop systems or open-loop systems as the following [19]:

- **The closed-loop system**: the closed-loop SWHPs is similar to GCHPs. It consists of water-to-water or water-to-air heat pumps linked to a submerged piping loop (coils) that transfers heat to or from the water body [19]. The heat pump transfers heat to or from the air in the building and then exchanges it to or from the lake by the working fluid circulating inside the submerged coil.
- **The open-loop system:** the open-loop SWHPs is similar to GWHPs. In these systems, the water-to-water or water-to-air heat pump unit pumps water from water body (i.e lake) through a heat exchanger and then returns it to the lake some distance from the point in which it was removed [19]. The water can be pumped directly to the heat pumps unit or to an intermediate heat exchanger that is connected to the unit with a closed piping loop.

The advantages of closed-loop SWHPs are that they have low investement costs, low operating costs, low pumping energy and low maintenance compared to other VGSHP and GWHP systems. Disadvantages are that they not suitable for public lakes and if the lakes are small and shallow, the variation of water temperature with outdoor conditions is wide [19].

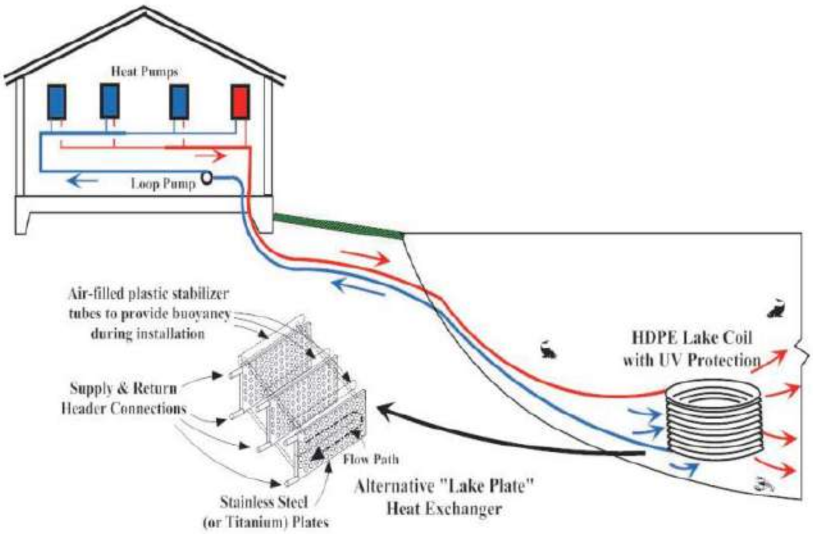

Fig 1.10 Closed-loop surface-water heat pump with two lake coil options [19]

1.3 Geothermal energy in the world

1.3.1 History of geothermal energy

1.3.1.1 Discoveries

Discoveries verify that the thermal energy created by the earth has been utilized by mankind since its existence [29]. Since the Paleolithic era, the indigenous American-Paleo Indians employed hot springs for bathing, heating and treat gastric health issues [20]. After that, Romans exploit the water of hot springs for public baths and balneology [30]. Geothermal water was also used by Chinese people in farming and treatment employing from the 4th century [20]. Centuries later, in 1300 AD, the geothermal heat was used for heating purposes by the oldest Icelanders [30].

Much later, in 15th century, the miners observed that below earth's surface the temperature of soil rise with depth [20], this was reported later by Alexander von Humboldt in 17th century when he found that the soil temperature increases by 3.8 °C per 100 m increase in depth in Freiberg, Saxony where was the first discovery of the geothermal gradient [29].

1.3.1.2 Development of geothermal power technologies

From the early 19th century to the present day, the primitive use of geothermal energy was further developed by numerous researchers. The timeline of noteworthy events is:

In 1897 for the first time, a low-pressure steam boiler working with the heat of geothermal water to produce steam for a steam engine was built by Francesco Larderel in Larderello, Italy [30]. This primitive installation is shown in the Appendix C.

In 1904, at the Larderello dry steam fields, the electricity power was produced from geothermal steam for first time in the world [30]. At first, the small generator which was tested by Piero Ginori Conti was only enough to light 5 electric light bulbs (shown in the Appendix C) [31]. Then, in the year 1915, the geothermal operation reached an electrical output of 5 MW [31].

In 1912, the first commercial geothermal power plant with a capacity of 250 kW was designed and installed near the Larderello fields (shown in the Appendix C). This technology was further developed during 1914, the unit was increased to a capacity of 8.5 MW and by 1944 reached a capacity of 127 MW [30].

In 1920, in Reykjavik in Iceland, the geothermal water was exploited to heat buildings for the first time ever [29]. It was only 6 years later, in 1926, a geothermal well was used for heating houses with an environment-friendly way in Klamath Falls [20].

In the late 1940s, the first direct exchange ground source heat pump was built by Robert C. Webber after modifying the concept of the geothermal ground source heat pumps which was first developed by Lord Kelvin in 1852 [32].

In 1958, in New Zealand, the first large-scale commercial power plant (Wairakei Power Station) was put into operation with an electric capacity of 192 MW [30].

In the 1960, in California in the United States, a geysers project consists of 21 power plant was constructed with a geothermal electric capacity of 750 MW which was sufficient to run San Francisco [29].

In the 1970s, the oil was replaced by the geothermal energy for heating buildings during the two major oil crises [32].

In the early 1980s, the total electrical capacity of the installed geothermal energy power plants in the world had reached 2,110 MWe and the direct-use installed capacity had reached 1,905 MWt [32].

By 1990, the installed electrical capacity has reached 5,832 MWe and the direct-use capacity has also grown 8,064 MWt [32].

From 1990 to 2000, the installed electric capacity of geothermal energy power plants increased by 3.2% per year to reach 2228 MW in the late 2000s [32].

1.3.2 Current situation of geothermal power generation

1.3.2.1 Direct use

The direct utilization of geothermal energy has been quite active over the last 20 years, especially geothermal heat pump applications (see Fig 1.11). The estimations showed that the installed thermal power for direct utilization at the end of 2019 is 107,727

MWt, a 52.0 % increase over 2015 [33]. The distribution of thermal energy used by category is approximately 58.8 % for ground source heat pumps, 18.0 % for bathing and swimming (including balneology), 16.0 % for space heating (of which 91.0 % is for district heating), 3.5 % for greenhouse heating, 1.6 % for industrial applications, 1.3 % for aquaculture pond and raceway heating, 0.4 % for agricultural drying, 0.2 % for snow melting and cooling, and 0.2 % for other uses [33].

Table D.1 (in the Appendix D) summarizes the installed thermal capacity (MWt), annual energy use (TJ/year and GWh/year) and the capacity factors by region in the end of 2019, respectively.

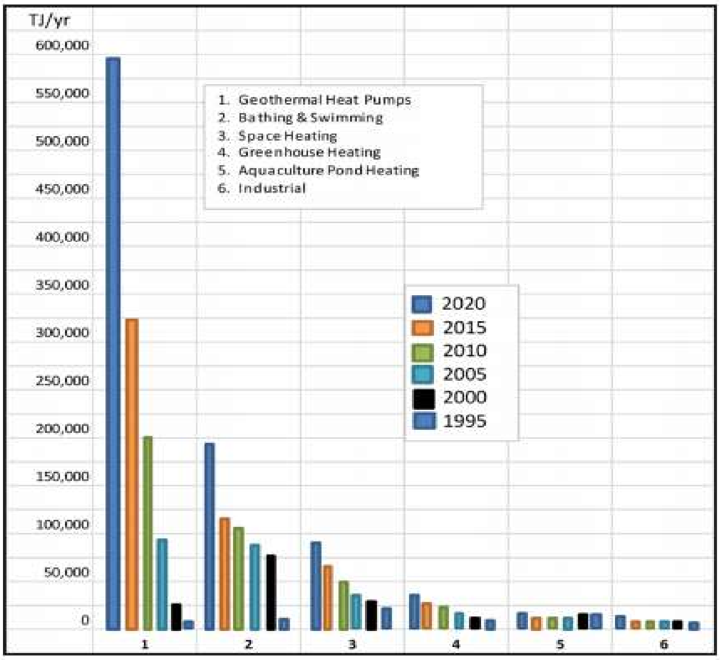

Fig 1.11 Comparison of worldwide direct-use of geothermal energy in TJ/yr from 1995, 2000, 2005, 2010, 2015 and 2020 [33]

1.3.2.2 Electric power production

Over the last 20 years, the production of electric power from geothermal energy resources worldwide has been continuously increasing (see Fig 1.12). In 2014, a total of 24 countries were using electric power from geothermal energy with an installed capacity of 12,800 MW, 0.4% of the world electric energy generation [34]. The distribution of worldwide installed capacity by types of power plants is approximately 57% produced by flashing units (both single and dual flashing), 26% produced by the dry steam units, 17% produced by the binary [34]. A world map of the installed capacity in 2015 is presented in the Appendix D.

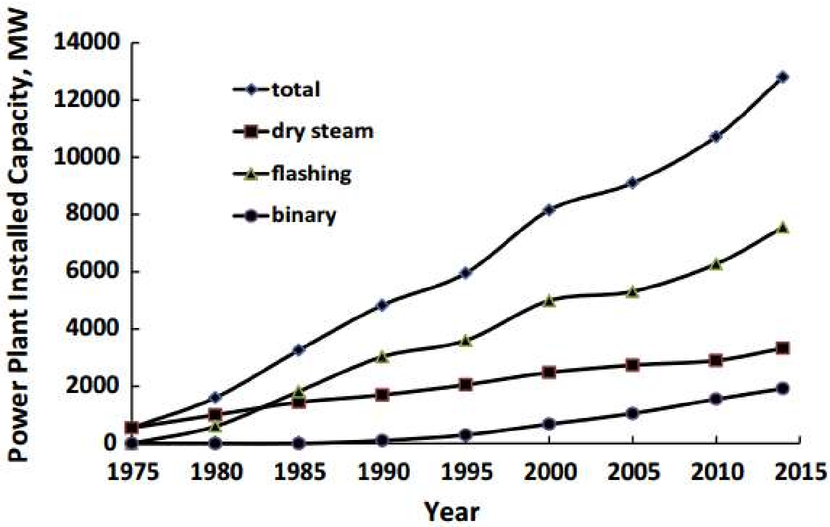

Fig 1.12 Globally installed capacity by type of geothermal power plant in the end of 2014 [34]

The major activities carried out for generation of geothermal electricity between 2015 and 2020 were analyzed. Reports indicate an increase of about 3.649 GW has been achieved (about 27%) in the last five year (2015-2020) [35].

1.3.3 The future of worldwide geothermal energy

1.3.3.1 Power production outlook

The researches that focus on the next-generation geothermal technologies and their production can provide an outlook on the future of geothermal energy and on where its applications will be heading in the coming years. Based on the ETP 2010 prediction scenario for the future of geothermal energy in the world that was proposed by IEA in 2011 [37], the total electricity production could reach 1400 TWh in 2030 and would increase to perhaps as high as 58,000 MW by 2050, about 3.5% of the total electricity production worldwide (see Fig 1.13).

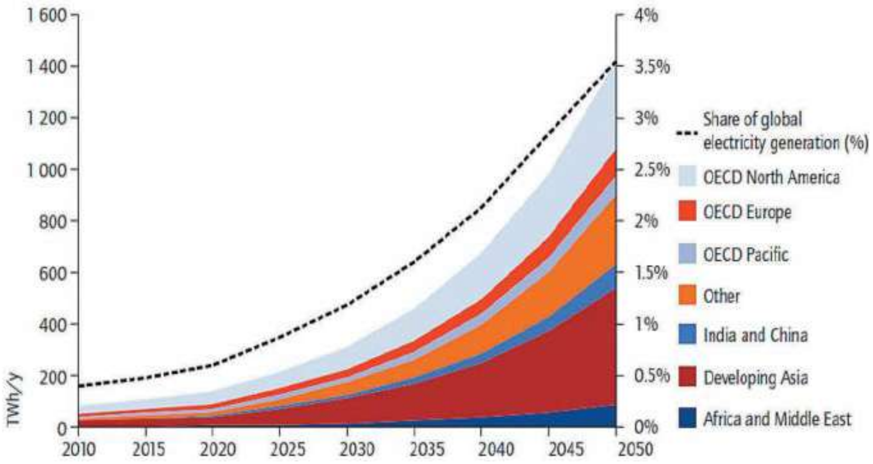

Fig 1.13 Future of geothermal power production until 2050 (IEA 2011) [37]

Among the three basic types of geothermal energy, the enhanced geothermal systems (EGSs) are expected to play a significant role by more than 50% of the total geothermal electricity production growth [37]. The classification of the predicted geothermal capacity by production technology is shown in Fig 1.14.

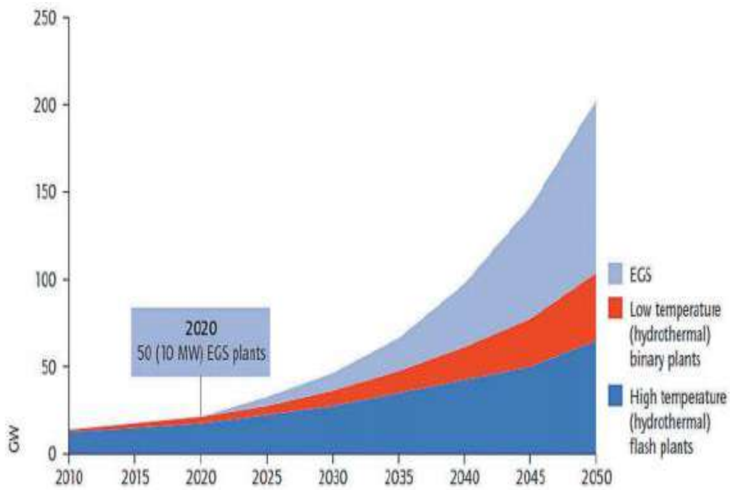

Fig 1.14 Classification of geothermal capacity by production technology [37]

1.3.3.2 Direct use outlook

The IEA reports the growth of the direct geothermal heat use with the exclusion of geothermal heat pumps. The direct geothermal energy use in the different regions around the world could increase to 1400 TWh in 2030 and would reach 5.8 EJ by 2050 [37], as shown in Fig 1.15.

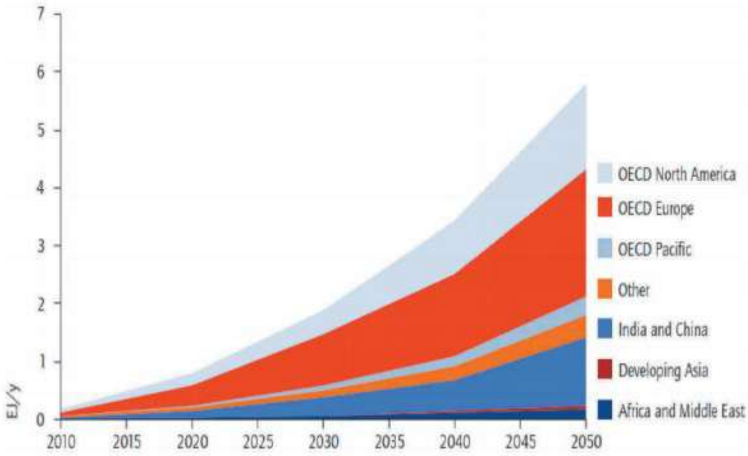

Fig 1.15 Future of direct use geothermal energy until 2050 (IEA 2011) [37]

1.4 Geothermal energy in Algeria

1.4.1 Geothermal resources in Algeria

Algeria has a diverse and relatively large geothermal potential. Most of these geothermal resources are in low-enthalpy form. Below we present a resource assessment for geothermal energy and its distribution over the entire territory of our country.

1.4.1.1 Geothermal heat flow and temperature gradient in Algeria

The geothermal heat flow that was evaluated based on temperatures measurements derived from geological and geophysical data sets in 230 oil wells is presented in Fig 1.16. The heat flow distribution map shows a large regional disparity which is mainly due to the diversity in the local geological structure caused by the large area of the country. The mean global heat flow for all the country yields a value of 82 mW m^{-2} with a standard deviation of 19 mW m^{-2} [38], this corresponding to a normal geothermal gradient of 30 °C/km (see Fig 1.17) [39].

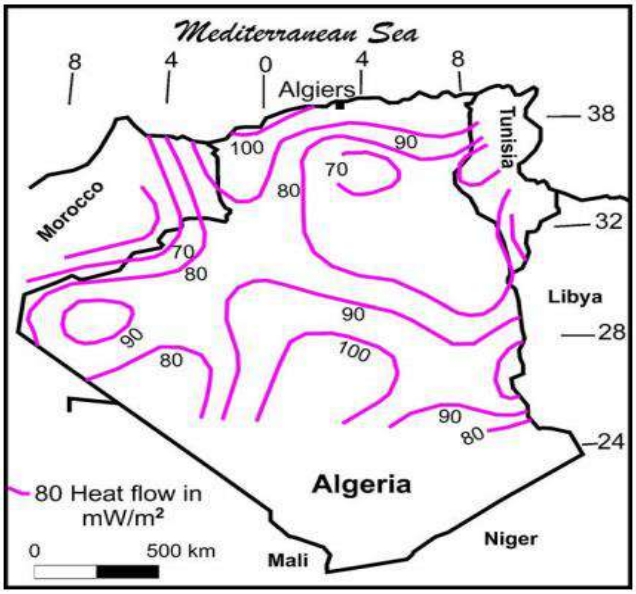

Fig 1.16 Heat flow map of Algeria [38]

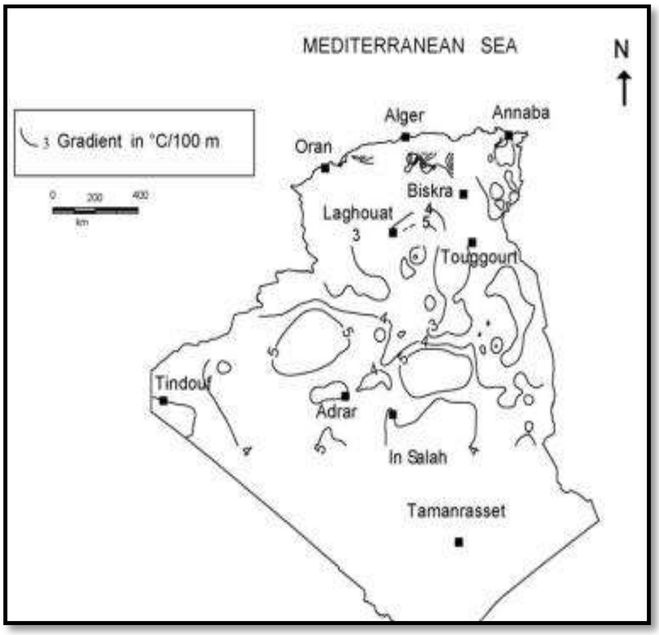

Fig 1.17 Geothermal gradient map of Algeria (modified from [39])

1.4.1.2 Geothermal reservoirs in Algeria

The database of the Algerian low-enthalpy geothermal energy resources that includes information on the effective thermal springs and the description of water resources in more than 240 sites around the country shows that the hot ground water is generally at neutral pH, total dissolved salts (TDS) range from 0.4 to 10 g/l and can reach a temperature in the range of 22-98.8 °C [40]. The highest spring temperatures recorded are [38]:

- 68.8 °C for the western area (Hammam Bouhnifia),
- 80.8 °C for the central area (Hammam El Biban),
- 98.8 °C for the eastern area in northern Algeria (Hammam Meskhoutine),
- 50.8 °C for the southern area.

The temperature and chemical data of all the Algerian hot springs are described in [38-43]. In general, the distribution of thermal springs and the compilation of geological, geochemical and geophysical data such as geothermal gradient and permeability have made possible the identification of three geothermal regions as presented in Fig 1.18 [38].

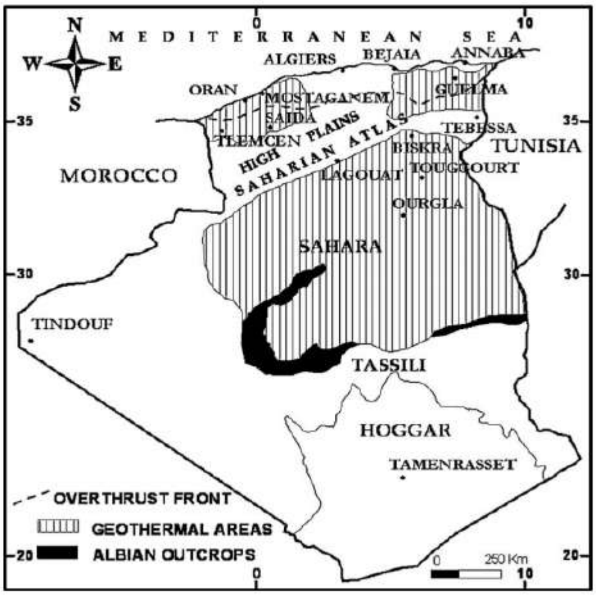

Fig 1.18 Main geothermal areas location in Algeria [38]

1.4.2 State of geothermal energy in Algeria

Geothermal utilization ratio in Algeria is small if compared to potential resources. The geothermal development has remained stagnant during the last decade although its exploration program was started since 1967 by the national oil company SONATRACH [38].

In 1982, the geothermal recognition studies of the northern and eastern parts of the country was undertook by the national electric power company SONALGAZ in association with the Italian company ENEL. From 1983, the program was extended to the whole northern part of the country by the Renewable Energies Center of Algeria (CDER) [38]. During the first stage of this program, a few studies have been undertaken to assess the geothermal potential and their possible uses. A description of databases on both the low-temperature geothermal resources and hot water resources of Algeria are presented.

By 2005, the statistics indicated that the installed geothermal capacity through the country reached 152.3 MWt in which 2.3 MWt is for greenhouse heating, 0.1 MWt for space heating, and the rest (149.9 MWt) for bathing and for balneology uses [44]. At the present time, additional efforts are being conducted to develop large projects with the establishment of the Geothermal Atlas in Algeria. However, the existing geothermal resources such as thermal springs and wells are using only for bathing, hydrotherapy and space heating like greenhouse heating in Ouargla and Ghardaia [44]. Despite the aspiration to install small power plant in the Bouhadjar zone [45], east Algeria, there are no examples in pilot plan experimentation that testing the use of geothermal energy for the electric production in the country.

1.4.3 Future development and policy

In the current situation, Algeria has aggressive plans for future development energy use. The Algerian government recently approved new renewable energies laws and provided substantial financial resources to investors and researchers to help them exploiting renewable energy resources, including the geothermal energy that is expected to reaches 15 MW of installed capacity by 2030 [46,47]. This will certainly enhance the geothermal power production in Algeria.

1.5 Conclusion

In this chapter, a general database of geothermal resources, all its exploitation techniques and its utilization around the world and in our country is presented and discussed in order to provide an outlook on the state of geothermal energy and where it will be heading in the future as well as identifying its promising technologies that could help achieve independence from fossil fuels. The main findings are:

- Based on the geothermal resource database, encouraging the exploitation of the huge geothermal energy can significantly help reduce the world’s use of oil resources.
- In recent years, the statistics indicate the world's interest in exploiting the shallow geothermal energy especially with the ground source heat pumps technologies.
- Algeria has important geothermal resources, indeed the geothermal maps of the country shows very good recourses in the northwestern part, the northeastern part and the south of the country.
- Despite the importance of the low enthalpy-geothermal resources in Algeria, its use is only limited to some direct applications such as balneological and agricultural uses.
- Since the GSHP technology is still not available in Algeria, it is time to benefit the high energy efficiency of these new technologies in order to reduce the large consumption of the building sector.
- Considering the geological specifications of most regions of Algeria and due to limitation in available groundwater with suitable thermal properties for both heating and cooling purposes, the closed loop systems are usually the best option.

In the following part, a review of the literatures dealing with the geothermal system including the ground heat exchanger which are to be invested will be presented.

CHAPTER 2

THE GSHP BACKGROUND AND LITERATURE REVIEW

2.5 Introduction

The main aims of this thesis focus on the pre-design and optimal control of GSHPs operation. This chapter therefore provides a literature review on recent researches and developments which deal with the cost-effective design methodologies and pre-investigation strategies for GSHP systems.

This chapter is organised as follows. Section 2.2 highlights the significance of identification the soil thermal properties and climate factors in the design of the GSHPs. Section 2.3 reviews the feasibility studies carried out for the design optimization and control of GSHPs. Section 2.4 summarises the reliable simulation models used for sizing the ground heat exchangers.

2.6 Implementation site factors

The design of geothermal heat exchangers strongly depends on the properties of the soil as they affect soil resistance, which is an indication of the amount of heat energy that can be transferred to/from the ground. In recent years, many studies dealing with the influence of soil types on ground heat pump performance have been published by various researches (design, simulation and testing of GSHPs). Deng et al. [48] examined the heat transfer in multilayered ground (coarse sand, clay, fine sand) with a vertical ground heat exchanger. The heat transfer rates during 24 hours of operation period were found to be discontinuous between soil layers and the effectiveness of heat distribution in coarse and fine sandy soils was higher by 62% and 27%, respectively, than in clayey soils as shown in Fig 2.1.

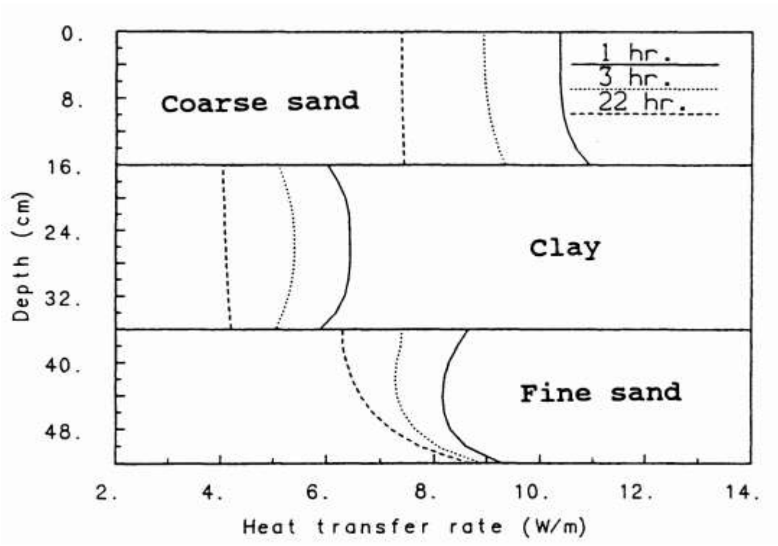

Fig 2.1 Computed heat transfer rates from the copper tube to the soil, with an Re of 16.800 and hot water temperature of 48 °C [48]

In the study of W. H. Leong et al. [49] three different soils with five different degrees of saturation (0, 12.5, 25, 50 and 100%) were used in computer simulations in order to determine the effect of soil type and moisture content on ground heat pump performance. It was found that the performance of the geothermal heat pump system strongly depends on the moisture content and the soil type (mineralogical composition) (see Fig 2.2). Therefore, they concluded that it is important to keep the soil moisture value at the highest possible levels.

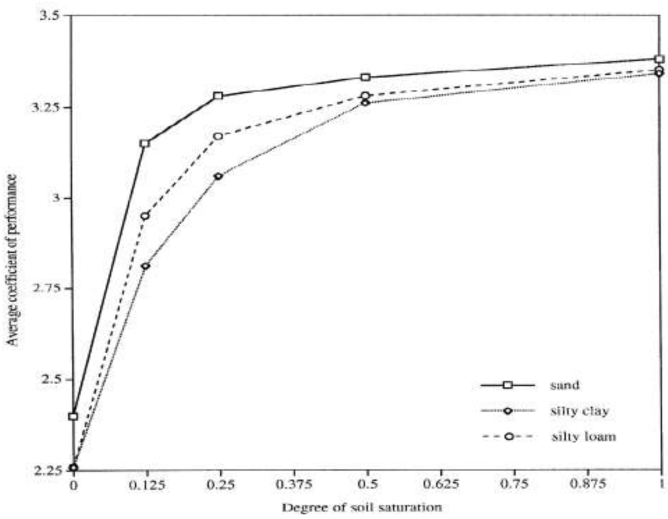

Fig 2.2 Variation of the average COP vs soil degree of saturation [49]

G. Radioti et al. [50] studied the effect of undisturbed ground temperature on the closed-loop geothermal systems. Experimental equipments consist of four borehole heat exchangers were tested using a 3D numerical model to present the heat loss. It was found in their study that the over or underestimation of the ground temperature can significantly overestimate the maximum extracted power and the heat pump coefficient of performance (COP). To limit the error in the COP and the extracted power to less than 5%, the error in the undisturbed temperature estimation should not exceed ±1.5 °C and ± 0.6 °C, respectively.

The actual loads of buildings and meteorological factors play also a significant role in the GSHPs performance and the design of the GHX. The heat transfer effectiveness between the ground heat exchanger pipe and the surrounding ground strongly dependent on the temperature of the surrounding soil which vary greatly with time and meteorological factors of implementation sites. This leads to significant differences in GSHP thermal performance from one region to another which changes the design criteria for the ground heat exchangers, especially for the horizontal ones, since they are the closest to the ground surface and the most affected by external factors. The performance and the feasibility of GSHPs have been investigated for different geological and climate conditions around the world. In the study of Noorollahi et al. [51] a vertical GSHPs installation was spatially analyzed and various optimum design parameters were investigated in order to achieve the minimum TAC (total annual cost) as an objective function for different geological and climate conditions. The procedure includes numerical modeling and optimization of GSHPs by Genetic Algorithm (GA), regional heating/cooling design load estimation and spatial data analysis for 234 cities in Iran. A regional scale energy-economic mapping was accomplished and Iran's provinces were prioritized based on the TAC weighted average which was found depends strongly on spatial data (see Fig 2.3).

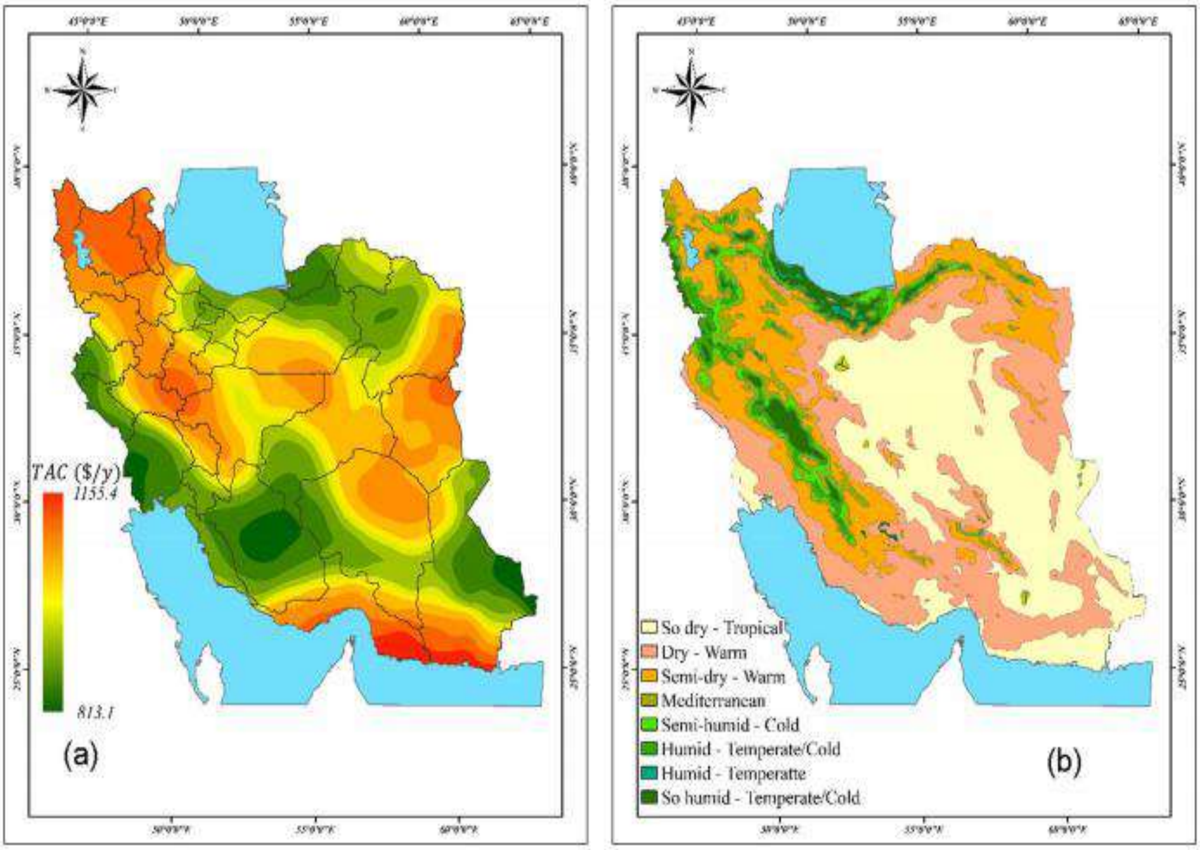

Fig 2.3 (a) Iran's economic priority map for GSHP system installation (b) Iran climates [51]

S, sanay et al. [52] investigates the effect of climate (tropical, temperate, and cold) on GCHPs operation. A sensitivity analysis of change in the total annual cost of the system and optimum design parameters with the climatic conditions and soil type were performed using Nelder–Mead optimization technique (NM) and genetic algorithm optimization technique (GA). Six soil types (damp clay, saturated sand, dray clay, dray sand, damp loam and dray loam) and seven climatic regions were considered: Three regions (No. 1–3) represent the cold climate, one region (No. 4) represents the temperate climate, and three regions (No. 5–7) represent the tropical climate. It was found that the total annual cost of the system and the optimum design parameters of GSHP are strongly dependent on soil conditions and climate type (see Fig 2.4).

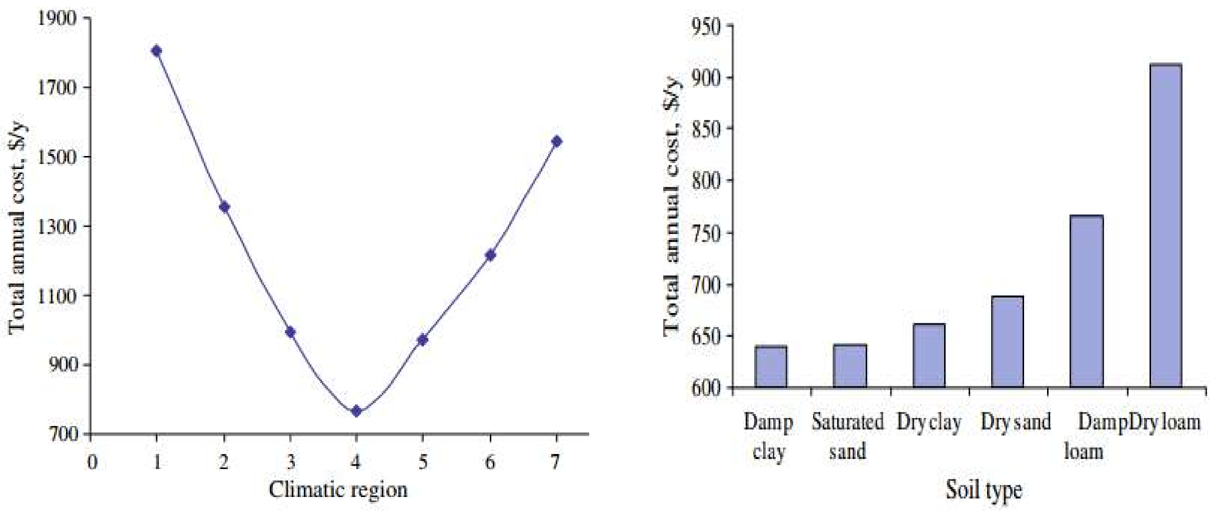

(a) **(b)**

Fig 2.4 The optimized TAC values in various (a) climatic regions and (b) soil type [52]

2.7 Design optimization of GSHP systems

The ground loop pipes or the ground heat exchangers, which are placed horizontally or standing vertically in ground, have the largest portion of investment cost in ground source heat pumps installation [52]. Compared with vertical GHXs, the horizontal GHXs require longer pipe length and ground surface area but they are typically less expensive due to the lower cost of drilling and refilling. However, the investment price remains relatively high compared to the air conditioning system. Therefore, the process of improvement of the system must be carried out during the sizing of GHX in order to obtain the most cost-effective design parameters and thus minimize the high installation cost of GSHP systems and avoiding the significant financial losses [52-54].

Over the last two decades, several studies have shown the importance of conducting a pre-design analysis to determine the influence of well properties on ground source heat pump performance and installation costs, modeling a software program based on a model of ground heat exchanger and evaluating the optimum technical characteristics of the overall GSHPs.

S, sanay et al. [55] presented a modeling and optimizing processes for a GSHP coupled with HGHX (Fig 2.5) by defining the total annual cost (total of investment and operation costs) as an objective function using Nelder–Mead and Genetic algorithm techniques to estimate the optimum design parameters of the system as well as the configuration of HGHX. Their study indicated that the system parameters (saturated temperature condenser and evaporator, inlet and outlet temperatures of the water source and GHX nominal pipe diameter) have a significant effect on ground coupled heat pump performance and the total annual cost of the system (see Fig 2.6). Therefore, it is necessary to pre-investigate the exploitation of closed geothermal systems before any field application in given climatic conditions in order to obtain optimum system parameters that ensure high efficiency and lower cost.

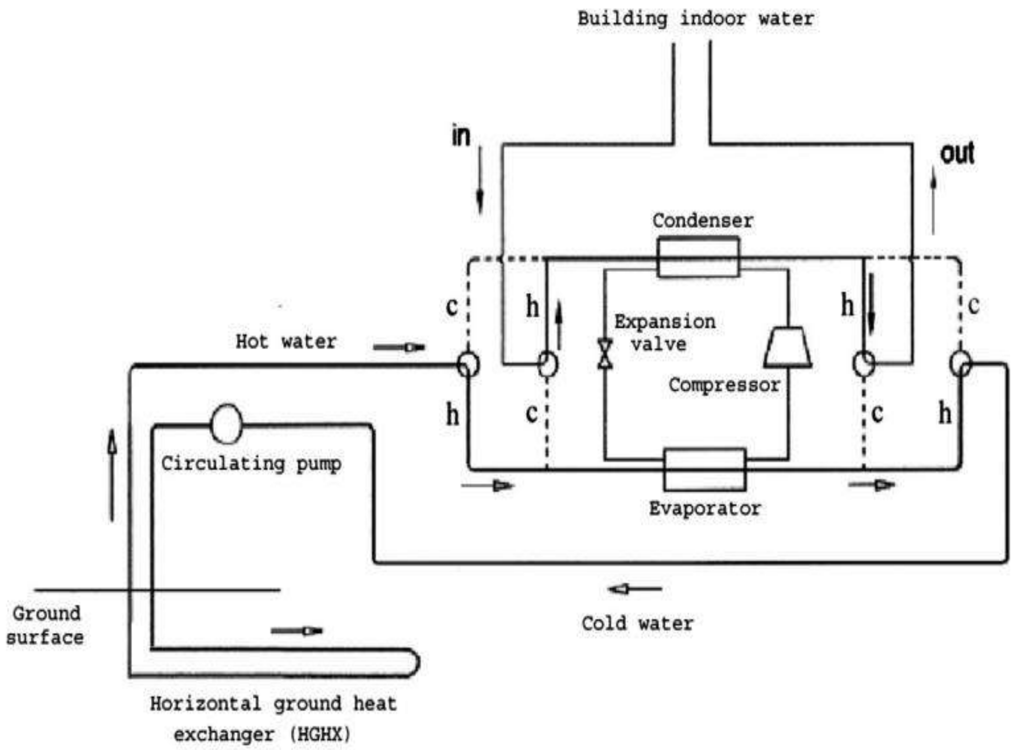

Fig 2. 5 A view of the studied GCHP with HGHX [55]

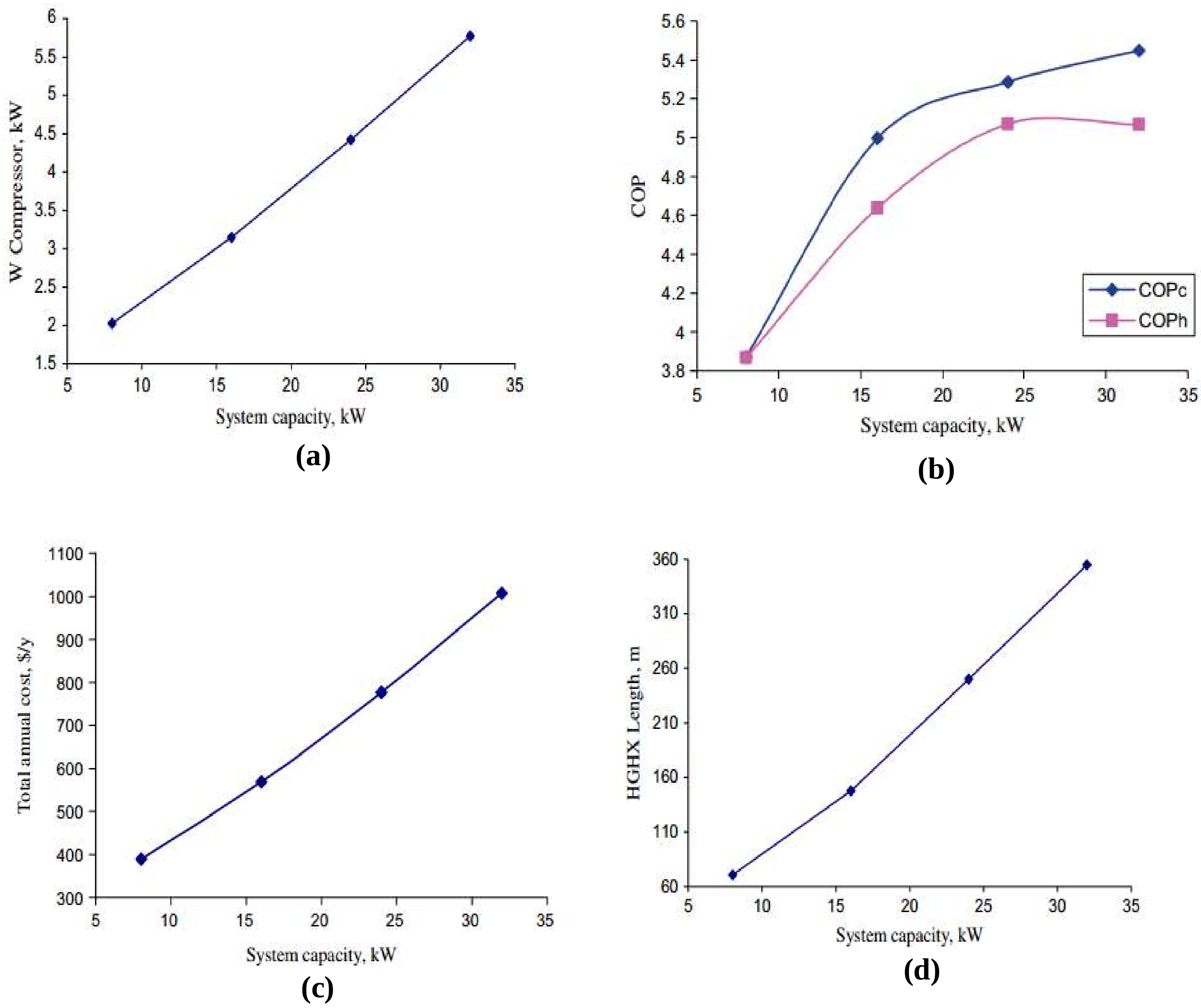

Fig 2.6 Change in the system capacity with (a) the compressor power consumption; (b) COP; (c) the optimized TAC and (d) the HGHX length [54]

Kayaci et al. [56] studied the energy and economic analysis of HGHX (see Fig 2.7) used for cooling and heating an office with a total conditioned space of about 200 m^2 in Turkey. The effect of all geometric properties of the designed horizontal GHX as well as the effects of the rate of increase in electricity prices was investigated by defining a reference function (total cost) as an optimization parameter. In their simulation results (see Fig 2.8), found that the number of parallel pipe, burial depth, pipe spacing, tube diameter and pipe length have a great impact on the performance of the GSHP and the reference function because it simultaneously affects the investment costs and the amounts of heat transferred to/from soil.

Thus, they concluded that it is feasible to examine all parts of GSHP system in the pre-design analysis to obtain the optimal design parameters that ensure a balance between system efficiency and total costs. Suggested values for all of these engineering properties are recommended.

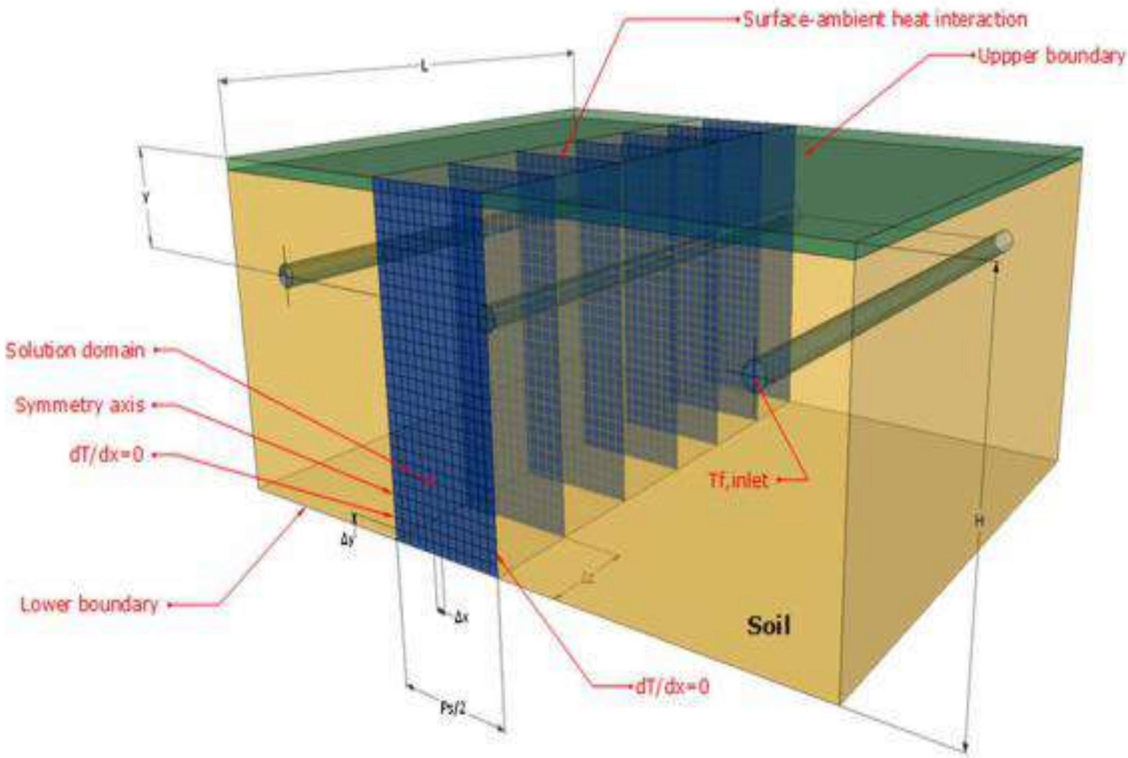

Fig 2.7 Ground heat exchanger and solution domain [56]

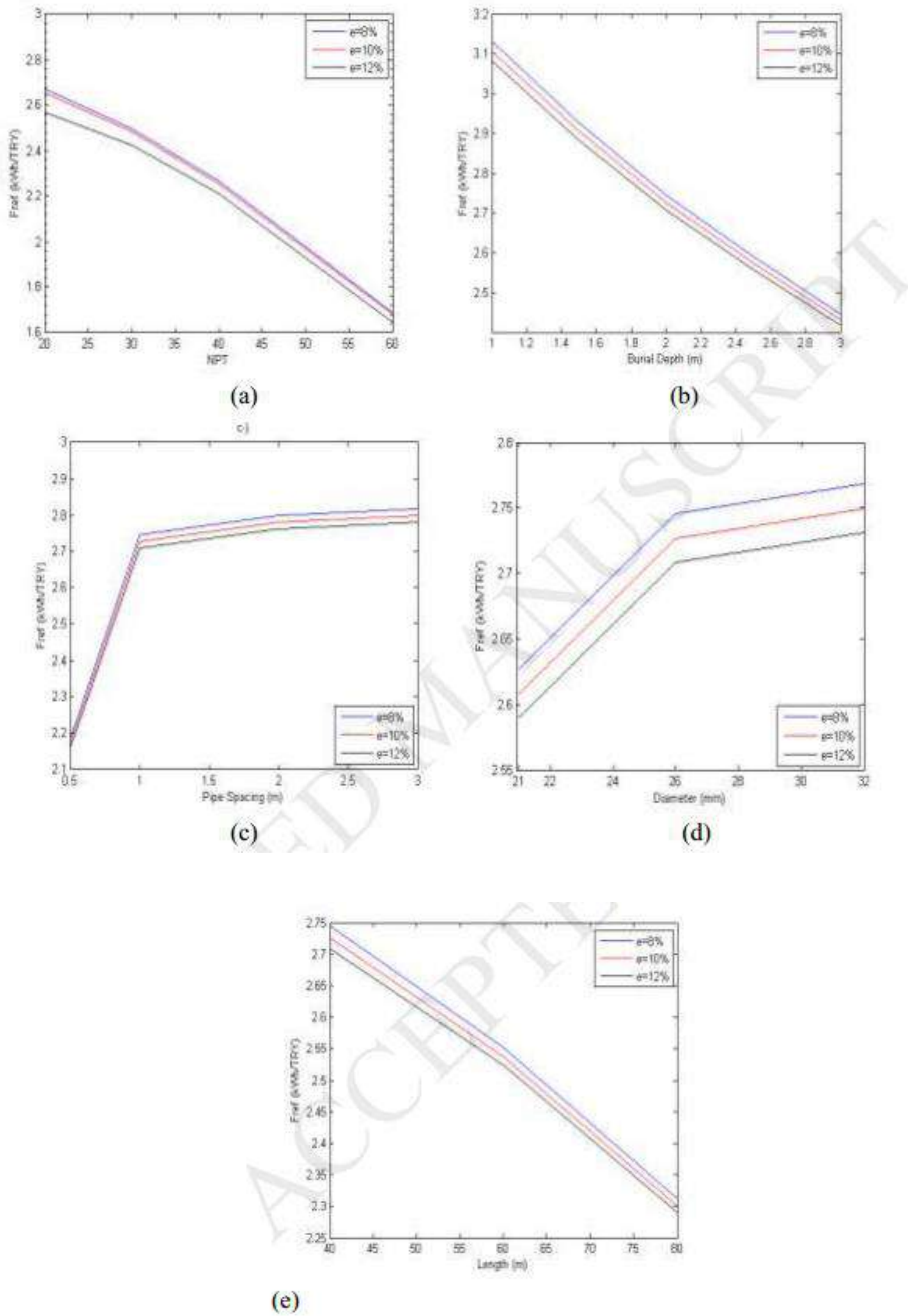

Fig 2.8 Variation of rate of increase in electricity prices on reference function for (a) NPT; (b) burial depth; (c) pipe spacing; (d) inner diameter; (e) length [56]

Mustafa et al. [57] the effects of various system parameters such as the burial depth of ground heat exchanger, the mass flow rate of the water antifreeze solution and the sewer water on the performance of ground source heat pumps were examined based on experimental analysis conducted in Turkey (see Fig 2.9). It was found that the poor design of the GSHPs caused lower performance factors when compared their results to other heat pumps operating under the same design conditions as shown in Fig 2.10. They concluded that it is necessary to conduct a pre-design analysis to determine optimal system parameters that will ensure minimum energy consumption and favorable costs with the help of GSHP simulation models.

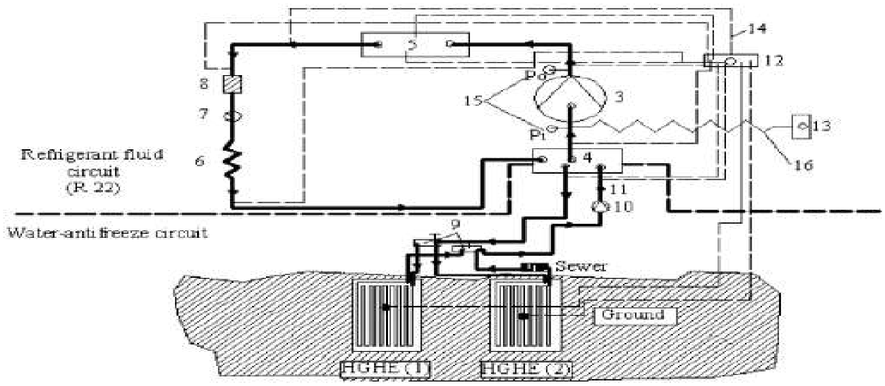

Fig 2.9 The schematic diagram of the experimental set-up [57]

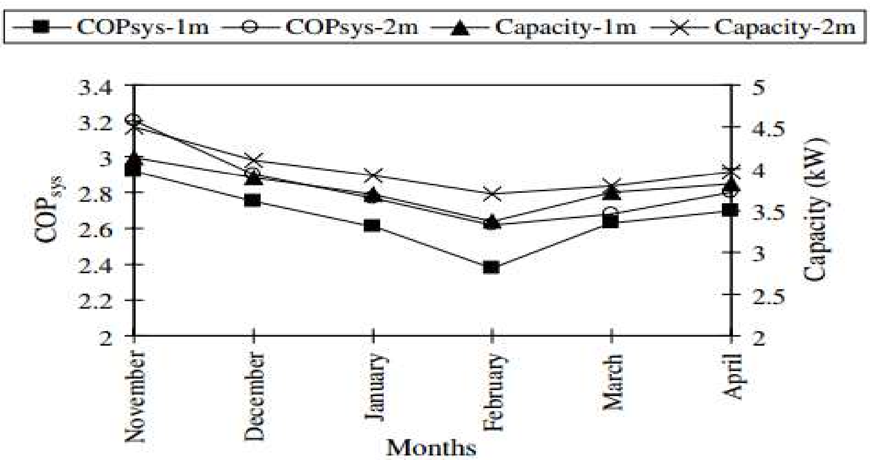

Fig 2.10 The monthly variation of COP_{sys} and the monthly variation of the space-heating rate of the GSHP system [57]

2.8 Modeling and dynamic simulation of GSHP systems

2.8.1 Computational design methods

There are many computational methods outlined in literature refer to simplified procedures applicable to GSHPs where the design depends on values of specific heat extraction rate related to ground thermal properties. Based on the work of Kavanaugh and Rafferty, the ASHRAE Handbook suggests relations for the required lengths of the GHX [19]. The design equations for heating and cooling loads are as follows:

For cooling:

$$L_{GHX,c} = \frac{q_a \ R_{ga} + Q_{con,c}(R_b + PLF_m R_{gm} + F_{sc} R_{gst})}{T_g - \frac{ELT + LLT}{2} + T_p} \tag{2.1}$$

For heating:

$$L_{GHX,h} = \frac{q_a \ R_{ga} + \ Q_{Eva,h}(R_b + PLF_m R_{gm} + F_{sc} R_{gst})}{T_g - \frac{ELT + LLT}{2} + T_p} \tag{2.2}$$

Where F_{sc} is the short circuit heat loss factor. $L_{GHX,c}$, $L_{GHX,h}$ are the required borehole field lengths for cooling and heating modes. PLF_m is the part load factor during the design month. q_a is the net annual average heat transfer to the ground. R_{ga},R_{gm}, R_{gst} are the effective thermal resistances of the ground for the annual, monthly, and daily pulses. T_g is the undisturbed ground temperature. ELT, LLT are the design heat pump inlet and outlet fluid temperatures. T_p is the temperature penalty. $Q_{con,c}$, $Q_{Eva,h}$ are the heat rate to/from ground at cooling and heating modes (W).

The heat rate to/from ground can be calculated using the following relations [19]:

The heat pump condenser heat rate to ground:

$$Q_{con,c} = \ q_{lc} \left(\frac{COP_c + 1}{COP_c} \right) \tag{2.3}$$

The heat pump evaporator heat rate from ground:

$$Q_{Eva,h} = q_{lh}\left(\frac{COP_h - 1}{COP_h}\right) \tag{2.4}$$

Where:

q_{lc} is the building design cooling block load and q_{lh} is the building design heating block load.

The borehole exit temperature is computed using the Equation (2.5) [58]:

$$T_{fo} = T_g + \frac{q_i}{2\dot{m}C_p} + \frac{q_i}{L_{GHX}} R_b + \frac{1}{2\pi L_{GHX}\mathrm{k}} \sum_{i=1}^{n} (q_i - q_{i-1})\ g\left(\frac{(t_i - t_{i-1})}{t_s}, \frac{r_b}{L_{GHX}}\right) \tag{2.5}$$

Where the length L_{GHX} is iterated until the exit temperature falls within the desired design value.

Min-Jun Kima et al. [59] proposed a design method for the horizontal spiral-coil GHXs (Fig 2.11) by modifying the boundary conditions of ASHRAE handbook equation which can be solved using the building load, heat pump specification, pipe dimensions, and ground thermal properties. A laboratory thermal response test was conducted to validate the proposed design method and the numerical modeling results were in good agreement with the experimental results. The design equation for the trench of the horizontal GHX is as follows:

$$L_{GHX} = \frac{q_a\, R_{ga} + q_{(lc,lh)}\left(\frac{COP_{(c,h)} \pm 1}{COP_{(c,h)}}\right) \times (R_b + PLF_{(mc,mh)} R_{gm} + F_{sc} R_{gd})}{T_{H,L} - \frac{T_{in-GHX} + T_{out-GHX}}{2}} \tag{2.6}$$

Where $T_{H,L}$ are the maximum and minimum ground temperatures at the installation depth of a horizontal GHX, it can be computed as follows [55].

$$T_{H,L} = \overline{T_g} \pm A_s\ exp[(-Z)(\frac{\omega}{2\alpha_g})^{\frac{1}{2}}] \times cos[\omega(t - t_0) - Z(\frac{\omega}{2\alpha_g})^{\frac{1}{2}}] \tag{2.7}$$

Where:

$\overline{T}_g$ is the average ground temperature, A_s is the amplitude of the soil surface temperature change throughout the year, and t is the elapsed time from January 1st. t_0 denotes the coldest day under the heating condition and the warmest day under the cooling condition of the year, α_g: is the ground thermal diffusivity, ω is the angular frequency of annual temperature variations (=2π/365), and z is the depth into the soil from the ground surface.

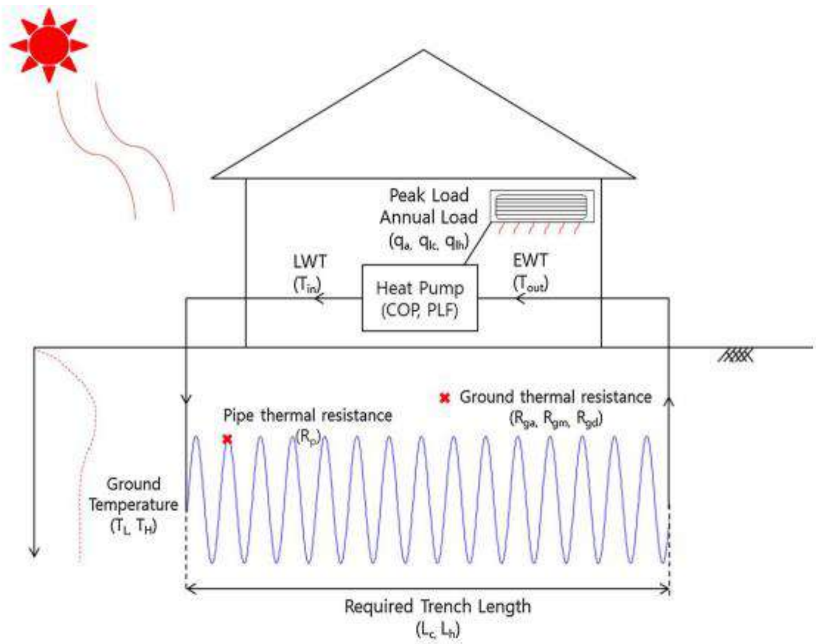

Fig 2.11 Conceptual diagram for design of a horizontal spiral-coil GHX [59]

Lamarche et al. [58] proposed a new design approach based on hourly load data which is mostly used for simulation purposes, but not for design due to longer simulation times. This new approach simulates the real thermal response of the individual hourly loads with the aid of ASHRAE handbook equation. The diagram given in Fig 2.12 describes the design algorithm of the new approach.

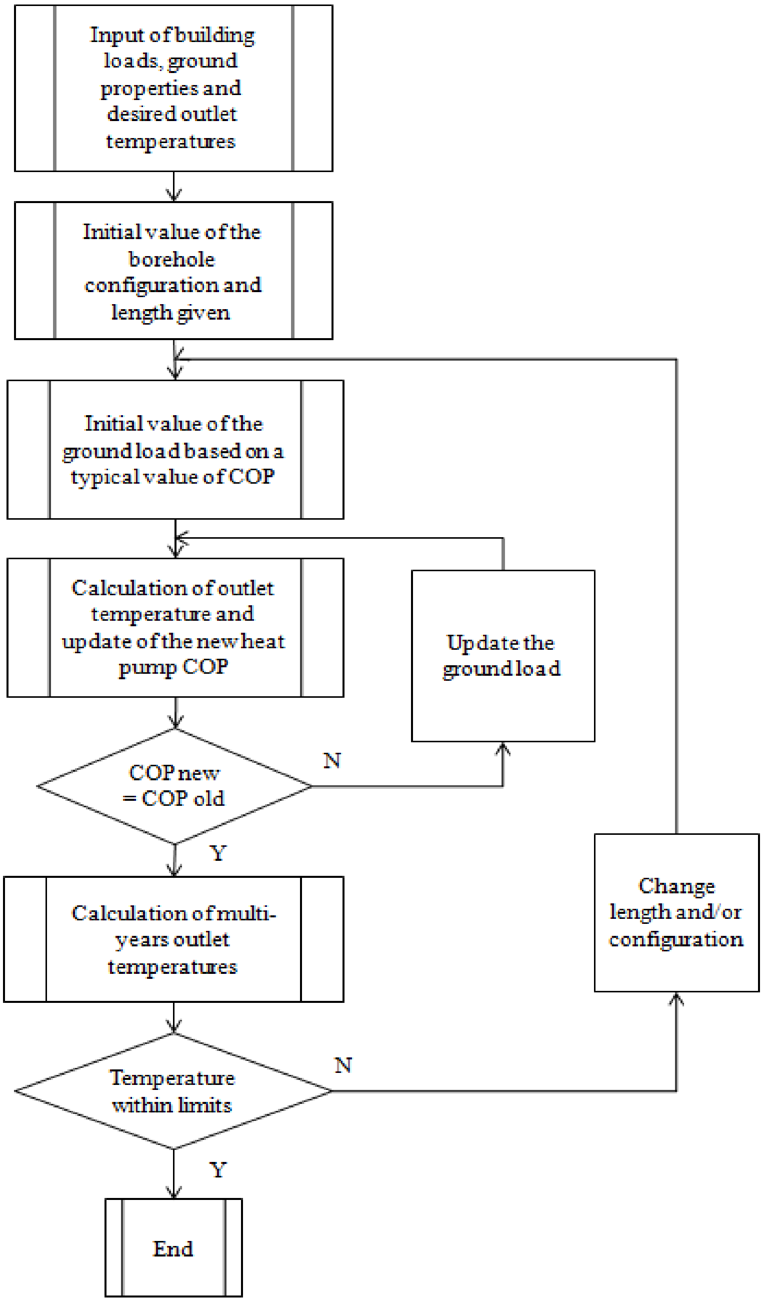

Fig 2.12 Design algorithm [60]

In this design approach, the total length of the GHX is iterated until the outlet temperatures of the ground heat exchangers meet the constrained design values. The use of this efficient scheme allows us to evaluate more precisely the physical effects, such as short-time thermal behavior, that will give more precise evaluation of the required borehole length [60].

2.4.2 Dynamic simulation models

Several dynamic models have also proven reliable in predicting the thermal behavior of the ground heat pump and the ground heat exchangers, and several studies have been published that have dealt with these models. e.g. Chao et al. [61] showed a comparison between the TRNSYS simulation results for different GHX models and the experimental data of a vertical ground source heat pump in order to show the ability of the dynamic model to reproduce the thermal behavior of the whole system. It was found that the TRNSYS model (Fig. 13) produced a better approach between the simulation results and the field data (see table. 2).

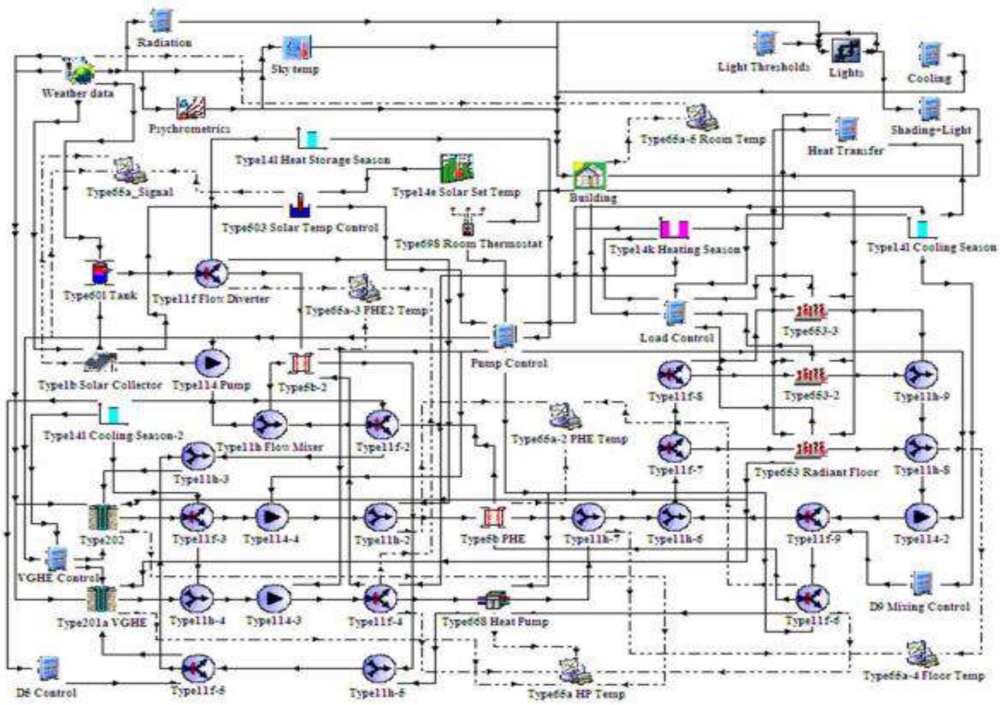

Fig 2.13 TRNSYS model of GCHPSSHS system [61]

Table 2.1 Comparison of energy parameters of system [61]

Energy parameters	Field data	557a	201a(0)	201a(1)	201a(2)	201a(2) relative deviation (%)
$Q_{g,c}$ (GJ)	5.10	4.69	4.97	4.98	5.01	1.76
$Q_{g,h}$ (GJ)	63.25	62.87	62.32	62.30	63.03	0.35
W_{hp} (kWh)	5457.7	5485.5	5310.7	5298.0	5452.4	0.10
COP	4.22	4.18	4.26	4.27	4.21	0.24

Mattia et al. [62] showed a new design approach based on a novel TRNSYS type of borehole to ground (B2G) model as one of the main components (see Fig 2.14). The model was developed for modeling the short-term dynamic performance of a borehole heat exchanger (BHE) with low computational time required. An experimental test was performed in order to validate the proposed model and good agreements were obtained between the numerical modeling and experimental results as shown in Fig 2.15.

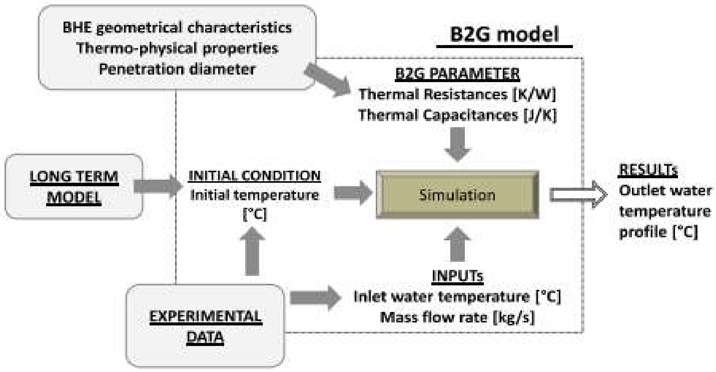

Fig 2.14 Calculation procedure of B2G model [62]

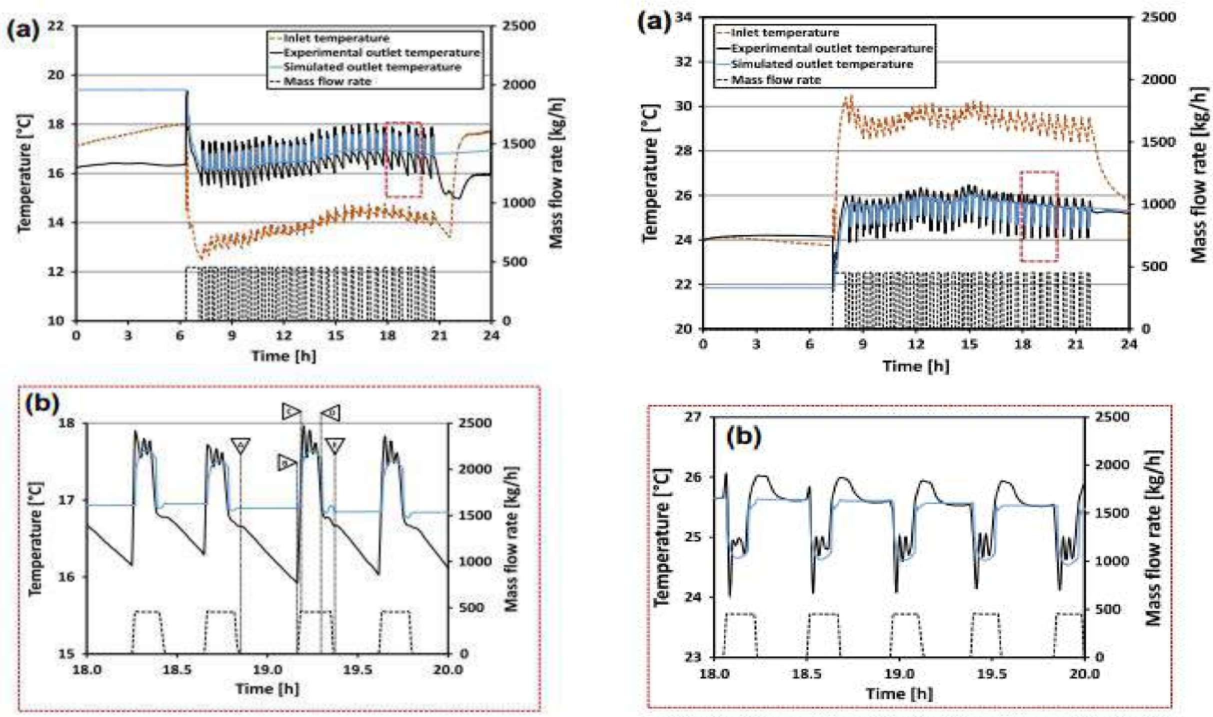

Fig 2.15 Experimental vs numerical outlet water temperature values for both heating and cooling cases [62]

2.5 Conclusion

In this chapter, a literature review on the significant factors affecting the operation of the GSHPs, pre-design analyses and optimization methods of the GHXs have been provided. Despite higher initial costs of GSHPs compared to conventional ones, the reviewed literature revealed that GSHPs can be confirmed as the most energy-efficient air conditioning system through appropriate design and optimization procedures. The important conclusions from this review include:

- Geological conditions can strongly influence the GSHPs performance. Accurate estimation of the soil thermal characteristics of the implementation sites is essential before the design and the installation of the GSHP system.
- The feasibility studies showed that GSHPs energy performance and its total investment and operating costs are also influenced by many factors, such as climate conditions and types of buildings and technology used. It is not possible to select a common conclusion about whether GSHPs are feasible for every building and climate conditions. It is necessary to evaluate the energy-economic performance of GSHPs on a case-by-case basis.
- A number of computational design methods have been developed for modeling and sizing ground heat exchangers. Due to the high computational time required, both analytical and numerical models are not suitable for simulation programs with hourly or sub-hourly time steps.
- Several dynamic simulation models and software programs are now available for appropriate design the GSHPs. However, it is hard to make sure that the designed GSHPs can give an optimal operation. Design optimization and operation control are very important to determine optimal values of the most-cost effective design

parameters in order to maximize the overall performance of GSHPs as well as to minimize the high initial cost of GSHPs.

Therefore, this thesis will focus on analyzing the energy-economic performance of GSHP systems under our Algerian desert climate. To maximize the benefits of the GSHPs use, the optimized GSHPs operation will also be calibrated.

CHAPTER 3

ENERGY-ECONOMIC ANALYSIS OF GSHP SYSTEM COUPLED WITH HORIZONTAL GROUND HEAT EXCHANGER

3.1 Introduction

The literature reviewed in Chapter 2 demonstrated that the pre-design of ground source heat pump systems is essential to reduce the high investment and operation costs as well as to improve the energy performance of the GSHP technology for any selected climate conditions. The ground heat exchanger is one of the major components in GSHP systems and it have the majority part of GSHP installation costs. For this purpose, this study focused specifically on the development of the design and optimisation procedures of the GHXs.

This chapter introduces the processes undertaken in the energy-economic modeling and optimisation of horizontal ground heat exchanger coupled ground heat pump system. It is organised as follows. Section 3.2 describes the general principles of the heat pump and vapor-compression cycle. A brief description of the developed model for multi-optimisation of HGSHPs is provided in Section 3.3.

3.2 Heat pump principles

The operation of the GSHPs basified by (1) heat source and sink, (2) heating and cooling distribution fluid, and (3) thermodynamic cycle. A view of the principal components in the GSHPs is shown in Fig 3.1.

It is clear that the studied system consisting of three circuits for both cooling and heating modes. The first circuit is on the external side in which the refrigerant exchanges heat with the ground loop that can be HGHX or VGHX depending on its application technic. The second circuit is the thermodynamic cycle or the vapor-compression cycle, which absorbs heat from the source circuit and delivers it into the load circuit. The third circuit is on the internal side in which the refrigerant exchanges heat with the building loop. It is either a radiant floor or a ceiling panel according to its installation in the building.

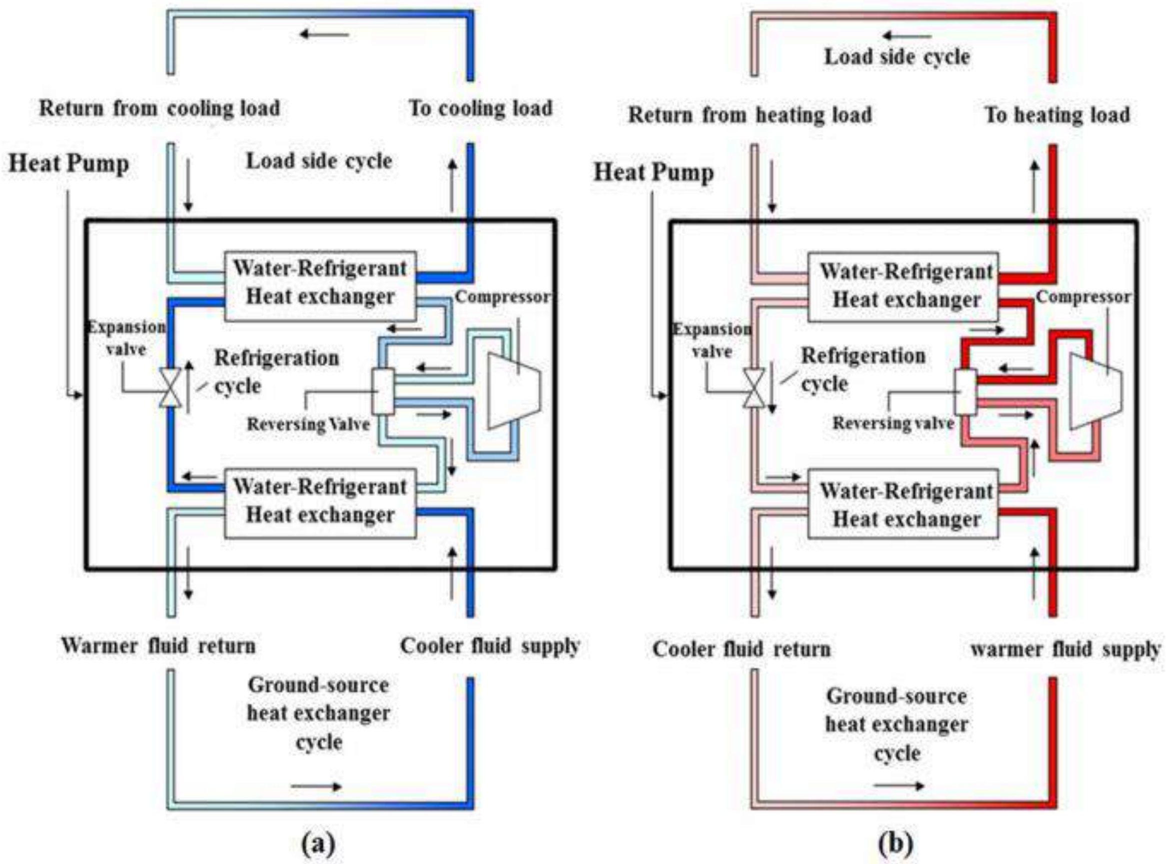

Fig 3.1 Principle diagram of a heat pump in both, (a) cooling and (b) heating modes [51]

The predominant form of the thermodynamic cycles is based on the vapor-compression cycle which made up of four fundamental processes: (1) expansion, (2) vaporization, (3) compression, (4) condensation. The states of the refrigerant throughout the vapor-compression theoretical cycle are illustrated in t-s and p-h diagrams in Fig 3.2. The refrigerant enters the compressor at state 1, as saturated vapor, and is compressed isentropically to the condensation pressure. The refrigerant pressure and temperature raises during this isentropic compression process to well above the temperature of the hot environment. The vapor then enters the condenser at state 2 where it gives up heat to the surroundings and leaves as saturated liquid at state 3. The new saturation temperature at this state is still greater than the temperature of the surroundings. The saturated liquid refrigerant at state 3 is throttled to the evaporation pressure by passing it through an expansion valve. The refrigerant temperature drops below the temperature of the cold environment during this process. The refrigerant enters the evaporator at state 4 as a low-quality saturated mixture, and completely vaporizes at a constant pressure and temperature by absorbing heat from the cold environment. The saturated vapor passes then to the compressor to complete the cycle and is ready to be recirculated [60,63].

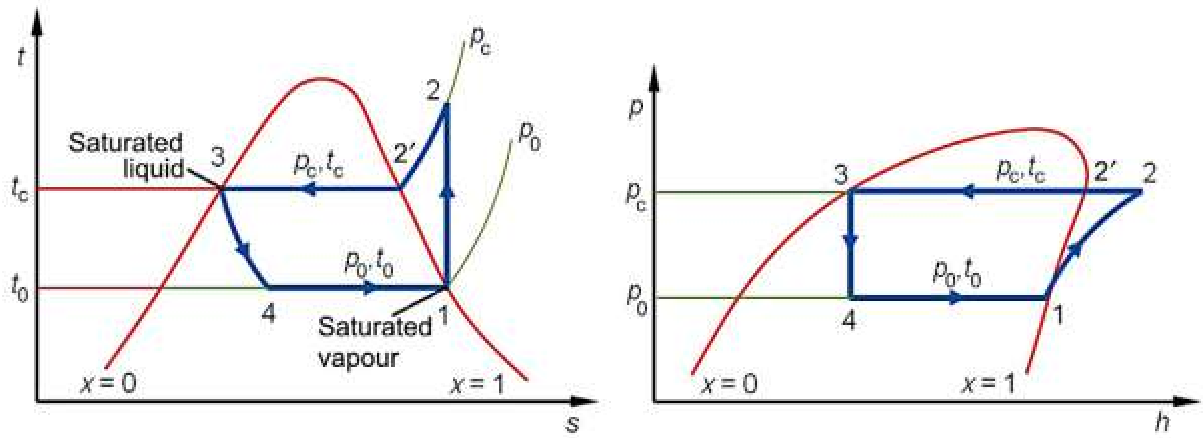

Fig 3.2 T–s and P-h diagrams of vapor-compression cycle for a heat pump [60]

3.3 Model development

As stated in previous sections, the model in this work focuses on pre-investigating the exploitation of geothermal heat pump for cooling and heating a residential unit under desert geological and climatic conditions. A simulation model of a HGSHPs has been proposed consisting of water-to-water heat pump, a water tank with immersed heat exchangers, a horizontal ground heat exchanger, water circulation pumps and a radiant floor system.

A novel method based on multi-year energy and economic analysis has been developed in order to achieve the two main goals of the model : reducing the total investment and operation costs as much as possible while ensuring a good system efficiency. The energy performance of GSHPs was evaluated with a developed TRNSYS model, which will be presented in Chapter 4. Then, the numerical outputs were used in the economic performance analysis to obtain the moste cost-effective design parameters of the HGHX. Because of the massive computations in the optimization process, a MATLAB code was used to evaluate the objective function based on Equations (3.31) and (3.32). The schematic diagram containing the algorithm procedure is shown in Fig 3.3.

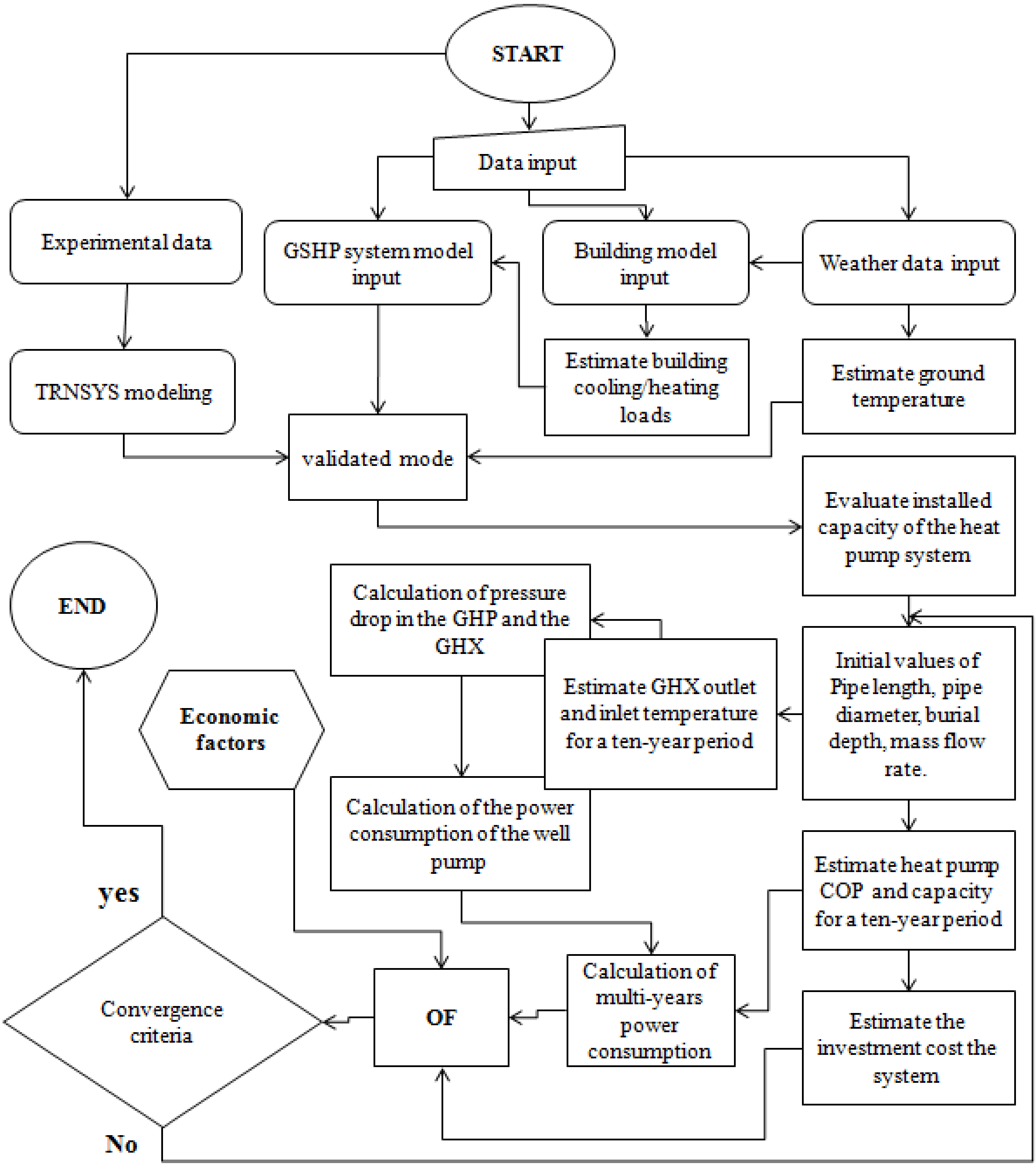

Fig 3.3 Block diagram of the optimization design procedure

3.3.1 Energy-economic modeling of GSHPs

3.3.1.1 Heat transfer analysis

Using the first law of thermodynamics, The heat transfer rate from radiant floor system to refrigerant via the evaporator in cooling mode is:

$$Q_{Evp,c} = \dot{m}_{w-RF,c}\, C_{p-H_2O} \left(T_{in-Evp} - T_{out-Evp}\right) \tag{3.1}$$

The heat transfer rate from refrigerant to radiant floor system via the condenser in heating mode is:

$$Q_{Con,h} = \dot{m}_{w-Con,h}\, C_{p-H_2O} \left(T_{out-Con} - T_{in-Con}\right) \tag{3.2}$$

The heat absorbed from the building, $Q_{b,c}$, in cooling and the heat transferred to the building,$Q_{b,h}$, in heating can be computed from the following equations:

$$Q_{b,c} = \dot{m}_{w-RF,c}\, C_{p-H_2O} \left(T_{out-RF} - T_{in-RF}\right) \tag{3.3}$$

$$Q_{b,h} = \dot{m}_{w-RF,h}\, C_{p-H_2O} \left(T_{in-RF} - T_{out-RF}\right) \tag{3.4}$$

The heat transfer rate from condenser to ground loop in cooling mode is:

$$Q_{Con,c} = \dot{m}_{w-Con,c}\, C_{p-H_2O} \left(T_{out-Con} - T_{in-Con}\right) \tag{3.5}$$

The heat transfer rate from ground loop to evaporator in heating mode is:

$$Q_{Evp,h} = \dot{m}_{w-Evp,h}\, C_{p-H_2O} \left(T_{in-Evp} - T_{out-Evp}\right) \tag{3.6}$$

The heat transferred to the ground, $Q_{g,c}$, in cooling and the heat absorbed from the ground ,$Q_{g,h}$, in heating can be computed from the following equations:

$$Q_{g,c} = \dot{m}_{w-GHX,c}\, C_{p-H_2O} \left(T_{in-GHX} - T_{out-GHX}\right) \tag{3.7}$$

$$Q_{g,h} = \dot{m}_{w-GHX,h}\, C_{p-H_2O} \left(T_{out-GHX} - T_{in-GHX}\right) \tag{3.8}$$

By proposing an infinitesimal element (Fig 3.4) ,Δx, of a GHX pipe in the water flow direction buried at a selective ground level in which the soil temperature considered constant, the heat exchange rate , ΔQ_g, transferred between water and soil through the element surface, ΔS, is given by the following expression:

$$\Delta Q_g = \frac{(T_w - T_g)}{R_{total}(x)} \tag{3.9}$$

Where:

T_g: represents the ground temperature, °C.

T_w: represents the average water temperature in the GHX, °C.

$R_{total}(x)$: represents the total thermal resistance through the infinitesimal element, Δx, of GHX pipe, (K/kw), can be computed from [51]:

$$R_{total}(x) = R_w(x) + R_p(x) + R_g(\text{x}) \tag{3.10}$$

Where:

R_w: represents the thermal resistance of the water flow, K/kW [51]:

$$R_w(x) = \frac{1}{h_w(\pi D_{i,GHX} \Delta x)} \tag{3.11}$$

R_p: represents the thermal resistance of the pipe wall, K/kW [51]:

$$R_p(x) = \frac{\ln \frac{D_{o,GHX}}{D_{i,GHX}}}{2\pi K_{GHX} \Delta x} \tag{3.12}$$

R_g: represents the thermal resistance of the soil, K/kW [51]:

$$R_g(x) = \frac{F}{U_s\left(\pi D_{o,GHX} \Delta x\right)} \tag{3.13}$$

Where:

h_w: represents the convection heat transfer coefficient of the water in GHX pipe, kW/(m^2 K).

$D_{i,GHX}$: represents the inner pipe diamete of the GHX, m.

$D_{o,GHX}$: represents the outer pipe diameter of GHX, m.

K_{GHX}: represents the thermal conductivity of GHX pipe, kW/(m K).

U_s: represents the heat transfer coefficient of soil, kW/(m^2 K).

F: represents the part-load factor of the GHX, for heating and cooling modes, can be computed from the following equations [55]:

$$F_c = \frac{t_c}{T_c} \tag{3.14}$$

$$F_h = \frac{t_h}{T_h} \tag{3.15}$$

Where t_c and t_h, represents the equivalent full-load hours in cooling and heating modes, h/y.

Thus, the heat transfer rate between the ground loop and the soil along the GHX pipe in cooling and heating modes can also be expressed as follows:

$$Q_{g,c} = \frac{(T_{w,c}-T_g)}{R_{total,c}} = \frac{[(T_{in-GHX}-T_{out-GHX})-T_g]}{\frac{1}{h_{w,c}(\pi\, D_{i,GHX,c}\, L_{GHX,c})}+\frac{\ln\frac{D_{o,GHX}}{D_{i,GHX}}}{2\pi\, K_{GHX}\, L_{GHX,c}}+\frac{F_c}{U_S\,(\pi\, D_{o,GHX}\, L_{GHX,c})}} \tag{3.16}$$

$$Q_{g,h} = \frac{(T_{w,h}-T_g)}{R_{total,h}} = \frac{[T_g-(T_{out-GHX}-T_{in-GHX})]}{\frac{1}{h_{w,h}(\pi\, D_{i,GHX,h}\, L_{GHX,h})}+\frac{\ln\frac{D_{o,GHX}}{D_{i,GHX}}}{2\pi\, K_{GHX}\, L_{GHX,h}}+\frac{F_h}{U_S\,(\pi\, D_{o,GHX,h}\, L_{GHX,h})}} \tag{3.17}$$

Where:

$L_{GHX,c}$: represents the required length of GHX in cooling mode, m.

$L_{GHX,h}$: represents the required length of GHX in heating mode, m.

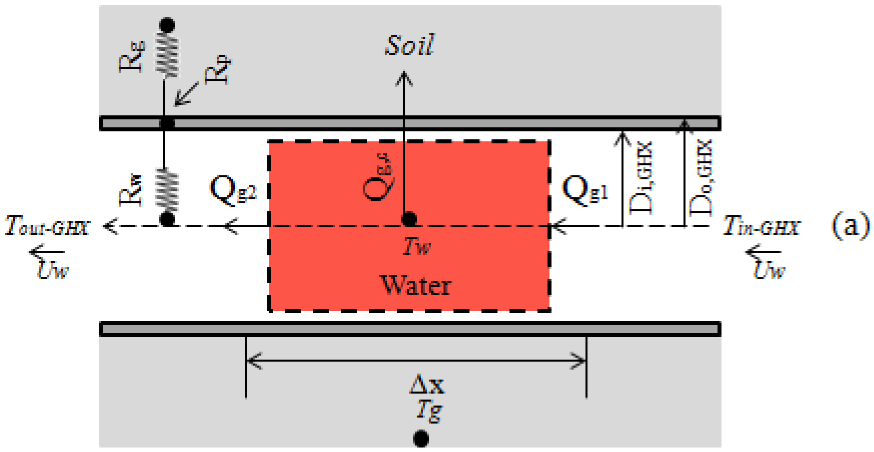

Fig 3.4 Descriptive scheme of an infinitesimal element of HGHX in (a) cooling cycle and (b) heating cycle

3.3.1.2 Energy performance analysis

3.3.1.2.1 Compressor power consumption

The compressor power consumption in cooling mode can be defined as the ratio between the heat absorbed from building and the heat pump coefficient of performance (COP_c) in cooling mode. It is obtained as shown below:

$$\dot{W}_{Com,c} = \frac{Q_{Evp,c}}{COP_c} \tag{3.18}$$

The compressor power consumption in heating mode is estimated by the ratio between the heat rejected into building and the heat pump coefficient of performance (COP_h) in heating mode. It can be expressed as follows:

$$\dot{W}_{Com,h} = \frac{Q_{Con,h}}{COP_h} \quad (3.19)$$

For the compressor:

$$W_{com} = Max\{W_{com,c}, W_{com,h}\} \quad (3.20)$$

3.3.1.2.2 Pumping power consumption

The pumping power consumption in heating and cooling modes are [52]:

$$W_{pump,c} = \frac{\dot{m_{w,c}}\, H_{pump,c}}{\rho_{w,c}\, \eta_{pump,c}} \quad (3.21)$$

$$W_{pump,h} = \frac{\dot{m_{w,h}}\, H_{pump,h}}{\rho_{w,h}\, \eta_{pump,h}} \quad (3.22)$$

Where H_{pump}, is the total pumping head in the HGHX (Δp_{GHX}) and heat pump (Δp_{GHP}).

For the circulating pump:

$$W_{pump} = Max\{W_{pump,c}, W_{pump,h}\} \quad (3.23)$$

3.3.1.2.3 The GHX pumping head

The total pumping head in the HGHX (H_{pump}) is defined as the sum of pressure drop in the straight portion of the GHX and in the bends [55], (see Fig 3.4) :

$$\Delta p_{GHX} = \Delta p_{straight} + \Delta p_{bends} \quad (3.24)$$

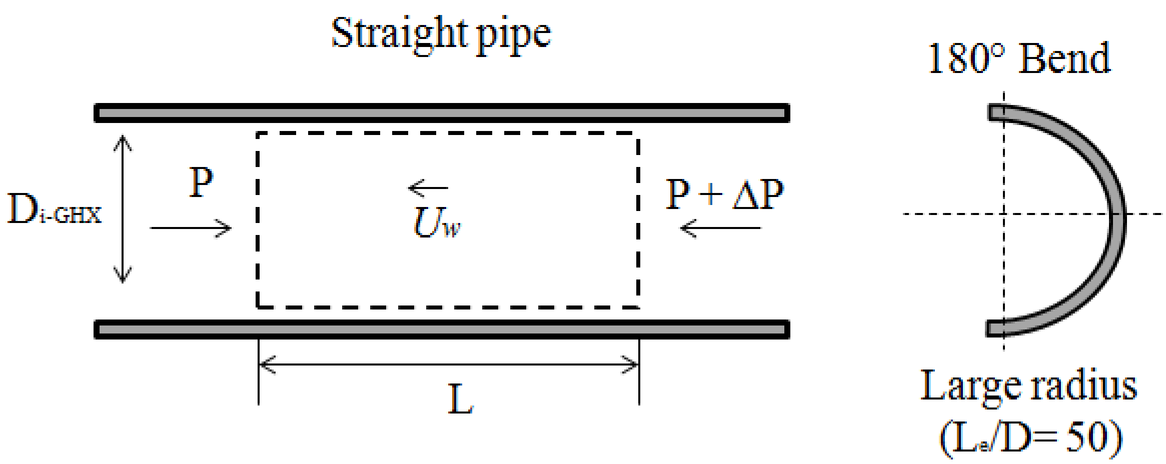

Fig 3.4 Force balance of a cylindrical fluid element within a pipe

Where:

$$\Delta p_{straight} = 4f \frac{L_{GHX}}{D_{i-GHX}} \rho_w \frac{U_w^2}{2} \tag{3.25}$$

$$\Delta p_{bends} = 4f \left(\frac{L_e}{D}\right) \rho_w \frac{U_w^2}{2} \tag{3.26}$$

Where:

($\frac{L_e}{D}$): represents the quivalent length in pipe diameters of 180° bends.

f: represents the friction coefficient.

U_w: represents the water velocity, m/s.

The calculation of the friction coefficient depends on the nature of the flow, laminar or turbulent. A recommended correlations for the smooth pipes are given as:

In laminar flow [64]:

$$f = \frac{16}{Re} \tag{3.27}$$

In turbulent flow [64]:

$$f = 0.046\, Re^{-0.2} \qquad \text{for} \qquad 3 \times 10^4 < Re < 10^6 \tag{3.28}$$

$$f = 0.079\, Re^{-0.25} \qquad \text{for} \qquad 4 \times 10^4 < Re < 10^5 \tag{3.29}$$

The reynolds number (Re) can be computed as [64]:

$$Re = \frac{U_w\, D_{i-GHX}\, \rho_w}{\mu_w} \tag{3.30}$$

Where:

ρ_w: represents the water density, (kg/m^3).

μ_w : represents the water dynamic viscosity, (Pa.s).

The properties of GHX water (including thermal conductivity, dynamic viscosity , density, and specific heat) in mean of GHX inlet and outlet water temperatures in cooling and heating modes ($T_{w,c}$ and $T_{w,h}$) were obtained from the tables of water thermophysical properties provided in Appendix E.

3.3.2 Economic analyses of GSHP system

Because of the high investment cost of the ground heat exchanger installation and the large cost of long-term electricity consumption, the objective of this part was to minimize the initial and operation costs of HGSHPs for the building cooling capacity in which the thermal performance of the GSHPs was considered (ie- COP). Thus, the design of GSHPs was implemented by defining an objective function to obtain the optimal values of GHX design parameters.

3.3.2.1 Objective function

An objective function, OF ($/kWh), was defined by dividing the total cost into the total seasonal thermal load:

In cooling season:

$$OF_c = \frac{TAC_c}{Q_{b,c} \times T_c} \tag{3.31}$$

In heating season:

$$OF_h = \frac{TAC_h}{Q_{b,h} \times T_h} \tag{3.32}$$

Where:

$Q_{b,c}$: is the annual cooling load, kW.

$Q_{b,h}$: is the annual heating load, kW.

T_c : is the total annual cooling operation hours, h/y.

T_h : is the total annual heating operation hours, h/y.

TAC: is the total annual cost which contains the investment and the electricity costs [66], was defined as:

$$TAC_{c,h} = CRF\ (C_{inv,c,h} + C_{elec,c,h}) \tag{3.33}$$

Where CRF, is the capital recovery factor [65]. It is expressed as:

$$CRF = \frac{i}{1-(i+1)^{-n}} \tag{3.34}$$

Where i and n, are the interest rate and the number of operation years, respectively.

Thus, the objective function can be reformulated by the following equation:

$$OF_{c,h} = OF_{inv,c,h} + OF_{elec,c,h} \tag{3.35}$$

Where:

$$OF_{inv,c,h} = \frac{CRF \times C_{inv,c,h}}{Q_{b,c,h} \times T_{c,h}} \tag{3.36}$$

$$OF_{elec,c,h} = \frac{CRF \times C_{ele,c,h}}{Q_{b,c,h} \times T_{c,h}} \tag{3.37}$$

3.3.2.2 The annual cost of the power consumption

The annual electricity consumption of GSHP systems includes the annual energy consumption of compressor and circulating pump:

$$E_{c,h} = E_{pump,c,h} + E_{comp,c,h} \tag{3.48}$$

The annual electricity consumption of the compressor, E_{comp} (kWh), can be determined as:

$$E_{comp,c,h} = T_{c,h}\ W_{comp,c,h} \tag{3.39}$$

The annual electricity consumption of the circulating pump, E_{pump} (kWh), can be determined as:

$$E_{pump,c,h} = T_{c,h} \frac{\dot{m_{w,c,h}} H_{pump,c,h}}{\rho_{w,h} \eta_{pump}} \tag{3.40}$$

Where $H_{pump,c,h}$ is the total pumping head in the HGHX (Δp_{GHX}) and heat pump (Δp_{GHP}).

Thus, the total annual electricity consumption, C_{elec} ($) can be obtained as follows:

$$C_{elec,c,h} = \left(E_{pump,c,h} + E_{comp,c,h}\right) E_{tariff} \tag{3.41}$$

where E_{tariff} ($/kWh), is the price of electricity for each kWh, which can be obtained from Sonelgaz [66].

And finally, the total cost of electricity consumption for ten-year period is obtained as follows:

$$C_{elec,c,h} = C_{elec,c,h,1} + \sum_{n=2}^{n=10} C_{elec,c,h,n}\, e \tag{3.42}$$

where e, is the increases in electricity prices.

3.3.2.3 The annual capital cost

For the total investment cost of GSHPs including the GHX, C_{inv} (\$), a reference function was defined as:

$$C_{inv,c,h} = C_{Pipe,c,h} + C_{earthwork,c,h} + C_{heatpump,c,h} + C_{pump,c,h} \tag{3.43}$$

For the cost of pipes, earthwork, pump and heat pump unit, the following cost functions were applied [54]:

$$C_{Pipe,c,h} = c_{Pipe}\,(NPT)\,L_{GHX,c,h} \tag{3.44}$$

$$C_{earthwork,c,h} = a_1\,(NPT)\,L_{GHX,c,h}\ Z_{c,h} \tag{3.45}$$

$$C_{heatpump,c,h} = a_2\, W_{com,c,h}^{a3} \tag{3.46}$$

$$C_{pump,c,h} = a_4 W_{pump,c,h}^{a5} \tag{3.47}$$

where :

c_{Pipe} : is the regional cost of polyethylene pipe per meter which depending on the diameter of pipes (provided in Appendix F), (\$/m).

NPT: is the number of parallel pipe.

Z : is the depth of the ground, m.

a_1 : is the regional price of the drilling and refilling,(\$/m^2).

a_2–a_5: are constant coefficients which were obtained based on the manufacturer's data according to the given required cooling and heating capacity and the regional price of the equipments.

3. 4 Conclusion

This chapter presents the processes undertaken in the modeling and optimisation of the proposed HGSHP system. With aid of TRNSYS software program and MATLAB code, a novel method based on multi-year energy and economic analysis has been developed in order to determine the optimal values of the most-cost effective design parameters of the system such as total GHX length, GHX pipe diameter, burial GHX depth etc, which can improve the economic feasibility of GSHP system in the long run and therefore compensate the high installation cost of GSHPs.

CHAPTER 4

TRNSYS DYNAMIC SIMULATION OF THE HORIZONTAL GROUND SOURCE HEAT PUMP

4.1 Introduction

A thorough understanding of the dynamic characteristics of GSHP system is useful for the development of optimal design strategies of GSHPs. For this purpose, this chapter presents the dynamic characterization of the entire ground source heat pump systems and describes its operating conditions.

This chapter is organised as follows. Section 4.2 describes the development of the simulation platform for the ground source heat pump including the horizontal ground heat exchanger systems. Section 4.3 analyzes the operating conditions of the proposed GSHPs.

4.2 Development of the simulation model

This section describes the development of the simulation model for the horizontal ground source heat pump system. The main purpose of the dynamic simulation is twofold: i) to examine the energy performance of ground source heat pump system under the Saharan conditions, and ii), to understand the effects of the GHX design parameters on the thermal performance of the overall GSHPs. A typical local building is used as a reference building and a water-to-water ground source heat pump combined straight horizontal ground heat exchanger is used as a reference air-conditioning system. The description of the HGSHP dynamic simulation model including detailed information on the building example as well as the operation conditions were presented in the following sections. The validation of the HGSHP simulation model which was performed by comparing its results with measured data obtained by experimental device will be presented in the following chapter.

4.2.1 TRNSYS model description

The entire model of the HGSHPs was simulated in the TRNSYS 16 simulation environment. Fig 4.1 and Fig 4.2 shows the simulation system developed for the cooling and the heating of the building exemple, respectively. The overall model is composed of four important sub-models: the building, the ground heat pump, the data acquisition (DAQ) system and the horizontal ground heat exchanger. This model includes the main components for the installation which can be provided from the TRNSYS library (standard models). It is summarized in Table 4.1.

The simulation time step was set as 5 min in order to capture any thermal behavior of the system during the simulation periods. The set point temperature for cooling is 25.5 °C when the compressor switch on and 26.5 °C when the compressor switches off and the set point temperature inside the water storage tank was set as 6 °C when the compressor switches on and 13 °C when the compressor switches off. In heating mode, the set point temperature is 24.5 °C when the compressor switches on and 23.5 °C when the compressor switches off and the set point temperature inside the water storage tank was set as 38 °C when the compressor switches on and 28 °C when the compressor switches off.

In order to simplify the simulation process, the following assumptions were integrated in the simulation system.

- Underground water is not considered;
- The ground loop fluid is assumed to be a pur water without additional thermal fluid;
- The average ground surface temperature is about 23.5 °C;
- The day of minimum ground surface temperature is 32.

Table 4.1 The technical information of the main system components and TRNSYS types

TRNSYS type	Type description
Type 56	Multi zone building model with refreshing floor
Type 668	Reversible water-to water heat pump
Type 556	Simple horizontal ground heat exchanger
Type 4c	Thermal storage tank with an immersed heat exchanger
Type 3b	Single speed circulating pump
Type 14h	ON/OFF differential controller
Type501	Soil temperature profile
Type109-TMY2	Formatted file data reader
Type65c	Graphical plotter
Type25f	Printer with output file

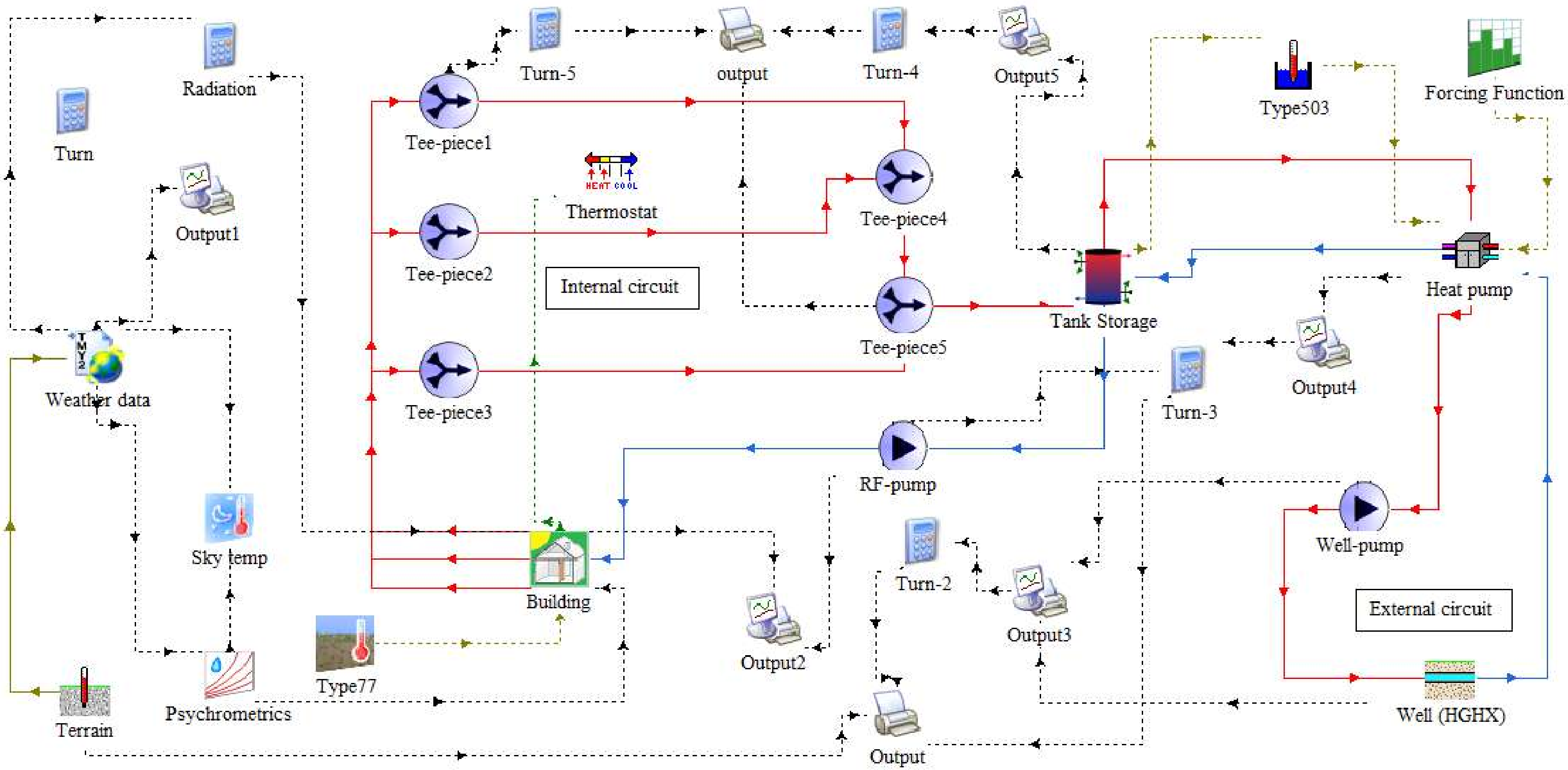

Fig 4.1 The TRNSYS model of HGSHP system in the cooling cycle

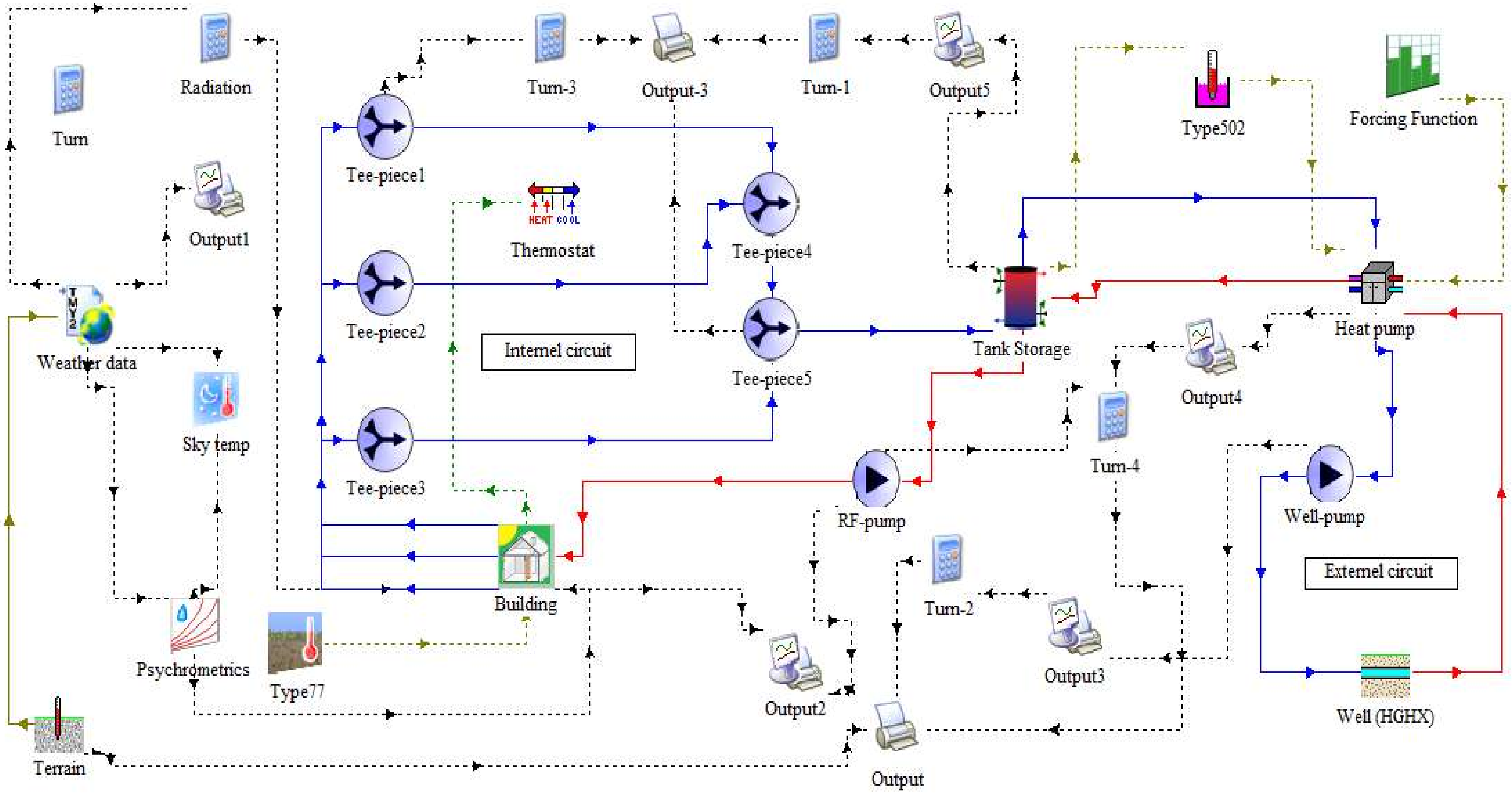

Fig 4.2 The TRNSYS model of HGSHP system in the heating cycle

4.2.1.1 Building thermal model description

A one-story residential house with a floor area of 95 m^2 and an internal height of 3 m was created in Room Arranger for the simulation performance analysis in the TRNSYS environment. The model of the building with northern orientation was divided into six thermal zones corresponding to the living requirements (three bedrooms, kitchen, living room and one toilet).

The following suggestions are also included in the house model and load characteristics topics:

- The walls made with 15 cm brick, 4 cm cement and 2 cm plaster, (see Fig 4.3a);
- The ground made with 1.5 cm floor ceramic, 6 cm concrete, active layer and 24 cm concrete, (see Fig 4.3b);
- The flat roof made with 20 cm heavy concrete block, 8 cm screed and 1 cm asphalt, (see Fig 4.3c);
- The house have eight double glazing windows with 2 m^2;
- The windows are primarily south-facing to block direct sunlight during the summer.

The properties of materials used in calculations of thermal simulation loads are given in Table 4.2.

Table 4.2 Materials properties

Layer	Conductivity (kj/h m k)	Capacity (kj/kg k)	Density (kg/m^3)
Cement	4.5	0.84	2000
Brick	3.2	1	1800
Plaster	5	1	2000
Floor	0.252	1	800
Concrete	7.56	0.8	2400
Asphalt	0.216	1.021	2100
Heavy concrete	6.12	0.84	2200

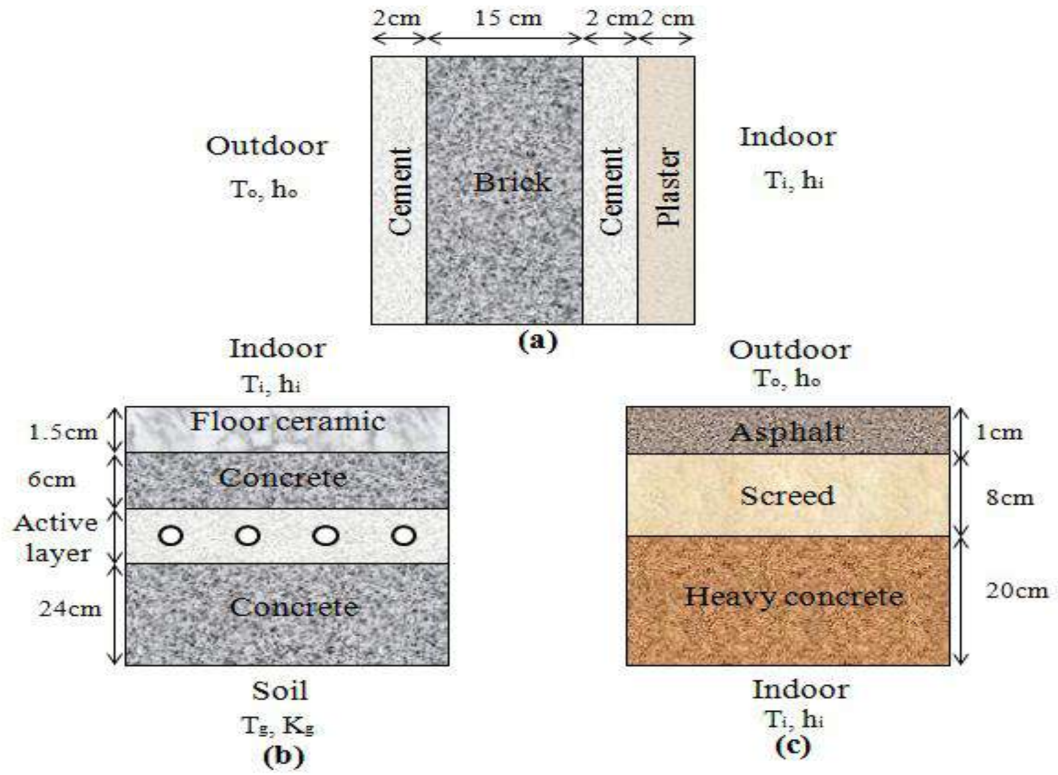

Fig 4.3 Typical building structures, (a) typical wall; (b) typical floor and (c) typical roof

The house model with all its technical specifications was imported into TRNSYS simulation model Type56. Fig 4.4 clearly shows the dimensions of the building thermal zones.

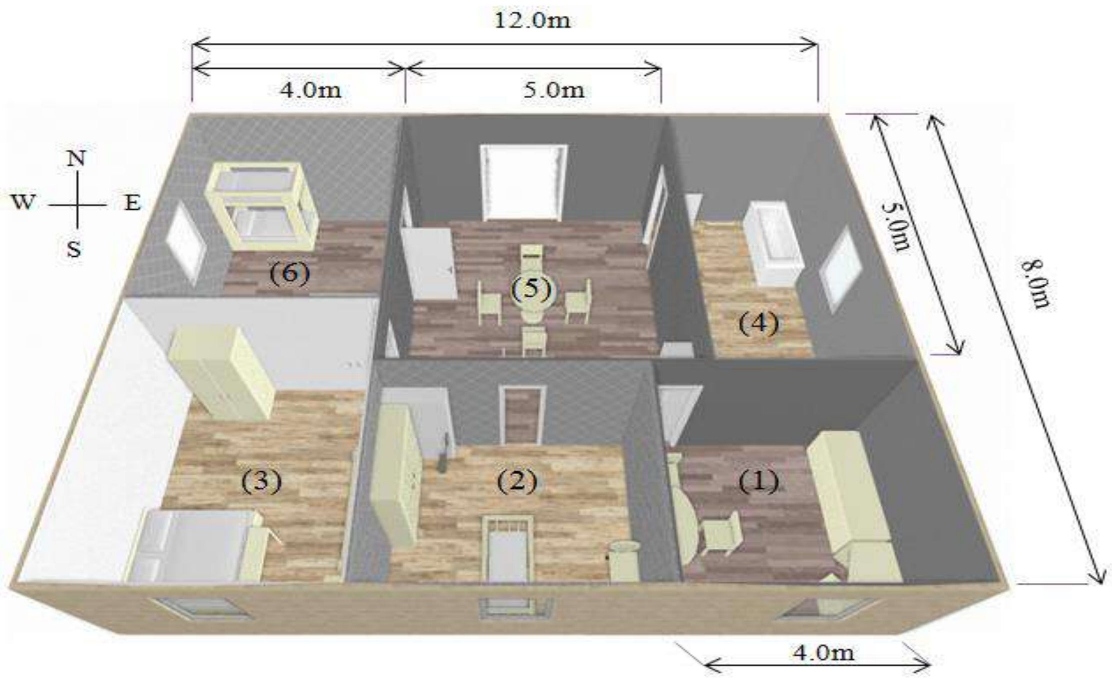

Fig 4.4 3D schematic view of the typical building (1): Zoon 1 (kitchen), (2), (3), (6): Zoon 2, 3, 6 (bedrooms), 4: Zoon 4 (bathroom) and (5): Zoon 5 (living room).

4.2.1.2 GHP description

In the proposed GSHPs under study, the TRNSYS mode, Type 668, which is based on the user-supplied data containing the heat pump parameters was used to simulate the water-to-water heat pump unit. The parameters of the water-to-water heat pump model were determined based on the product specification available from the manufacturers and based on the design load so that its nominal capacity is adequate for the thermal loads of the building. During the simulation, the cooling and heating capacity and power consumption of the heat pump unit can be obtained and controlled according to the specified parameters.

4.2.1.3 Storage tank

The reversible water to water heat pump is designed to satisfy the cooling demands of a large area, so to adapt it to our case study, we proposed a water storage tank (insulating tank) of 1 m^3 to increase the thermal inertia of the system. In the simulation environment, the storage tank was directly connected to the two inputs of the GHP unit and on the other hand linked through a small circulation pump to ensure the circulation of water in the RF system. The TRNSYS model Type4c was used to simulate the variable inlets storage tank of GSHP systems.

4.2.1.4 Radiant floor system

In the TRNSYS program, the TRNBuild model was equipped with a radiant floor system that provides cooling to the various zones, the circuit of the RF system consists of a multilayer (Cross-linked polyethylene) heat exchanger with 0.017 m of outside diameter and with a 0.02 m distance between the pipes. The heat exchangers are distributed throughout the ground floor to ensure a uniform internal temperature distribution.

4.2.1.5 Ground heat exchanger

For the horizontal ground heat exchanger, TRNSYS model Type 556 was used. This component model simulates the heat transfer process between the ground and a series of pipes which were designed according to the thermal loads of the building. This series is composed of straight ground heat exchanger installed horizontally at different depths in the ground. It consists of HDPE (high-density polyethylene, PE 100, type SDR11) pipe with different inner diameters where the circulating fluid (water) flows as a heat transfer fluid.

4.2.1.6 Forcing function model

A forcing function model was developed to control the heating and cooling operations of the water-to-water heat pump unit. In the simulation, the time intervals between the compressor on and off may not be proportional to those in the experiment. For this purpose, a TRNSYS component model Type14h was used to facilitate the process of controlling the timing function of the compressor so that it works within the time ranges specified based on the experimental data.

4.2.2 Weather data

In the TRNSYS program, the weather data is typical meteorological year (TMY). Therefore, the actual weather data that is presented in the next sections was collected from weather stations and converted to TMY2 data format by an actual meteorological data processor.

4.3 The operating conditions analysis

4.3.1 Regional factors

4.3.1.1 Geological background

As a future working project, the optimized HGSHPs is mainly proposed to meet the thermal comfort requirements of a house model under climatic conditions of Ouargla city, Algeria. The city of Ouargla is situated in north-eastern of the Algerian Sahara, it is located at 164 m altitude, 31° 57’ N latitude and 5° 21’ E longitude and covers a total area of about 163.233 km^2. The hydraulic drilling that crosses the Saharan territory indicates that this area is mainly covered with Tertiary and Quaternary materials [69], which are characterized by a sandy limestone majority in the surface layers of lithological classifications, as it is evident in the Fig 4.5.

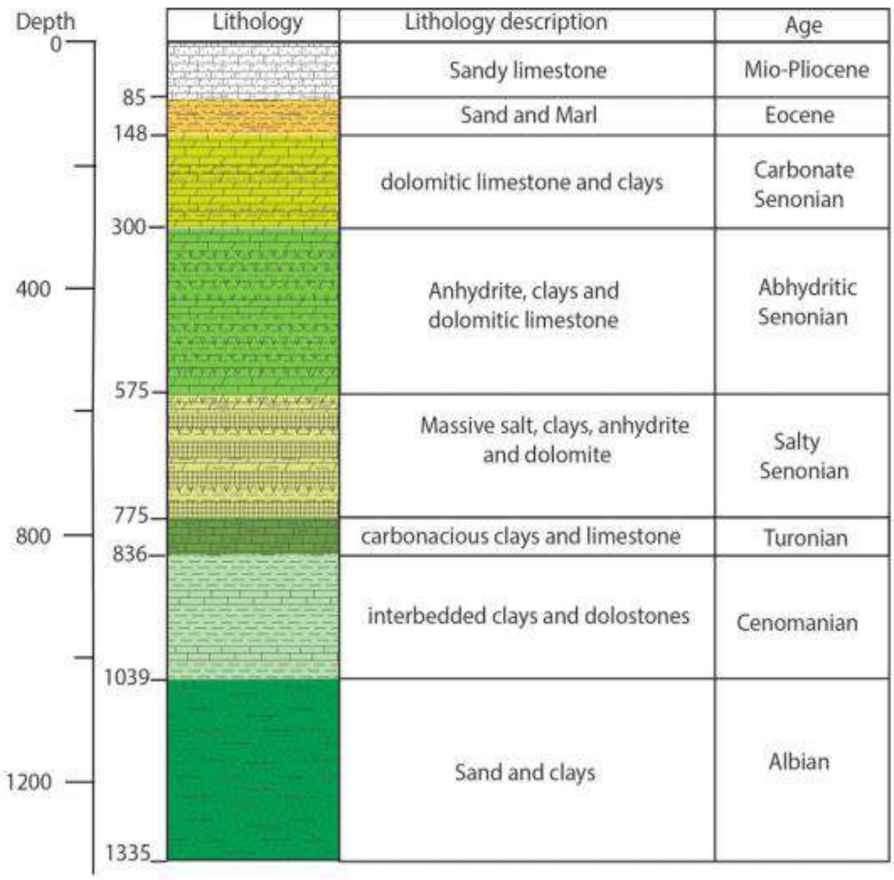

Fig 4.5 Stratigraphic log of Hdeb 1 drilling [69]

4.3.1.2 Actual meteorological data

As already mentioned in the previous sections, the meteorological factors are very important database to represent the most important physical phenomena related to the calculation of thermal loads, surface soil temperatures and to obtain the undisturbed soil temperature measurements in deeper formations. The average, minimum and maximum monthly variation of temperatures, including the average monthly variation of the wind speed and relative humidity measured with the meteorological weather station of Ouargla during the year 2019 were collected and displayed in Fig 4.6.

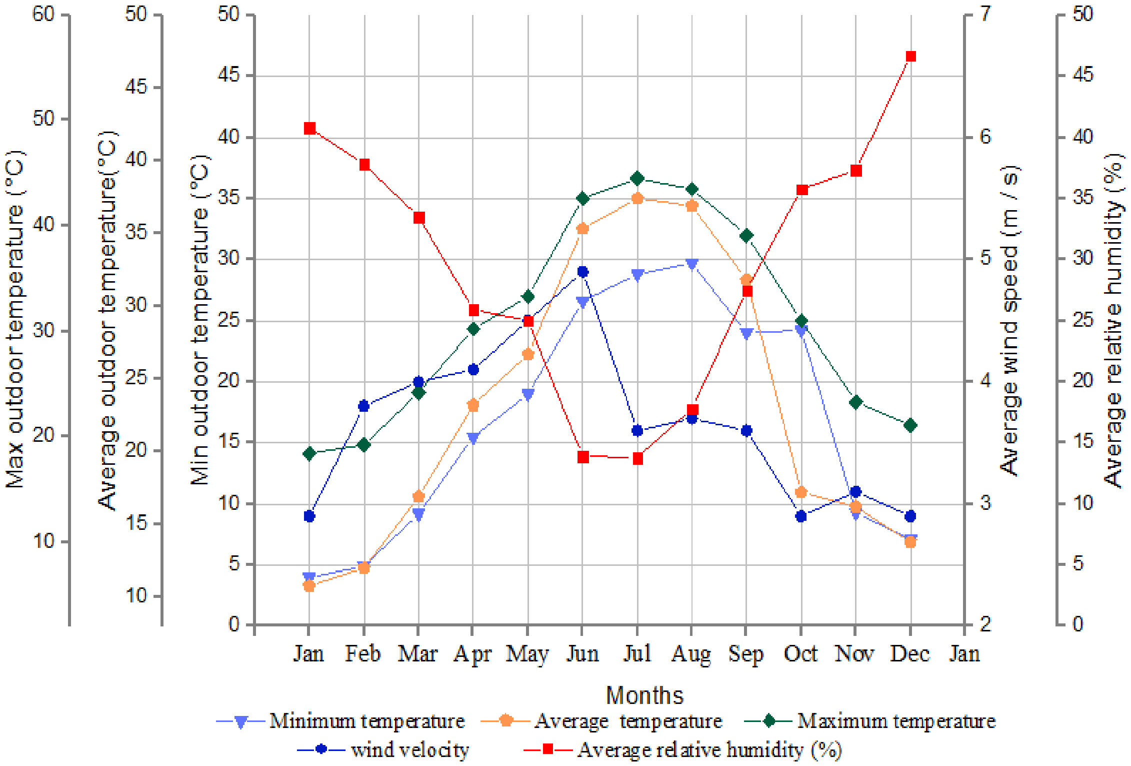

Fig 4.6 The min max average monthly variation of outdoor temperatures and the average monthly variation of relative humidity and wind speed in the year 2019

It is clear from Fig 4.6 that this region has a hot dry climate, which is characterised by a mild winters and a very hot-dry summers, indeed, the temperature can reach more than 45 °C in the summer season that lasts more than 5 months.

4.3.1.3 Soil thermophysical properties

The soil thermophysical properties, particularly the thermal conductivity, are essential for the assessment of the regional geothermal field in the implementation site and they play a major role in heat transfer efficiency between the ground and the GHXs. In this study, according to the previous data, the soil thermophysical properties were collected by taking into account the moisture contents. The soil thermal properties including thermal conductivity, specific heat and density for the soil at the surface layer of the most territories in Ouargla were tabulated in Table 4.3.

Table 4.3 Thermophysical properties of the soil.

Parameter	Values
Thermal conductivity of soil (W/m.K)	0.93
Specific heat of soil (J/kg.K)	1390
Density of soil (Kg/m^3)	1780

4.4.2 Annual energy consumption

In this work, the dailay load profile was categorized into four time periods for both heating and cooling as illustrated in Fig 4.8a and Fig. 4.8b, respectively, this categorization was mainly designed for ground recharge purposes by assuming that there is no cooling or heating demand during the transition periods. In order to calculate the annual thermal loads according to the thermal comfort standards [70], the cooling thermostat was set as 26 °C from 10:00 to18:00 and from 20:00 to 06:00 for all the spaces. The heating thermostat was set as 23,5 °C from 15:00 to 11:00. Fig 4.7 presents the simulation submodel built in TRNSYS, where the building thermal behaviour was modelled using Type 56.

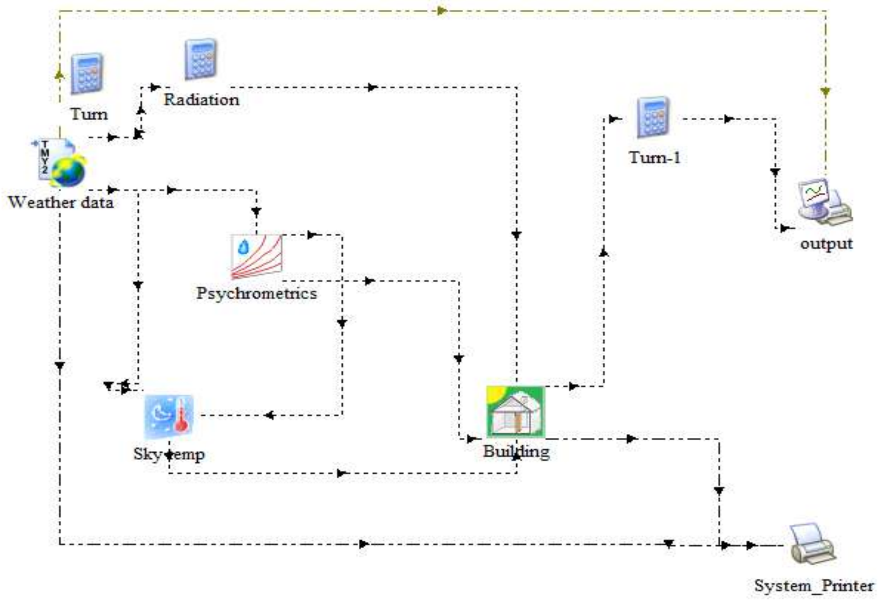

Fig 4.7 Scheme of the TRNSYS sub model used to simulate the thermal energy loads

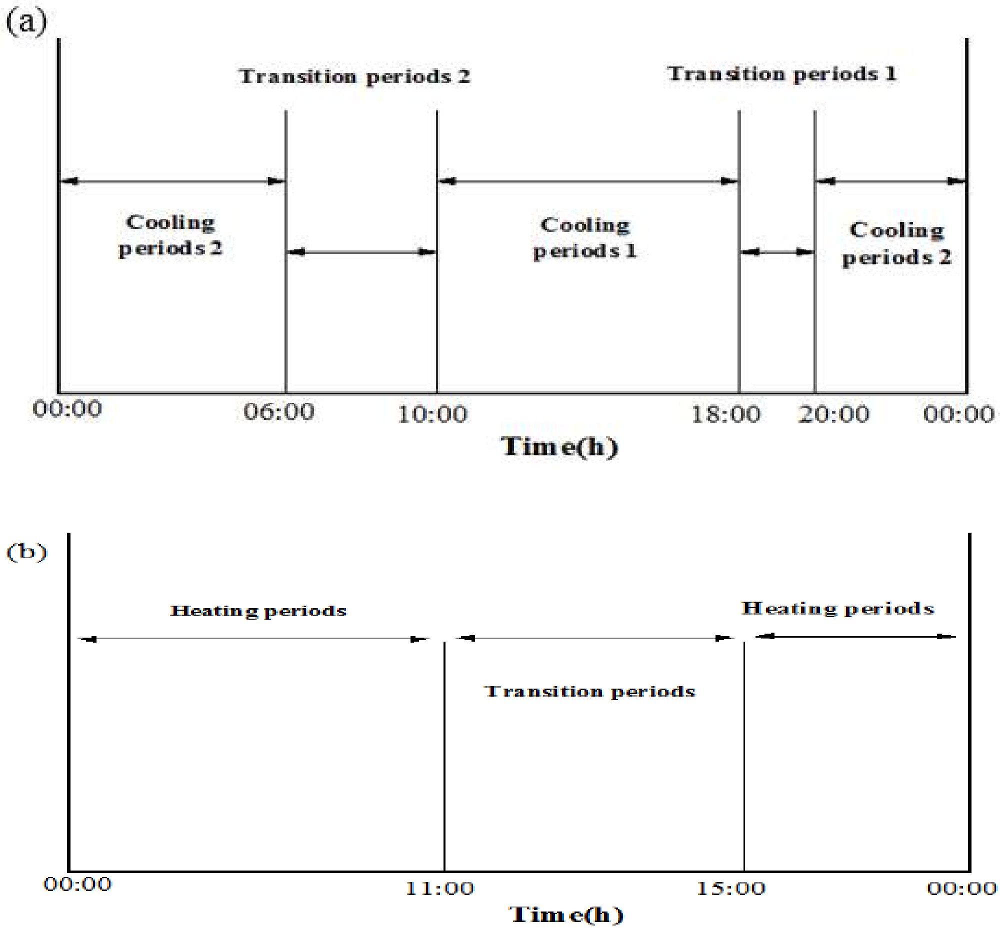

Fig 4.8 Daily cooling, heating and transition periods

Fig 4.9 shows the variation of the annual building thermal loads which were obtained using the TRNSYS simulation software based on the weather data of the south climate. According to the load simulation results, the heating period started from 1 November to 30 March and the cooling period started from 15 May to 31 October, the remaining periods were considered as transition periods. The heating loads of the building reaches the maximum in January with about 4.7 kW and the cooling loads exceed 7 kW in July.

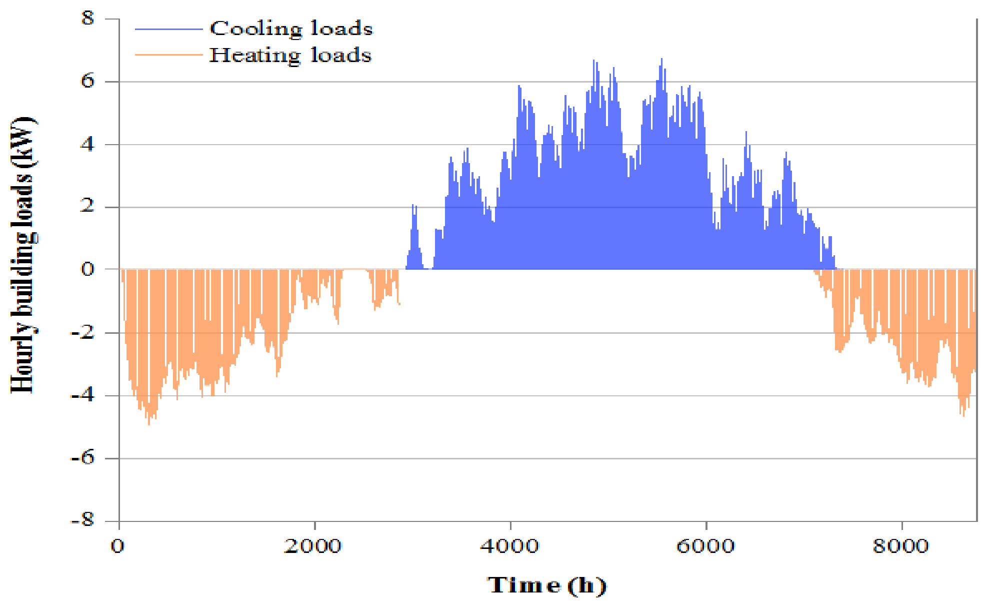

Fig 4.9 Hourly cooling and heating loads of the proposed building

4.3.3 Variation of the soil temperature

As mentioned previously, the design of geothermal heat exchangers strongly depends on the undisturbed soil temperature (i.e. the soil temperature before any heat injection or extraction). The undisturbed soil temperature strongly affects the soil resistance [50,51], which limits the heat exchange between the soil and the GHX wall [55], and thus affects the GSHP performance coefficient as well as the design parameters of the system.

The initial subsurface temperature distribution T_s can be computed as a function of the time of year and the depth below the ground surface as the following correlation [50]:

$$T_g = \overline{T_g} - A_s * \exp\left[-Z\left(\sqrt{\frac{\pi}{365*\alpha_g}}\right)\right] * cos\left[\frac{2\pi}{365}\left(t_{now} - t_{shift} - \frac{Z}{2} * \sqrt{\frac{365}{\pi*\alpha_g}}\right)\right] \qquad (4.1)$$

Where:

$\overline{T_g}$: is the mean value of the ground surface temperature for a location of Ouargla city over an entire year, °C;

A_s: is the amplitude that the surface temperature experiences throughout a year at the location;

t_{shift}: is the difference in time between the beginning of the year and the occurrence of the minimum surface temperature.

Fig 4.10 shows the undisturbed soil temperature profiles over a year for the given climate. It can be observed that the amplitude of the soil temperature signal decreases as the depth increases. In the upper 3 m, where soil temperature is affected by the external factors of climatic conditions, the soil has a big thermal slope. In deeper distances that correspond to the thermally stable zone, the soil mean temperature is almost constant.

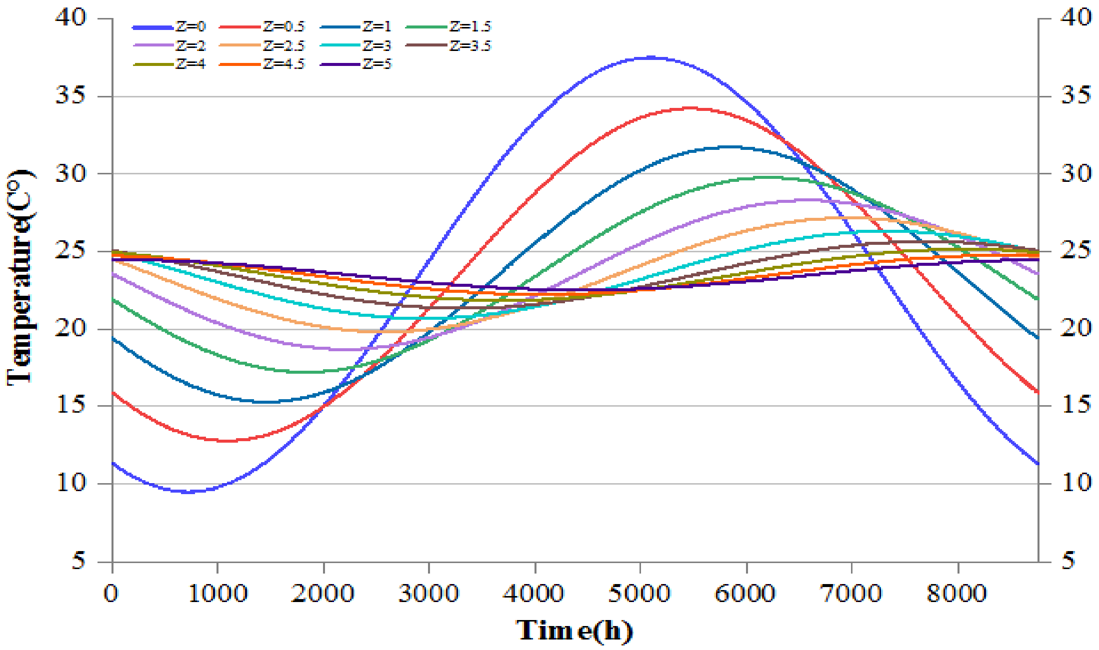

Fig 4.10 Variations of soil temperature with depth (m), Ouargla city

4.5 Conclusion

In this chapter, the development of the TRNSYS dynamic simulation model that has been used to evaluate the performance of the horizontal ground source heat pump system was presented. The operating conditions were also analyzed and the annual energy consumption as well as the variation of soil temperature were assessed by using TRNSYS software.

CHAPTER 5

EXPERIMENTAL VERIFICATION OF THE HORIZONTAL GROUND SOURCE HEAT PUMP SYSTEM MODEL

5.1 Introduction

The validation of the dynamic simulation models of the ground source heat pump and ground heat exchangers is requisite befor the pre-design process. This chapter describes the design and implementation of the horizontal ground source heat pump system of the CRTEn projet and presentes its experimental data used to validate the developed models used in this study. This chapter is organised as follows. The design and installation of the ground source heat pump system of the CRTEn projet are presented in Section 5.2. Section 5.3 provides the uncertainty analysis in the experimental tests. Then, the validation of the dynamic simulation model of the entire GSHPs was performed in section 5.4.

5.2 CRTEn ground source heat pump projet

5.2.1 System location

The horizontal ground source heat pump experimental system is installed in a test office at the Laboratory of Thermal Processes (LPT) of the Research Center and Technologies of Energy (CRTEn), Borj-Cédria. The city of Borj-Cédria is situated in the northern Tunisia in the middle of North Africa's Mediterranean coast, it is located at 36° N latitude and 10° E longitude. The CRTEn location is shown in Fig 5.1.

Fig 5.1 Location of the CRTEn (from [71])

1.2.1 System description

A schematic view of the studied system is shown in fig 5.2. The system consists mainly of three loops: the building loop (RFs), the refrigerant loop (vapor-compression cycle) and the ground loop (GHXs).

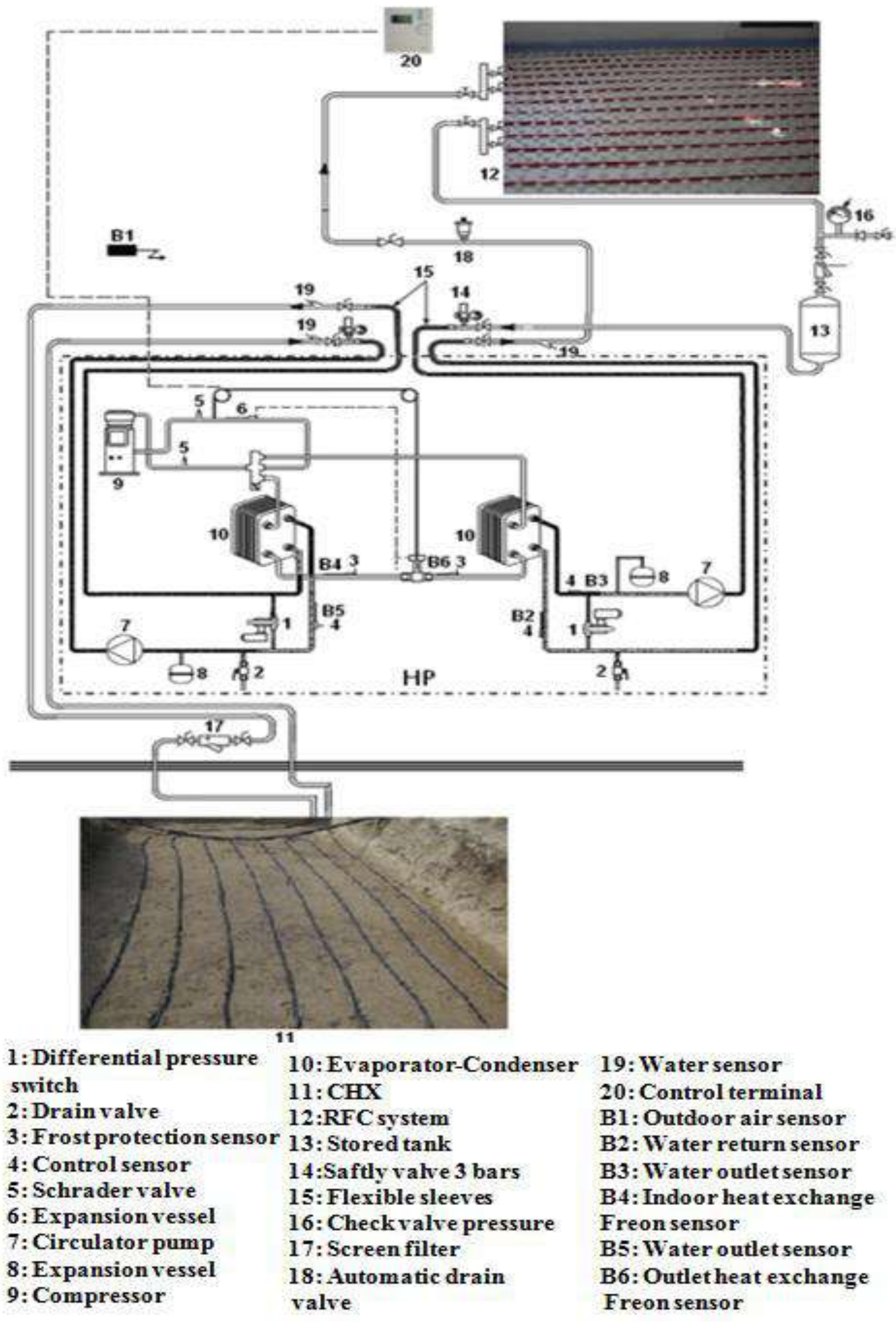

Fig 5.2 Schematic diagram of the HGSHP experimental system (modified from [72])

5.2.2.1 Description of the test building

The test building is a north facing office room located at the test rig of the Laboratory of Thermal Processes (LPT) in the CRTEn (see Fig 5.3). It had a floor area of 12 m^2 (3 m × 4 m) and an internal height of about 3 m. The building structure had two external walls made with a double pane of 15 cm hollow bricks and 3 cm plaster on each side and a layer of 5 cm air insulation in between. The test office room had also a south facing window with 3 m^2. The roof is flat and made with 20 cm heavy concrete block, 8 cm screed and 1 cm asphalt.

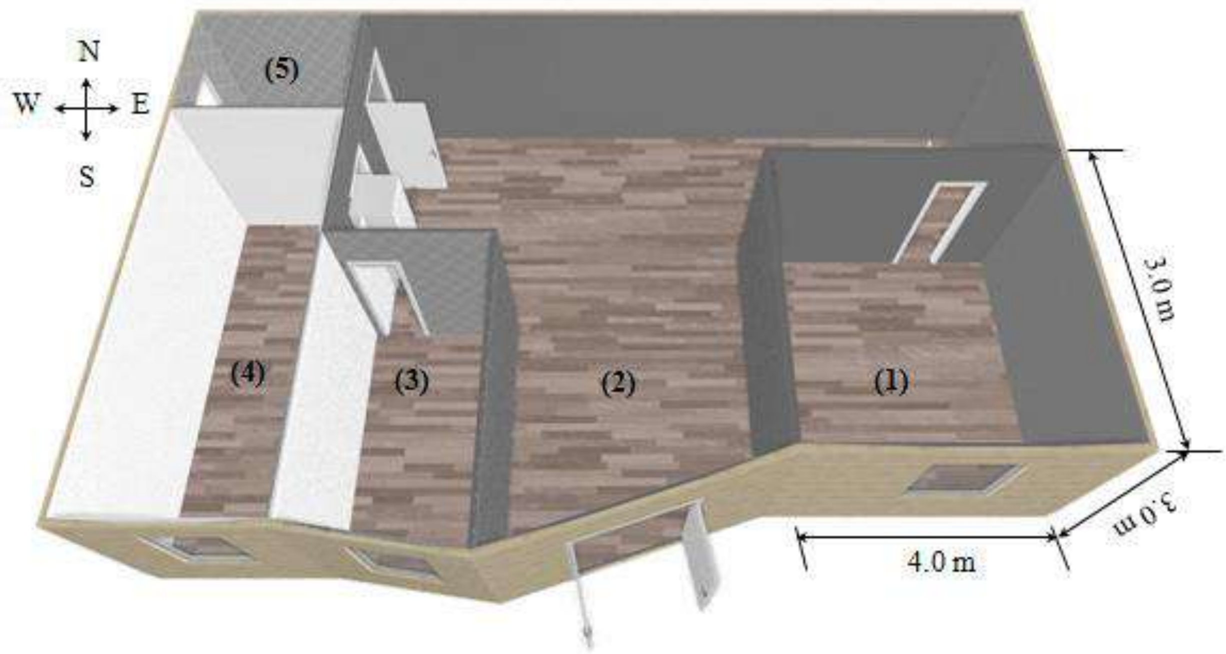

Fig 5.3 3D plan of the measurements side of thermal processes laboratory (1): Test room, (2): test rig, (3) and (4): Office and (5): bathroom

5.2.2.2 Description of the radiant floor

The test building is equipped with a radiant floor system consists of a multilayer heat exchanger installed with homogeneous distribution in the whole floor of the test room (Fig 5.4). The technical properties of the RF heat exchanger are shown in Table 5.1.

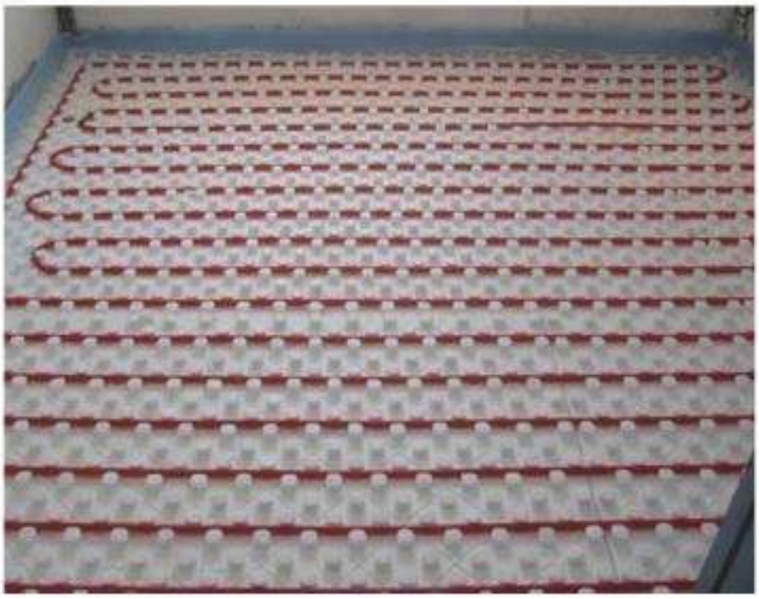

Fig 5.4 The radiant floor system [73]

Table 5.1 Technical Specification of the multilayer heat exchanger.

Parameter	Specification	Unit
Diameter	0 .016	m
Thickness	0.0055	m
The distance between the pipes	0.02	m
Tube spacing	0.015	m
Conductivity	0.4	(W m^{-1} K^{-1})
Maximum operating temperature	95	° C
Minimum operating temperature	- 40	° C
Continuous pressure at 70	10	Bars
Burst pressure	80	Bars
Tube roughness	0.0004	mm

The outlet and the inlet of the RF installation are connected to a hydraulic collector (7 in Fig 5.5). The collector is made up of a supply manifold which has a supply line coming from the storage tank and secondary lines exiting from the manifold towards the radiant floor system, a return manifold which has a secondary lines coming to the manifold from the radiant floor system and a single return line exiting from the manifold towards the storage tank, a flow meter (adjustment from 0.5 to 5 l/min) integrated into the supply manifold, two manual taps and two draining taps of 1/2-inch.

Fig 5.5 Tube collector

5.2.2.3 Description of The heat pump unit

The geothermal heat pump unit that provides the air conditioning for the test building is a reversible water-to-water, manufactured by Ageo CIAT (Fig 5.6). It is fitted with scroll compressor, brazed plate heat exchangers, built-in double hydraulic modules and complete electronic controls. The GHP is equipped with two circulating pumps to circulate water in the internal and external circuits (see Fig 5.7). The technical properties of GHP unit are shown in Table 5.2.

Fig 5.6 The heat pump unit.

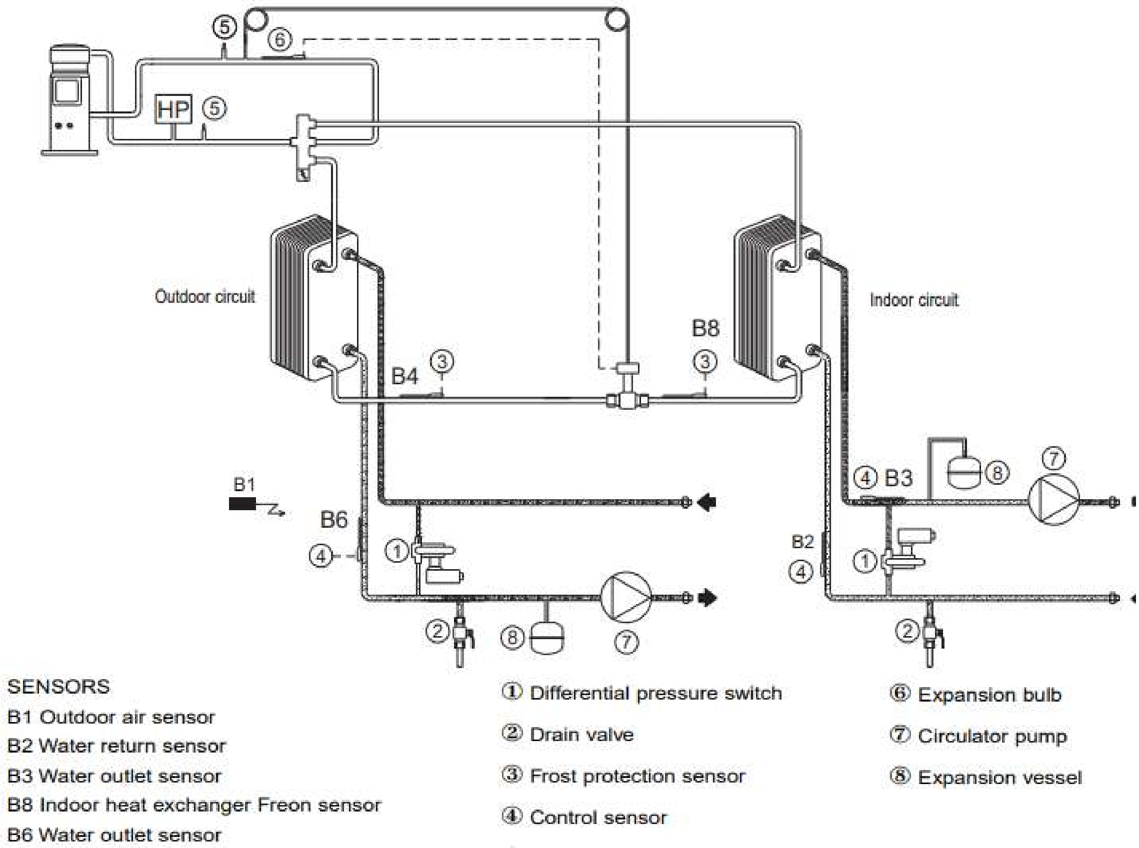

Fig 5.7 Schematic diagram of the CIAT water-to-water heat pump

Table 5.2 Technical Specification of the reversible water to water heat pump

Parameter	Specification	Unit
Type	AGEO 50 HT	
Refrigerant	R410A	
Heating capacity	16.1	KW
Inlet / outlet temperature	40.0 /45.0	°C
Flow rate	1-2.77	m^3/h
Cooling capacity	12.2	KW
Inlet / outlet temperature	12.0 /7.0	°C
Flow rate	1-2.1	m^3/h

5.2.2.4 Storage tank

A water tank of 0.1 m^3 was integrated between the heat pump unit and the radiator panel to increase the thermal inertia of the system. A view of the insulating tank was shown in Fig-5.8.

Fig 5.8 Insulating tank

5.2.2.5 Description of The GHX system

The geothermal filed is a horizontal ground heat exchanger (Fig 5.9) consists of a high-density polyethylene (PEHD) tube installed in 1 m of depth in the ground. Their technical properties are regrouped in Table 5.3.

Fig 5.9 The horizontal GHX [74]

Table 5.3 Technical Specification of the ground heat exchanger

Parameter	Specification	Unit
Pipe material	High density polyethylene	
Diameter	0.025	m
Thickness	0.0023	m
Length	100	m
Tube spacing	0.5	m
Conductivity at 23 °C	0.48	$(W\ m^{-1}\ K^{-1})$
Density at 23 ° C	0.945 to 0.955	g/cm^3
Coefficient of linear expansion	0.2	mm/mk

5.2.2.6 Description of the buried tank

According to the GSHP usage standards, the normal operation of the external circuit requires a water mass flow rate of around 0.58 kg/s and a minimum water volume of about 214 L. For this purpose, a storage tank of about 200 L was integrated into the external circuit to supply the needed water for the ground heat exchanger. The buried tank was installed horizontally at 1 m of depth under the ground surface (see Fig 5.10).

Fig 5.10 buried tank [73]

5.2.3 Data acquisition system

During the test procedures all the measurement sensors were connected to a multichannel digital Agilent type HP, which was linked to a Microsoft software program that stock the results every 1 min during 3 days to record any unexpected thermal behavior for the entire system (Fig 5.11).

Fig 5.11 The measurement system

5.2.3.1 Measuring instruments

5.2.3.1.1 Thermocouples type K

A K-type thermocouples (accuracy ±1 °C) (Fig 5.12) were used to measure the ambient temperature and the temperatures indoors at different levels in the center of the test office. The technical characteristics of the K-type thermocouples are presented in table 5.4.

Fig 5.12 K-type thermocouple [73]

Table 5.4 Technical specification of the K-type thermocouple

Parameter	Value	Unit
Conversion coefficient	40	µV/°C
Temperature range	200e 1370	°C
Accuracy	±1	°C

5.2.3.1.2 PT500 temperature sensor

The temperature measurements of the water at the inlet and the outlet of GHX are performed using two wires PT500 resistance thermometer sensors (accuracy ±5.71%) (Fig 5.13). The technical specification of PT500 thermometer sensors are presented in table 5.5.

Fig 5.13 PT500 temperature sensor [73]

Table 5.5 Technical characteristics of PT500 thermometer sensors.

Parameter	Value	Unit
Length of sensor	45	mm
Immersion depth with direct mounting	27.5	mm
Temperature range	0e 150	°C

5.3 Uncertainty analysis

Instrument conditions and calibration, reading errors and others can lead to a number of experimental uncertainties. Therefore, the uncertainty analysis is important to provide the accuracy of the experiment. In this experimental tests, an uncertainty analysis was performed for both measured and calculated parameters. According to Holman [75], The uncertainties of the measured parameters and calculated parameters (R) which depending on x_1, x_2, x_3........, x_n can be estimated from the Eq 5.1.

$$W_R = \left[\left(\frac{\partial R}{\partial X_1} W_1 \right)^2 + \left(\frac{\partial R}{\partial X_2} W_2 \right)^2 + \left(\frac{\partial R}{\partial X_3} W_3 \right)^2 + \cdots + \left(\frac{\partial R}{\partial X_n} W_n \right)^2 \right]^{1/2} \tag{5.1}$$

Where w_1, w_2, w_3,...,w_n, are the uncertainties in the independent measured variables. Illustrative examples of calculating uncertainty in a measured and computed result are shown in Appendix G.

The total uncertainties in the inlet and outlet water temperatures of the ground heat exchanger were estimated to be 5.71% and 5.14% , respectively. The total uncertainty in the calculated heat exchange rate at the external circuit of the GSHPs is about 11.75%, whereas the total uncertainty in the calculated heat exchange rate at the internal circuit was around 5.19%. For the COP of the water-to-water heat pump, the uncertainty was found to be 0.54%. The total uncertainties for other measured parameters were summarized in Table 5.6.

Table 5.6 Total uncertainties for measured parameters

Items	Unit	Total uncertainty (%)
RF outlet emperature	°C	±2.00
RF intlet emperature	°C	±1.71
Outdoor temperature	°C	±3.89
Indoor temperature	°C	±3.48
Ground temperature	°C	±3.57
GHX circulating water mass flow rate	kg/s	±0.14
RF circulating water mass flow rate	kg/s	±0.14
Compressor power input	kW	±0.50
Circulating pumps power input	W	±0.50

5.4 Model validation

This section presents the validation of the TRNSYS model against experimental measurements of one of the three heat exchangers of the CRTEn ground source heat pump project. In order to test the reliability of the simulation model that we have developed, all the technical characteristics of the experimental device as well as the climate teste building have been integrated into the developed TRNSYS types. The following assumptions have been made:

- The model has been validated with the consideration of the experimental measurements of mass flow, pipe length, pipe diameter, burial depth as inputs for the HGHX type.
- The number of horizontal nodes has been increased in order to increase the accuracy at the expense of simulation time.
- Average value of function (time interval) was imposed by the library (TESS) controller to correctly reproduces the evolution of the on/off cycle of the heat pump unit over the simulation periods.
- In order to ensure good accuracy in predicting the response of the drill, the thermophysical properties of the soil and the backfill material around the horizontal buried pipes were precisely determined before being integrated in the HGHX type.

As the case of heating has similar validation results (i.e. trends) as that of the cooling case, only the results of cooling model validation are presented in this section. The validation results will mainly aim to evaluating the ability of the model to qualitatively represent the observed physical phenomena in pilot plan experimentation. The experimental measurements has been compared against the simulated inlet and outlet fluid temperature of the GHX, the heat exchange rate to ground and the coefficient of performance. Fig. 5.14 and Fig. 5.15 reports the comparisons between the experimental measurements and simulation results in terms of the heat exchange rate to ground and the COP of the GSHP in the cooling mode operation. We can observe from this illustration that the maximum error between the simulated and the measured COP does not exceed ±4.9% and the maximum error between the simulated and the measured heat exchange is about ±10%.

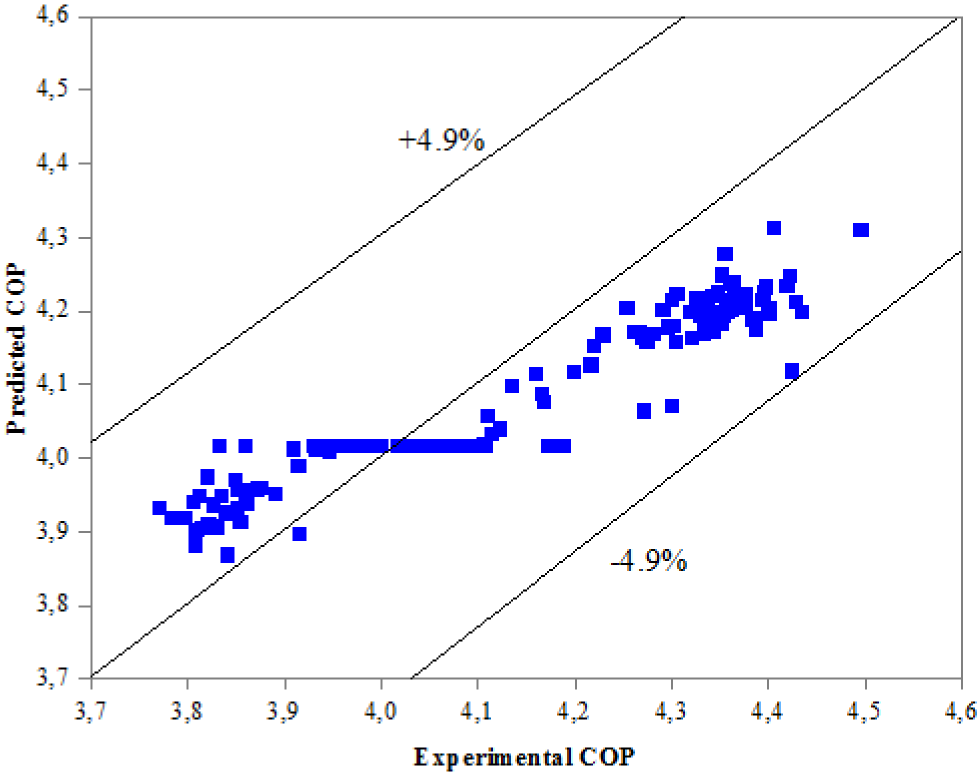

Fig 5.14 Experimental vs numerical coefficient of performance of the GSHP, cooling mode

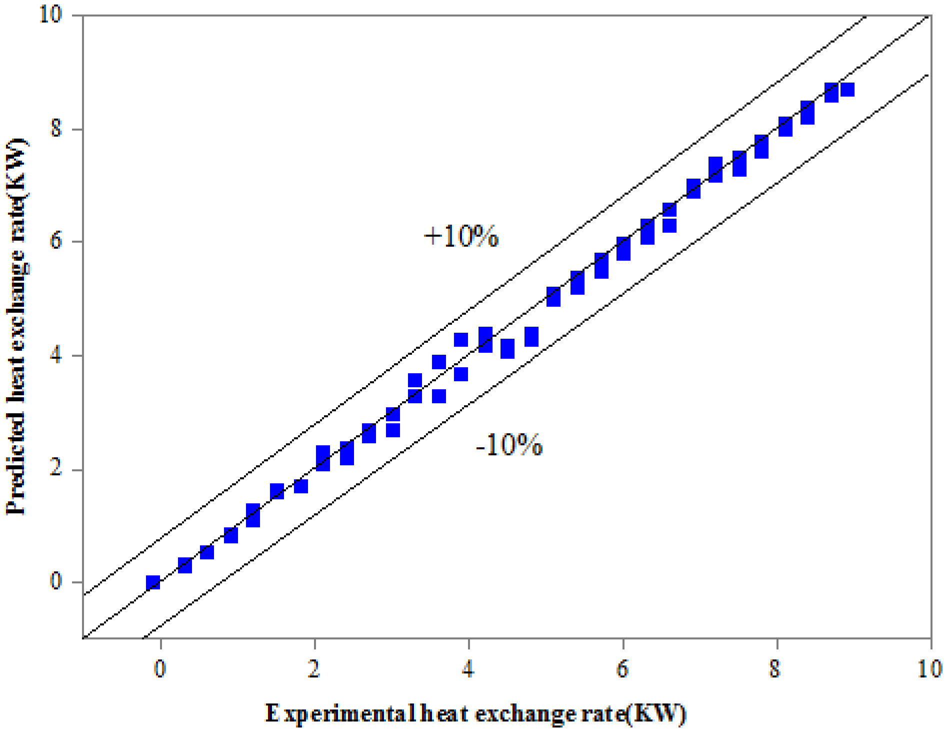

Fig. 5.15 Experimental vs numerical heat exchange rate to the ground, cooling mode

Fig 5.16 illustrates the comparisons between the measured and the simulated indoor temperatures of the test building. It can be seen that the simulation model can provide acceptable estimates. The relative errors between the simulated and measured indoor temperatures were within the range of ±4.16%, the same for the outlet and inlet water temperature of the GHX and the heat exchange rate from the building, the maximum relative-error does not exceed ±1.4C%, ±2.3C% and ±0.5%, respectively.

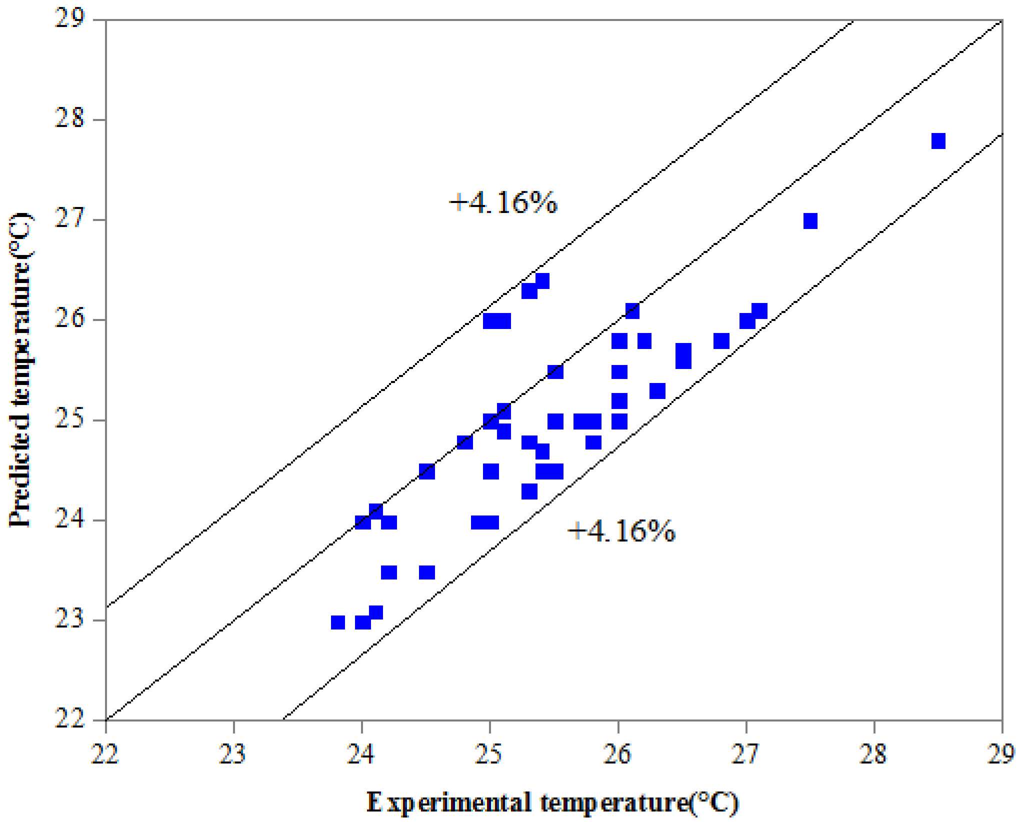

Fig. 5.16 Experimental vs numerical indoor temperature, cooling mode

5.5 Conclusion

In this chapter, the TRNSYS model of the simulated system was evaluated through a detailed experimental data. The investigations were based on the HGSHP system implemented in the Research and Technology Center of Energy (CRTEn), Tunisia. The working conditions including the building specifications, the GHX parameters, the soil properties, the climate conditions and others were used as inputs in the TRNSYS simulation.

Based on the typical working conditions, the analyses showed that the simulation results agreed well with the expremental measurements with a maximum accuracy of about ±10% was found in prediction of the heat exchange rate to the ground, which mean that the detailed TRNSYS simulations is able to reproduce the thermal behavior of the HGSHP with a high accuracy. Therefore, it can be concluded that by means of the GSHP model developed in TRNSYS environment, the GHP system and the drill outputs can be pre-investigated individually based on meteorological and geological databases which can further facilitate the good design and control of the GSHP systems.

CHAPTER 6

FEASIBILITY ANALYSIS OF HORIZONTAL GROUND SOURCE HEAT PUMP SYSTEMS FOR SAHARAN CLIMATE

6.1 Introduction

This chapter presents an energy performance and economic feasibility studies of horizontal ground source heat pump system for Saharan climate and more particully for the southest of Algerienne sahara. The main aim of this chapter is to quantify the extent to which the local climate affects the energy performance and the economic feasibility of implementing HGSHP systems.

This chapter is organised as follows. The results of energy and economic feasibility analysis are presented in Section 6.2. A brief summary of the key findings is provided in Section 6.3.

6.2 Effects of design parameters on the performance of GSHPs

The performance of a GSHPs depends on a range of design parameters such as length, diameter and burial depth of the ground heat exchanger, and operating parameters such as mass flow rate, thermal loads, temperature settings and operation schedules. Based on the TRNSYS model presented and validated in the last chapters and with the aid of MATLAB code, a parametric study was performed in order to investigate the effects of the different design parameters of the GHX on the energy performance of GSHPs, as well as to evaluate the influence of the working conditions on the overall cost of the system.

The optimal design of the GSHPs was obtained by considering the long time operating costs and the first investment costs simultaneously under technical and economic conditions. Thus, the effect of the GHX design parameters on both the objective function and the performance of GSHP were investigated for ten years of cooling and heating periods in different cases as summarized in the Table 6.1. The system operating conditions and the constant economical factors were collected in Table 6.2.

Table 6.1 Design parameters of all cases

Cases	L_{GHX} (m)		D_{i-GHX} (m)		Z (m)		$\dot{m}_{w-GHX}$ (Kg/s)	
	Cooling	Heating	Cooling	Heating	Cooling	Heating	Cooling	Heating
Case 1	200	200	0.029	0.029	1	1	0.5	0.5
Case 2	300	300						
Case 3	400	400						
Case 4	500	500						
Case 5	600	600						
Case 6	700	700						
Case 7	800	800						
Case 8	900	900						
Case 9	1000	1000						
Case 10	500	300	0.018	0.018				
Case 11			0.0227	0.0227				
Case 12			0.029	0.029				
Case 13			0.0363	0.0363				
Case 14			0.0363	0.0227	0.5	0.5		
Case 15					1	1		
Case 16					1.5	1.5		
Case 17					2	2		
Case 18					2.5	2.5		
Case 19					3	3		
Case 20					1	0.5	0.25	0.25
Case 21							0.5	0.5
Case 22							0.75	0.75
Case 23							1	1
Case 24							1.25	/
Case 25							1.5	/
Case 26							1.75	/
Case 27							2	/

Table 6.2 The list of input parameters used in economic analysis

T_c = *720 (h/y)*	a_1 = *6* $(\$/m^2)$
τ_c = *4320(h/y)*	a_4 = *308,9*
T_h = *540 (h/y)*	$a_5 = 0.25$ *f*or pump power of 0.02–0.3 kW
τ_h = *3240(h/y)*	$a_5 = 0.45$ *f*or pump power of 0.3–20 kW
n = *10 (y)*	$a_5 = 0.84$ *f*or pump power of 20–200 kW
i = *10%*	$E_{traiff} = 0.014\$$ *for power consumption of 0-125 (KWh)*
η_{pump} = *80%*	$E_{traiff} = 0.034\ \$$ *for power consumption over 125 (KWh)*
e =10 %	$CRF = 0.1627$

6.2.1 Energy-economic performance of GSHPs

6.2.1.1 Effect of the pipe length

In this section, the effect of pipe length on the energy and economic performance of the HGSHPs is investigated by assuming constant mass flow rate, pipe diameter and burial pipe depth (Cases 1-9). The total annual power consumption from compressor and circulating pump as well as the total electricity costs for the first year and ten year of operation for different pipe lengths were collected in Table 6.3. The change in the trench, circulating pump, GHP unit costs as well as the total investment costs are shown in Table 6.4. For both heating and cooling, the coefficient of performance of the GSHP and the objective function values are shown in Fig. 6.1 (left) and (right), respectively.

Table 6.3 Annual power consumption and electricity costs vs different pipe lengths

Pipe length	Annual power consumption (kWh/y)				Cost of power consumption ($)			
	Compressor power consumption		Circulating pump power consumption		First year operation		Ten years operation	
	Heating	Cooling	Heating	Cooling	Heating	Cooling	Heating	Cooling
200	2987.55	3371.4	1365.95	1571.33	146.07	166.52	2328.07	2653.91
300	3091.5	3371.4	1759.71	2087.47	163.34	184.42	2603.3	2939.33
400	3091.5	3355.2	2262.27	2716.91	180.78	205.7	2881.21	3278.45
500	3222.45	3259.8	2740.64	3320.23	201.92	223.33	3218.16	3559.33
600	3252.15	3142.8	3236.85	3942.14	220.17	240.85	3508.98	3838.53
700	3262.1	3094.2	3733.54	4562.12	237.4	260.67	3783.65	4154.51
800	3268.35	3031.2	4226.41	5174.35	255.07	279.73	4065.16	4458.22
900	3296.7	2930.4	4713.01	5791.3	272.93	297.64	4349.93	4743.65
1000	3306.15	2849.4	5203.51	6418.89	290.28	316.6	4626.4	5045.91

Table 6.4 The investment costs vs different pipe lengths

Pipe length	The investment costs ($)							
	Cost of trench		Cost of circulating pump		Cost of GHP unit		Total investment cost	
	Heating	Cooling	Heating	Cooling	Heating	Cooling	Heating	Cooling
200	958	958	248.91	195.96	1926	1926	3132.91	3079.96
300	1437	1437	234.7	222.68	1926	1926	3597.7	3585.68
400	1916	1916	262.8	250.72	1926	1926	4104.8	4092.72
500	2395	2395	286.49	274.4	1926	1926	4607.49	4595.4
600	2874	2874	308.76	296.44	1926	1198	5108.76	4368.44
700	3353	3353	329.25	316.57	1926	1229	5608.25	4898.57
800	3832	3832	348.14	335.03	1926	1229	6106.14	5396.03
900	4311	4311	365.64	352.45	1926	1229	6602.64	5892.45
1000	4790	4790	382.3	369.15	1926	1229	7098.3	6388.15

In cooling mode, as expected, the results demonstrates that an increase in pipe length leads to an increase in the $\mathrm{COP}_c$of the heat pump and the first investment cost. In the initial stage, the electric power consumption of the compressor decreases with the increase of pipe length, which reduces the objective function until getting a minimum point at 500 m of pipe length (Case 4, optimal point). After this stage, the system investment caused by increased heat exchanger area as well as the excavation works exceeds the decrease of operating cost which explain the increase in the objective function with higher pipe lengths.

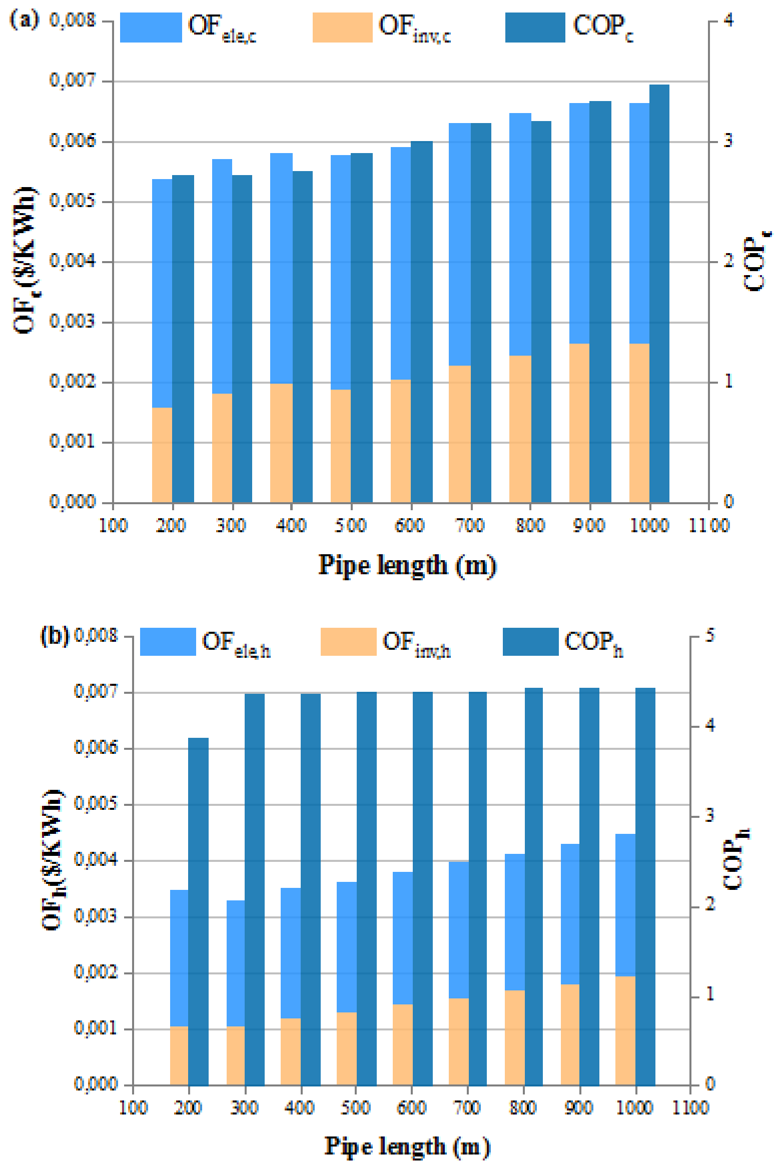

Fig 6.1 Effect of HGHX length on the objective function and the COP of the GHP, (a) cooling mode and (b) heating mode

For heating mode, the coefficient of performance, the electric power consumption and the first investment costs increase with the increase of heat exchanger length. Based on Eq- (3.32) and (3.33) (Chapter 3) and considering the fact that $C_{inv,h}$ *and* $C_{elec,h}$ increase with GHX length, the variation of objective function with length depends on the increment magnitude of $Q_{b,h}$ and the sum of $C_{inv,h}$ and $C_{elec,h}$. Referring to cases 2, the increment magnitude of $Q_{b,h}$ is greater in this piont (optimal length), and thus, the value of OF_h has decreased.

6.2.1.2 Effect of the pipe diameter

The variations of the objective function and the performance coefficient of the GSHP system as function of pipe diameter in constant mass flow rate, burial depth and pipe length (Cases 10-13) for both heating and cooling modes are shown in Fig 6.2. Results illustrate that the objective function and the COP of the GSHP were directly affected by pipe diameter values. In cooling mode, the electric power consumption of the compressor and the well pump decreases with the increase of the pipe diameter (see Table 6.5), indicating a degradation in the objective function of about 63.16% from 0.02 m to 0.04 m of outer pipe diameter

Table 6.5 Annual power consumption and electricity costs vs different pipe diameters

Pipe diameter	Annual power consumption (kWh/y)				Cost of power consumption ($)			
	Compressor power consumption		Circulating pump power consumption		First year operation		Ten years operation	
	Heating	Cooling	Heating	Cooling	Heating	Cooling	Heating	Cooling
0.02	2430	3371.4	16800.05	31170.7	662.25	1193.55	10554.7	19022.19
0.025	3056.4	3371.4	5145.13	9879.76	279.59	454.8	4456	7248.42
0.032	3087.45	3259.8	1757.57	3321.86	163.13	223.38	2599.87	3560.23
0.04	3121.2	3020.4	760.22	1344.17	129.69	146.45	2067.01	2334.19

Table 6.6 The investment costs vs different pipe diameters

Pipe diameter	The investment costs ($)							
	Cost of trench		Cost of circulating pump		Cost of GHP unit		The total investment cost	
	Heating	Cooling	Heating	Cooling	Heating	Cooling	Heating	Cooling
0.02	1143	1905	647.83	751.69	1129	1926	2919.83	4582.69
0.025	1251	2085	380.37	448.21	1926	1926	3557.37	4459.21
0.032	1437	2395	234.58	274.46	1926	1926	3597.58	4595.46
0.04	1698	2830	214.99	182.66	1926	1229	3838.99	4241.66

For heating mode, although there is a slight increase in the electric power consumption from the compressor with increasing the pipe diametre (see Table 6.5.), the significantly decrease in the circulating pump power consumption is far exceed this increased amount of power consumption which decreases the objective function by 66.53% from 0.02 m to 0.04 m of outer pipe diameter. Referring to Fig 6.2b, the coefficient of performance of the GHP unit was decreased with pipe diameter more than 0.0363 m (optimal pipe diameter) which can be explained by the considerable decrease in the velocity of the fluid that caused by the increased pipe surface.

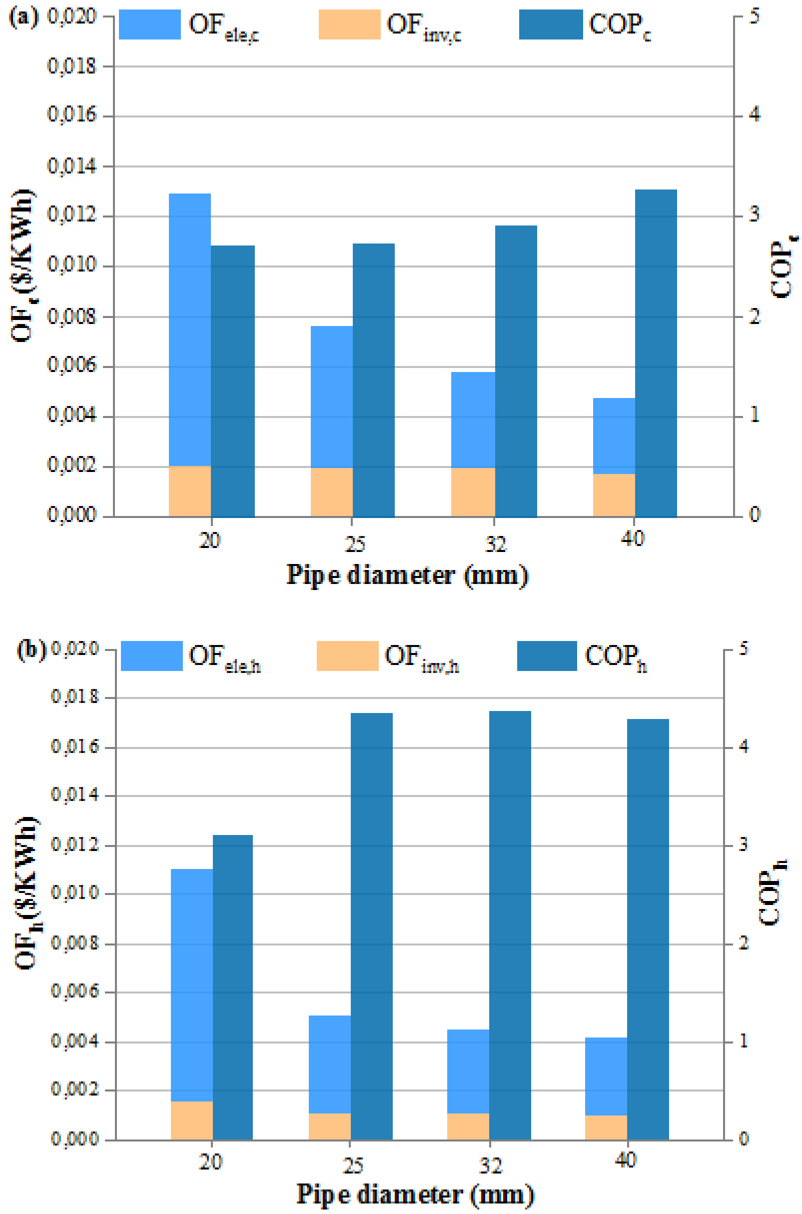

Fig 6.2 Effect of HGHX diameter on the objective function and the COP of the GHP, (a) cooling mode and (b) heating mode

6.2.1.3 Effect of the burial depth

To determine the optimal burial depth in which we must put the GHX pipes a series of simulations were carried out. Results which plotted the objective function and the COP of the GSHP as functions of the burial pipe depth in constant mass flow rate, pipe diameter and pipe length (Cases 10-19) for both heating and cooling modes are shown in Fig 6.3. With increasing the burial depth in cooling season, the electric power consumption of the compressor decreases (see Table 6.7), and the COP increases as a result of the improvement in the amounts of heat transferred to soil in the lower depths. But it is clear that from 1 m of depth (Case 11, optimal point), the investment cost caused by the increased cost of earthworks (7 in Table 6.8) is far exceeds the decrease of operating cost, which explain the increase in the objective function by more than 7.22 % from 1 m to 3 m of burial depth.

Table 6.7 Annual power consumption and electricity costs vs burial depth

Burial depth	Annual power consumption (kWh/y)				Cost of power consumption ($)			
	Compressor power consumption		Circulating pump power consumption		First year operation		Ten years operation	
	Heating	Cooling	Heating	Cooling	Heating	Cooling	Heating	Cooling
0.5	3080.7	3223.8	1760.84	1358.51	163	154.01	2597.95	2454.6
1	3091.5	3020.4	1758.44	1364.52	163.3	147.16	2602.6	2345.44
1.5	3114.45	2836.8	1754.74	1371.19	163.96	141.02	2613.24	2247.6
2	3140.1	2710.8	1750.28	1375.6	164.7	136.8	2624.96	2180.36
2.5	3161.7	2624.4	1746.21	1384.12	165.31	134.1	2634.65	2137.3
3	3190.05	2561.4	1741.37	1387.3	166.12	132.02	2647.65	2104.21

Table 6.8 The investment costs vs burial depth

Burial depth	The investment costs ($)							
	Cost of trench		Cost of circulating pump		Cost of GHP unit		The total investment cost	
	Heating	Cooling	Heating	Cooling	Heating	Cooling	Heating	Cooling
0.5	987	2080	234.77	183.54	1926	1926	3147.77	4189.54
1	1437	2830	234.63	183.90	1926	1229	3597.63	4242.9
1.5	1887	3580	234.41	184.31	1926	1229	4047.41	4993.31
2	2337	4330	234.14	184.57	1926	1198	4497.14	5712.57
2.5	2787	5080	233.89	185.09	1926	1198	4946.89	6463.09
3	3237	5830	233.60	185.28	1926	1198	5396.6	7213.28

Actually, with increasing the GHX depth in heating season, the objective function has been increased but the improvement of the COP values was almost negligible. Therefore the GSHPs tend to have optimal values on the lower end of this depths range.

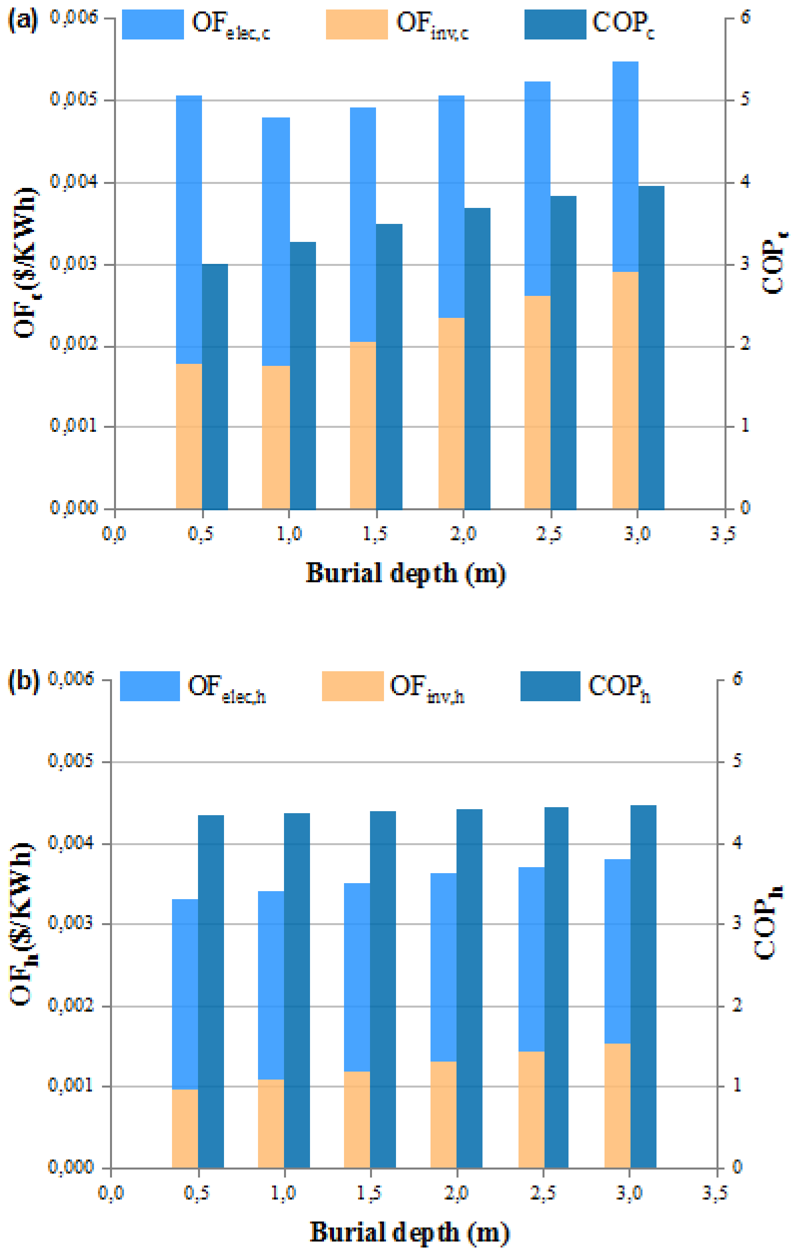

Fig 6.3 Effect of burial depth on the objective function and the COP of the GHP, (a) cooling mode, (b) heating mode

6.2.1.4 Effect of the mass flow rate

The total annual power consumption from compressor and circulating pump as well as total electricity costs for the first year and ten year of operation for different mass flow rates were collected in Table 6.9. The change in the trench, circulating pump, GHP unit costs and the total investment costs are shown in Table 6.10.

Fig 6.4 displays the objective function and the coefficient of performance of the GSHP as function of mass flow rate in constant burial depth, pipe diameter and pipe length (Cases 20-27) in heating and cooling operations. In the initial stage (Cases 20-23 for cooling operation and cases 20-21 for heating operation), the COP increases and the electric power consumption of the well pump decreases with the increase of mass flow rate of water circulating in the GHX, which explain the decline in the objective function until getting a minimum value at 1 kg/s (optimal point) in cooling mode and 0.5 kg/s (optimal point) in heating mode. In higher mass flows rate, the pressure drop in the GHX was increased gradually with the increase of fluid velocity that increases the electric power consumption of the well pump and simultaneously reduced the COP values.

Table 6.9 Annual power consumption and electricity costs vs mass flow rate

Mass flow rate	Annual power consumption (kWh/y)				Cost of power consumption ($)			
	Compressor power consumption		Circulating pump power consumption		First year operation		Ten years operation	
	Heating	Cooling	Heating	Cooling	Heating	Cooling	Heating	Cooling
0.25	3246.75	2802.6	336.99	310.66	119.36	103.04	1902.4	1642.22
0.5	3082.05	3020.4	1760.84	1364.52	163.05	147.16	2598.7	2345.44
0.75	3076.65	3083.4	5088.66	3754.66	278.33	232.28	4435.97	3702.01
1	2430	3301.2	15625.59	8005.34	621.5	387.33	9905.23	6173.06
1.25	/	3542.4	/	14489.75	/	620.69	/	9892.27
1.5	/	3709.8	/	23534.97	/	940.35	/	14986.79
1.75	/	3785.4	/	35907.16	/	1372.26	/	21870.34
2	/	3853.8	/	51758.71	/	1924.65	/	30673.97

Table 6.10 The investment costs vs mass flow rate

Mass flow rate	The investment costs ($)							
	Cost of trench		Cost of circulating pump		Cost of GHP unit		Total investment cost	
	Heating	Cooling	Heating	Cooling	Heating	Cooling	Heating	Cooling
0.25	987	3580	175.42	159.96	1926	1229	3088.42	4968.96
0.5	987	3580	265.22	231.58	1926	1229	3178.22	5040.58
0.75	987	3580	345.81	298.26	1926	1229	3258.81	5107.26
1	987	3580	457.76	360.41	1129	1926	2573.76	5866.41
1.25	/	3580	/	418.03	/	1926	/	5924.03
1.5	/	3580	/	471.93	/	1926	/	5977.93
1.75	/	3580	/	524.50	/	1926	/	6030.50
2	/	3580	/	574.70	/	1926	/	6080.70

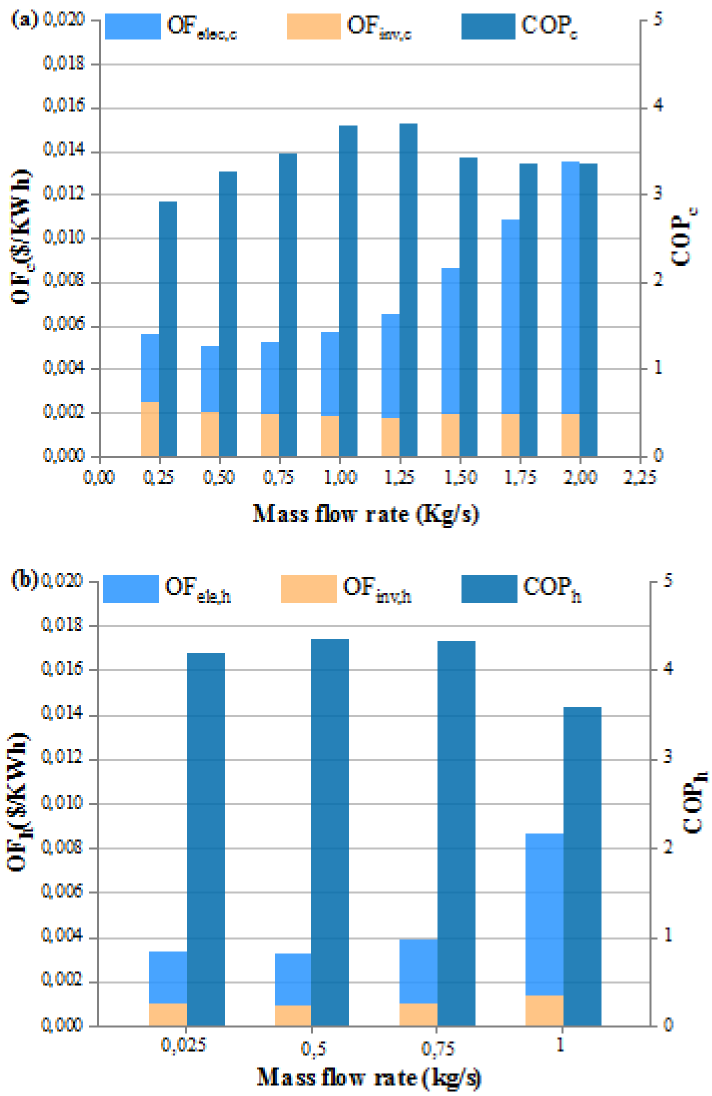

Fig 6,4 **Effect of mass flow rate on the objective function and the COP of the GHP, (a) cooling mode, (b) heating mode**

6.2.2 Thermal behavior of HGHX:

For further understanding the effect of the design parameters on the performance of the GSHP system, the effect of the pipe length, pipe diameter, burial depth and mass flow rate on the inlet and outlet temperature of ground heat exchanger for both the cooling and the heating were shown in Fig 6.5 and Fig 6.7, respectively. The results demonstrate that outside the range of the optimal design parameters, the poor design significantly affects the thermal behavior of the horizontal ground heat exchanger and therefore the overall performance of the GSHP system.

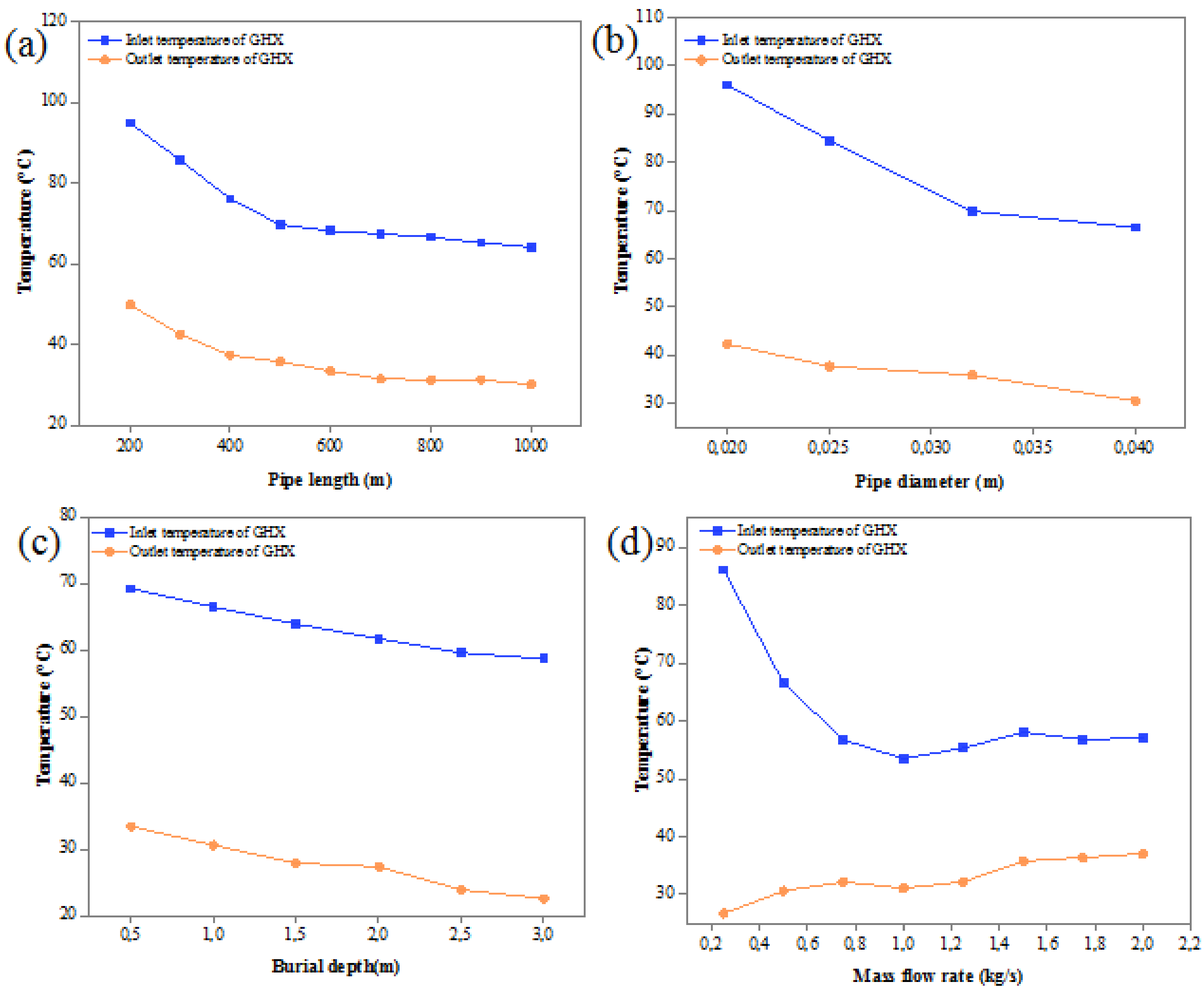

Fig 6.5 The maximum outlet and inlet GHX temperature vs (a) pipe length, (b) pipe diameter, (c) burial depth and (d) mass flow rate in cooling mode

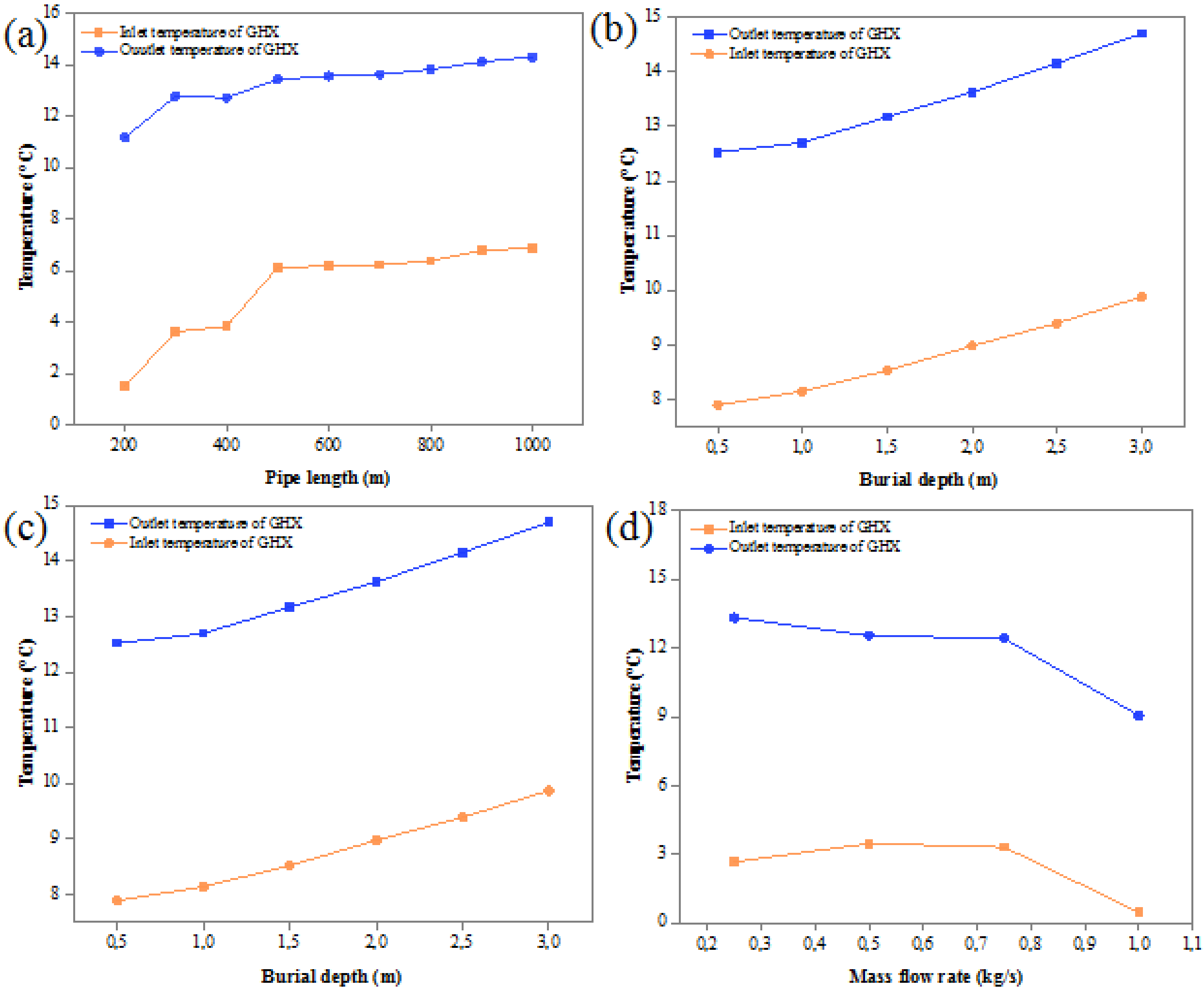

Fig 6.6 The maximum outlet and inlet GHX temperature vs (a) pipe length, (b) pipe diameter, (c) burial depth and (d) mass flow rate in heating mode

6.3 Conclusion

This chapter presented a feasibility analysis of using horizontal ground source heat pump systems to provide space heating and cooling for a typical building under Saharan climate condition. The effect of the design parameters such as pipe length, pipe diameter, burial depth and mass flow rate on both the energy performance and the economic feasibility of the ground source heat pump were investigated through a detailed simulation models developed by using TRNSYS and MATLAB. The main conclusions of this chapter are as follows:

- The thermal performance coefficient decreases and the total electric power consumption increases as the pipe diameters decrease for both cooling and heating mode. The small pipe diameters are not practical.
- Increasing the burial depth more than 1 m greatly affects the first investment total cost by increasing the price of earthworks and excavation. For every 0.5 m of additional depth the return on investment is deteriorated by 12% for cooling operation and by 3.03% for heating operation, whereas the system COP performance is improved by 4.9% in cooling and by 0.49% in heating.
- The electric power consumption of the well pump increases sharply when the water velocity in the GHX pipe increases. Lower mass flow rates (1–1.5 kg/s for cooling and 0.5–0.75 kg/s for heating) are more suitable for GSHP operation in this case.
- For ten-year economical cooling operations of HGSHPs, suggested values for pipe length, burial depth, inside pipe diameter and mass flow rate for this case are 500, 1, 0.0363 m and 1 kg/s respectively.
- For ten-year economical heating operations of HGSHPs, suggested values for pipe length, burial depth, inside pipe diameter and mass flow rate for this case are 300, 0.5, 0.029 m and 0.5 kg/s respectively.
- The use of the optimal design strategy is great importance to achieve better performance of the GSHP systems. It is worthwhile to mention that the proposed optimization of the ground heat exchangers design brings certain amount of energy savings that minimize the objective function, i.e., lowest cost, and therefore establish the most-cost effective design parameters for the specific design configuration analyzed. The obtained optimum values of all effective parameters in objective function are summarized in Table 6.11 for cooling and heating operations.

Table 6.11 The list of optimum design parameters including the results values of elements of the objective function

Cooling	Heating
$L_{GHX,c} = 500\ (m)$	$L_{GHX,h} = 300\ (m)$
$D_{i-GHX,c} = 0.0363\ (m)$	$D_{i-GHX,h} = 0.029 (m)$
$Z_c = 1\ (m)$	$Z_h = 0.5\ (m)$
$\dot{m}_{w-GHX} = 1\ (kg/s)$	$\dot{m}_{w-GHX} = 0.5\ (kg/s)$
$W_{com,c} = 4.5\ (kW)$	$W_{com,h} = 5.6\ (kW)$
$W_{pump,c} = 1{,}85\ (kW)$	$W_{pump,h} = 0{,}54\ (kW)$
$E_c = 6838{,}06\ (kWh/y)$	$E_h = 4842{,}89\ (kWh/y)$
$C_{elec,c} = 6173{,}06$ (\$)	$C_{elec,h} = 2598{,}70$ (\$)
$C_{heat\ pump,c} = 1926$ (\$)	$C_{heat\ pump,h} = 1926$ (\$)
$C_{pump,c} = 360.18$ (\$)	$C_{pump,h} = 265{,}22$ (\$)
$C_{earthworks,c} = 2250$ (\$)	$C_{earthworks,h} = 987$(\$)
$OF_c = 0{,}00568108\ (\$/kWh)$	$OF_h = 0{,}00329648\ (\$/kWh)$

CHAPTER 7

CALIBRATION THE OPTIMIZED OPERATION OF THE HORIZONTAL GROUND SOURCE HEAT PUMP

7.1 Introduction

Besides design optimisation, optimal operation control is another essential step to check the operation of the entire GSHP system that works within the desired conditions. In this chapter, investigating the effects of all optimum design parameters on the operation of the HGSHPs were performed in order to (a): maximising the system efficiency, (b): further minimising the power consumption of both heat pump and water circulating pumps and (c) ensure that the optimal operation of the HGHXs is within the recommended temperature specifications. This chapter is organised as follows. Section 7.2 presented the performance test of the optimized HGSHs and analyzed its thermal behavior in long term operation. The key findings in this chapter are summarised in Section 7.3.

7.2 The optimized HGSHPs operation analysis

In this section, the optimized values of all the design parameters were performed in the HGSHP model in order to envisage the effectiveness of the HGSHPs for air-conditioning a typical building with 95 m^2 of surface under weather factors of a Saharan climate. The effect of HGSHPs long run on both the drill outputs and soil temperature were also assessed.

7.2.1 Drill outputs

7.2.1.1 GHX parameters and soil temperatures estimation

The variation of the GHX outlet water temperature and soil temperature are very important to evaluate the GSHP performance in long term. The GHX inlet and outlet water temperatures of the optimized GSHPs and the average soil temperature around the HGHX for the first year and for ten years in Ouargla were shown in Fig 7.1, Fig 7.2, Fig 7.3, Fig 7.4 and Fig 7.5. For both heating and cooling seasons, the GHX inlet and outlet water temperature and the soil temperature were not significantly changed. The GHX inlet and outlet water temperatures for ten years presented relatively parallel trend and the average soil temperature around the GHX was stably equal in all this period. Therefore, the employment of the

HGSHPs is very suitable for buildings of Ouargla in the long term. According to ASHRAE standard [19], the optimum value for the maximum GHX outlet water temperature is typically 5 to 8°C less than the undisturbed ground temperature in heating season. Buildings in warmer climates or those with high internal cooling loads tend to have optimal values on the lower end of this range. For cooling, the maximum outlet water temperature of GHX is 11 to17°C greater than the undisturbed soil temperature to guarantee the proper heat exchange between soil, GHX water and GHP refrigerant . In warm climates (Ts > 15°C) the optimal level tends to the minimum for this range (i.e 11°C).

As shown in Fig 7.2 (b) and Fig 7.4 (b), the maximum difference between outlet and inlet GHX water temperature ranging between 22 to 22.2°C in cooling season and ranging between 9.19 to 9.2°C in the heating. Referring to Fig 7.1, the maximum difference between the outlet GHX water temperature and soil temperature is 14.5°C in cooling and 4.7°C in heating. Due to the very hot climate, these values showing that the simulation results present an acceptable agreement with ASHRAE guidelines constraints.

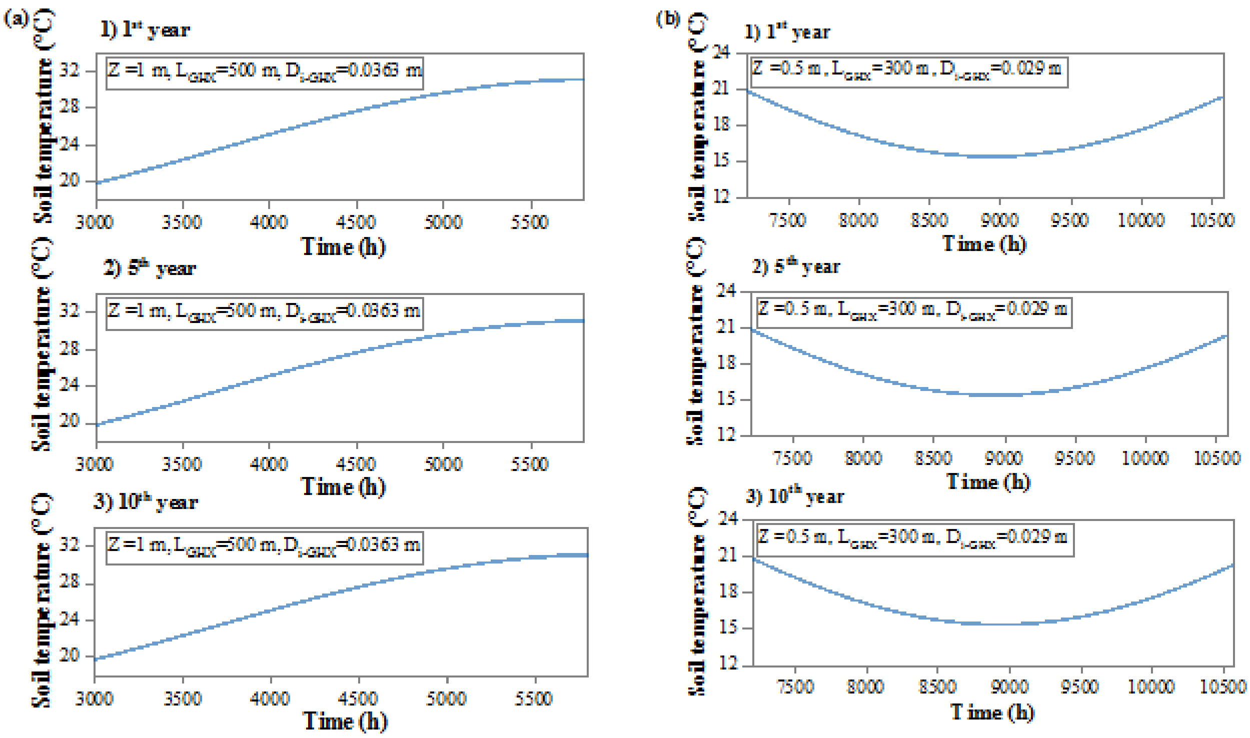

Fig 7.1 Variation of average soil temperature surrounding the ground heat exchanger at the first, fifth and tenth year of (a) cooling period and (b) heating period

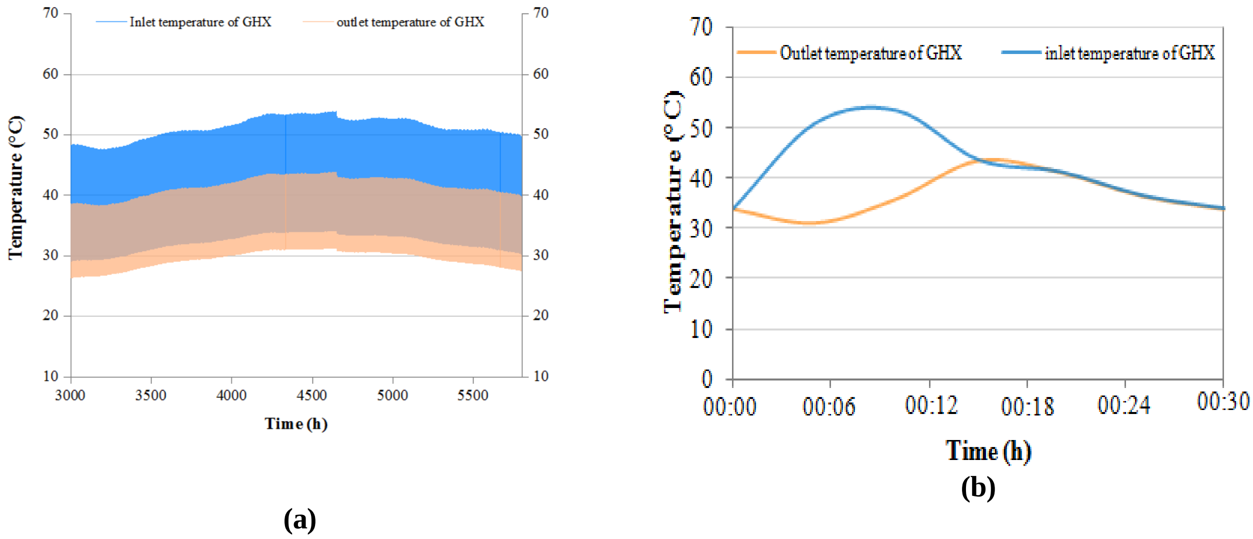

Fig 7.2 Evolution of water temperatures at the external circuits in (a) the first year of cooling mode period and (b) typical cooling day for L_{GHX}=500 W/m, $D_{i\text{-}GHX}$ = 0.0363 m and Z = 1 m

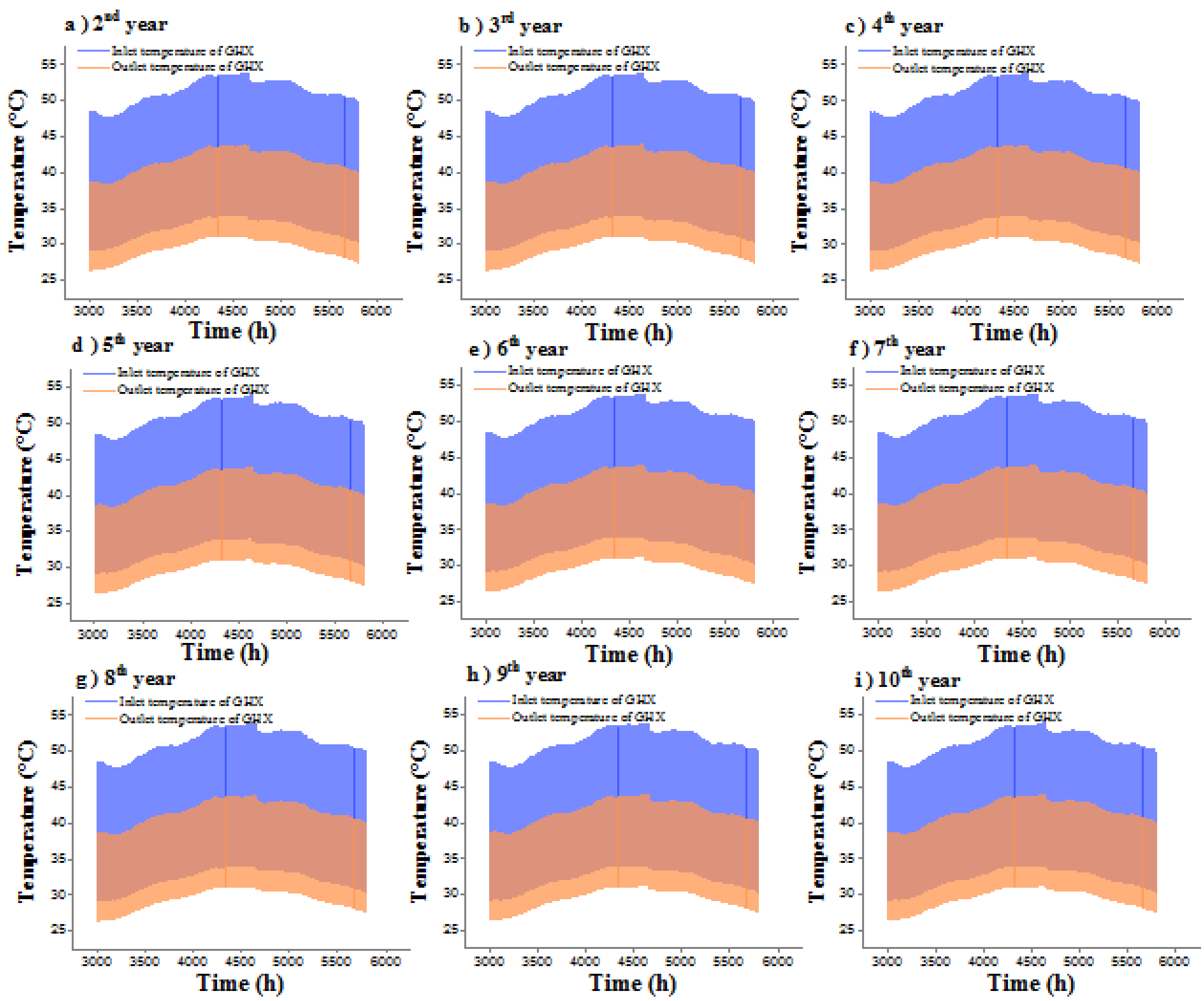

Fig 7.3 Variation of GHX inlet and outlet water temperatures in nine years of cooling period for L_{GHX}=500 W/m, $D_{i\text{-}GHX}$ = 0.0363 m and Z = 1 m

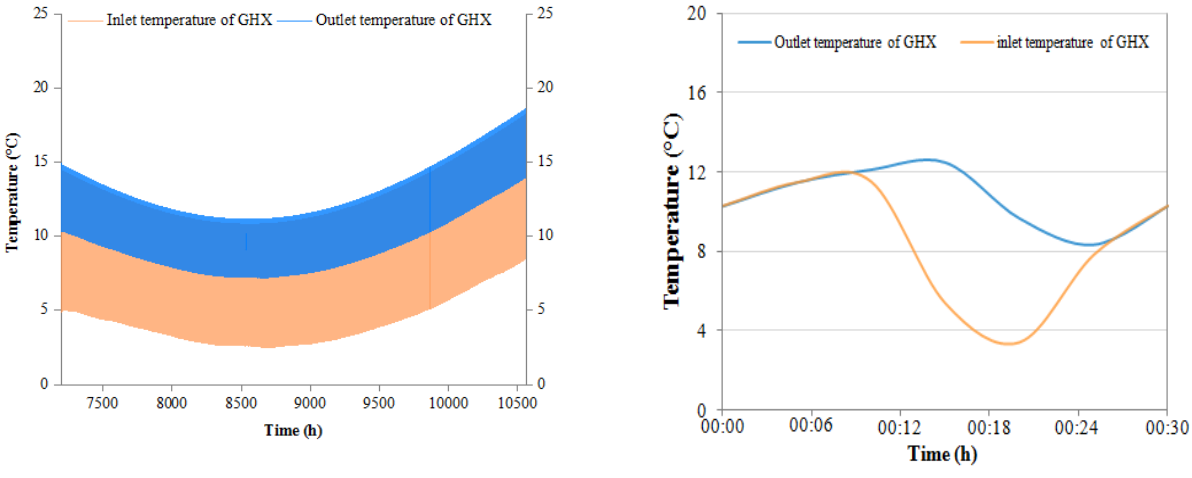

(a) **(b)**

Fig 7.4 Evolution of water temperatures at the external circuits in (a) the first year of heating period and (b) typical heating day for L_{GHX}=300 W/m, $D_{i\text{-}GHX}$ = 0.029 m and Z = 0.5 m

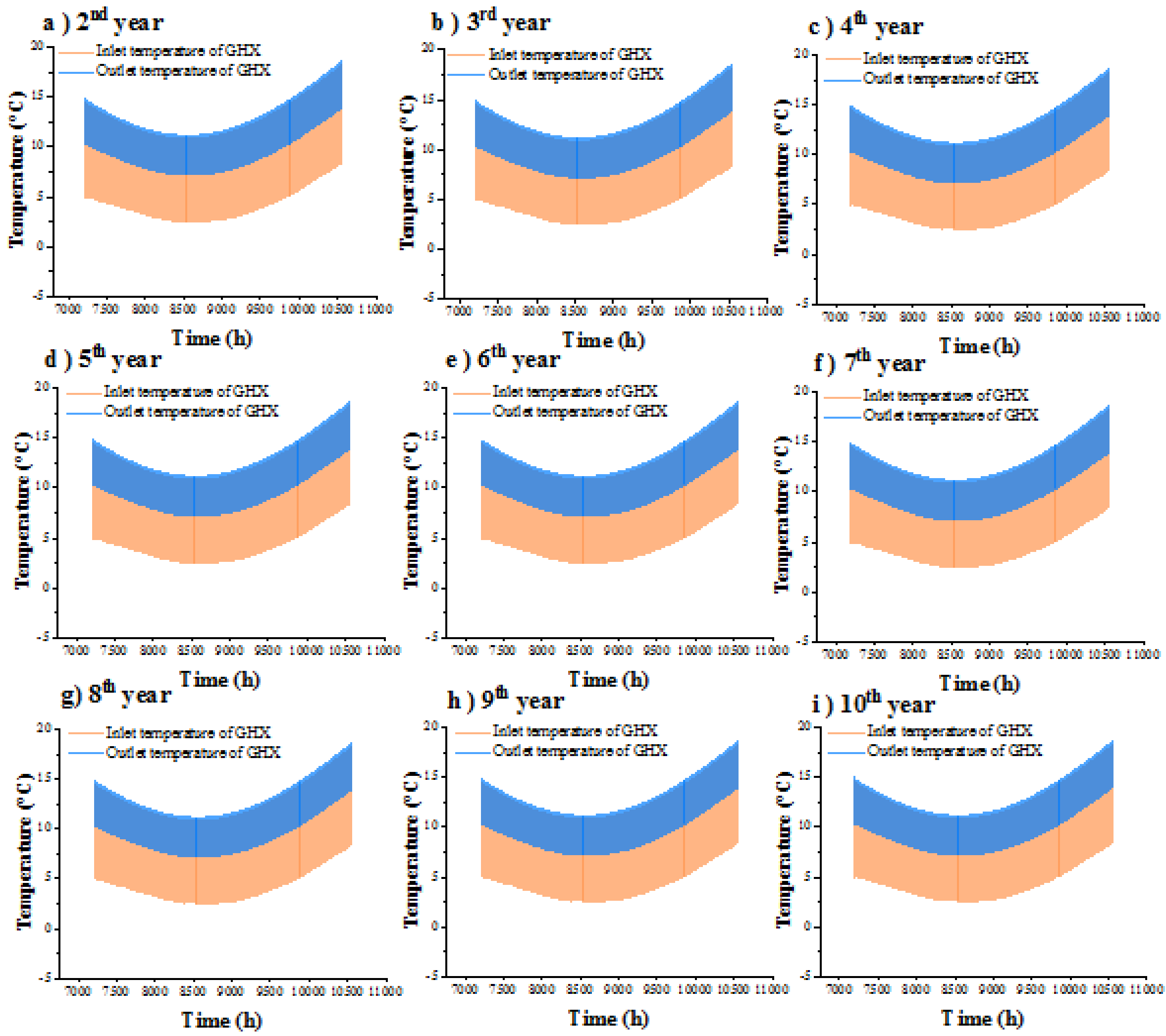

Fig 7.5 Variation of GHX inlet and outlet water temperatures in nine years of heating period for L_{GHX}=300 W/m, $D_{i\text{-}GHX}$ = 0.029 m and Z = 0.5 m

7.2.1.2 The heat transfer

The amount of heats injected into ground during the cooling season and the amount of heat absorbed from the ground in heating season are shown in Fig 7.6 and Fig 7.7, respectivelly. Results illustrate that the heats rejected from the GHX into ground in cooling vary between 0.37 and 83.6 kW and the heat absorbed from the ground in heating rang between 0.22 and 15.2 kW, which reflect the high potential of saharan territories to meet the thermal needs of the GSHP system for heating and cooling operations.

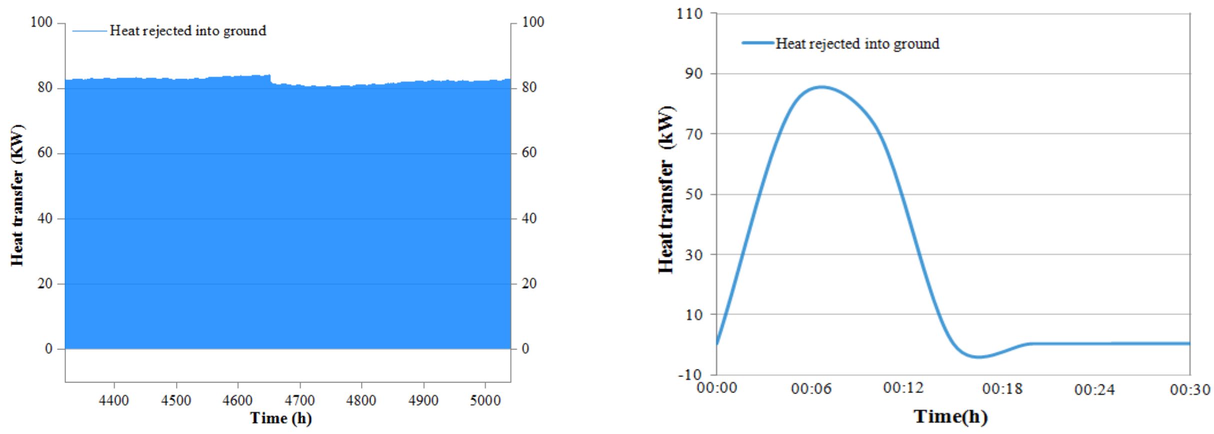

(a) (b)

Fig 7.6 Evolution of the heat injected into the ground in (a) the first year of cooling period and (b) typical cooling day for L_{GHX}=500 W/m, $D_{i\text{-}GHX}$ = 0.0363 m and Z = 1 m

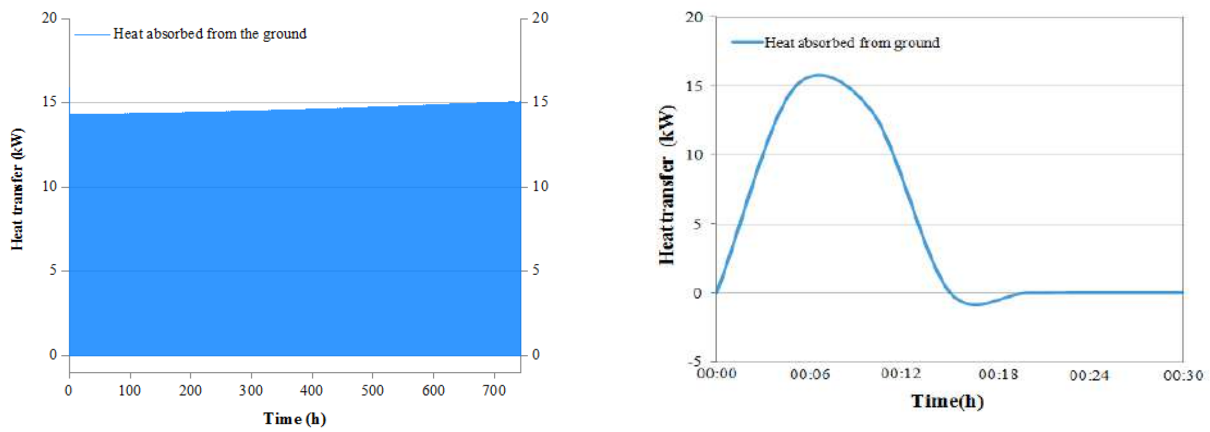

(a) (b)

Fig 7.7 Evolution of the heat absorbed from the ground in (a) the first year of heating period and (b) typical heating day for L_{GHX}=300 W/m, $D_{i\text{-}GHX}$ = 0.029 m and Z = 0.5 m

7.2.2 RF system outputs

7.2.2.1 Building thermal conditions

In order to show the reliability of the optimized HGSHPs for refreshing and heating the different typical building zones, we represent in Fig 7.8 and Fig 7.9 the variations of indoor and outdoor climat conditions during typical days of cooling mode (July 1 until July 30) and heating mode (January1 until January 30) in the first year of operation for different scenarios.

In the first state, without the HGSHP system and for an outside air temperature and relative humidity ranging between 25.92 to 48.72°C and 10 to 57.96%, respectively in summer and vary between 2.06 to 21.12 °C and 29.08 to 100%, respectively in winter, it was observed that the indoor temperature in cooling season vary between 37.44 to 41.96°C and ranging between 13.62 to 20.42 °C in heating season, while the indoor relative humidity ranges between 25.48 to 33% in cooling season and vary between 29.54 to 55.71% in heating season.

In the second state, with the HGSHP system, the indoor air temperature ranges between 23.5 to 27 °C while the relative humidity values ranges between 58.31-73.97% in cooling mode. For the heating mode, the indoor air temperature ranges between 23 to 26.5 °C while the relative humidity values ranges between 23.77-32.23%. These results demonstrate the effectiveness of the optimized HGSHP system for cooling and heating in the selected climate that experience high-temperature days in summer and relatively cold days in winter.

Fig 7.10 and Fig 7.11 show the RF inlet and outlet water temperature in heating and cooling operations. We can note from these figures that in cooling mode the RF inlet and outlet water temperature varie periodically between 6.95-13.1 °C and 12.2-16.1°C, respectively. For heating mode, the RF inlet and outlet water temperature range between 29-37.5°C and 27.9-31.11°C, respectively. The periodic change in the inlet and outlet RF system water temperature is due to the compressor on/off operation, which depends on the water temperature inside the storage tank.

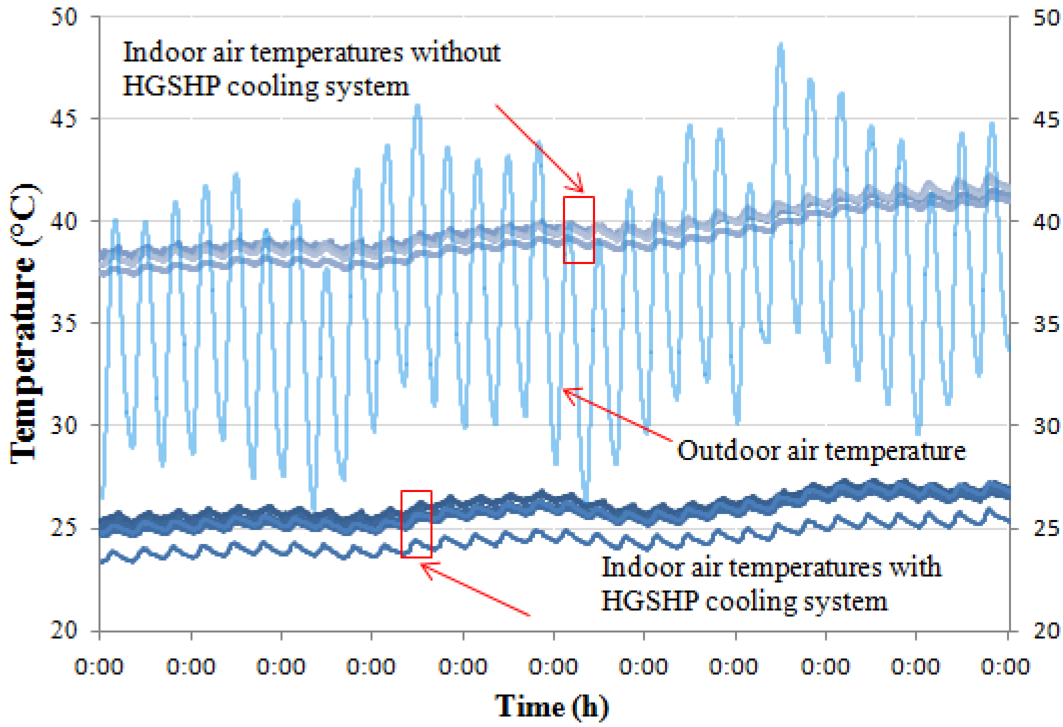

(a)

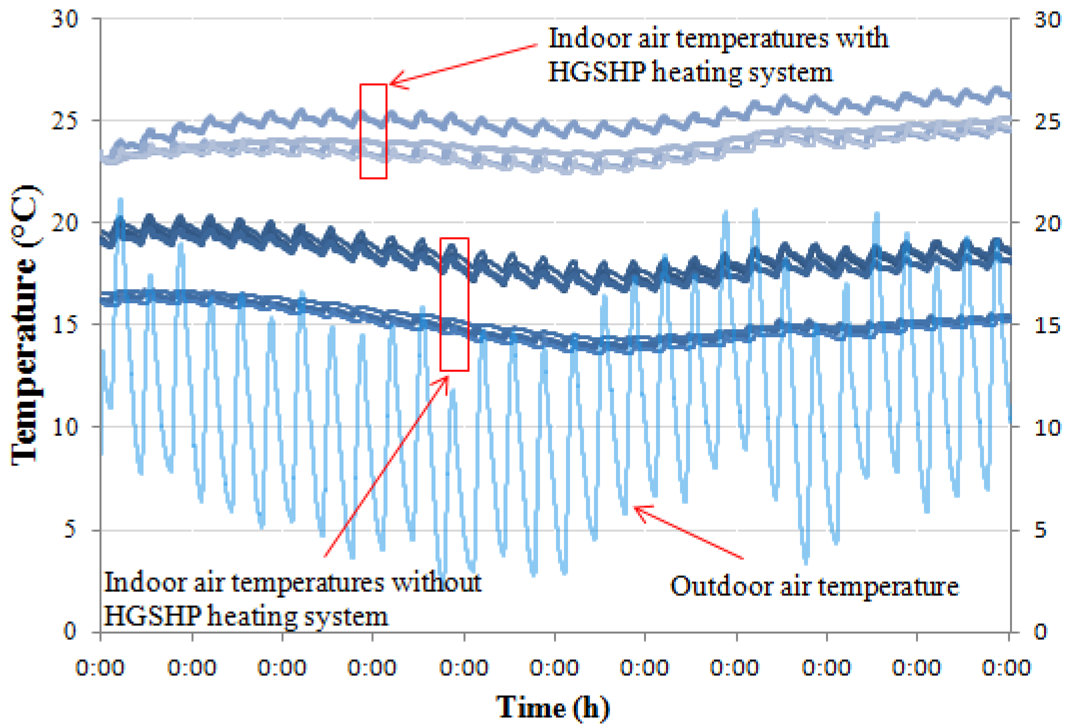

(b)

Fig 7.8 Comparison between indoor and outdoor temperatures in (a) typical cooling days (July-1 until July-30) and (b) typical heating days (January-1 until January-30)

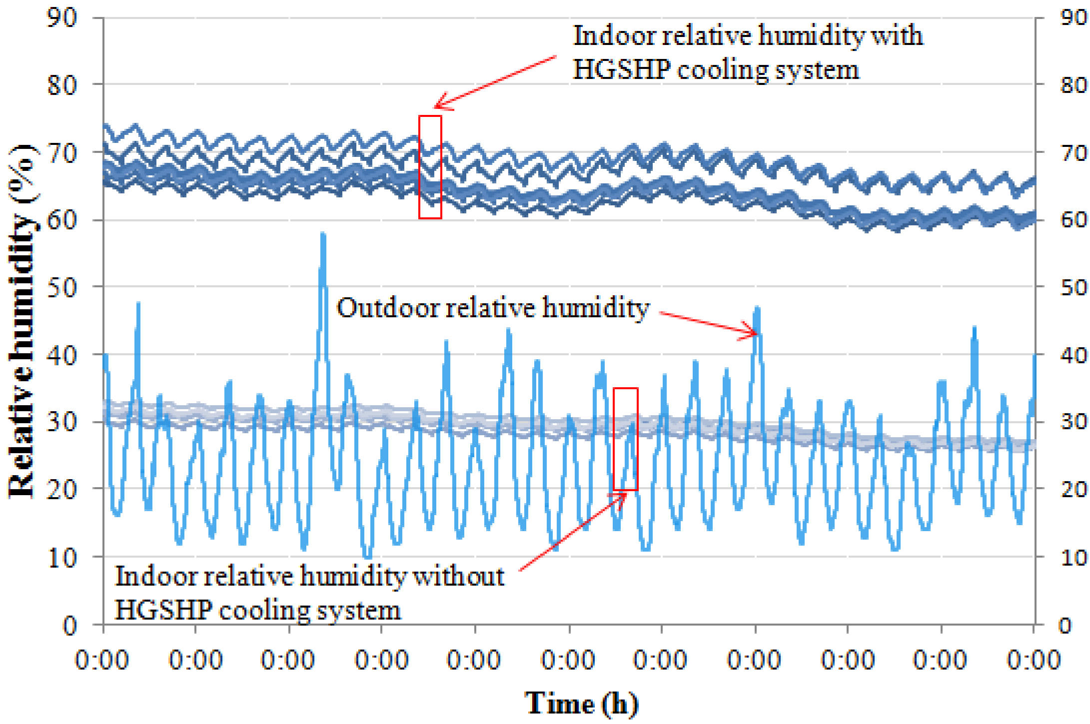

(a)

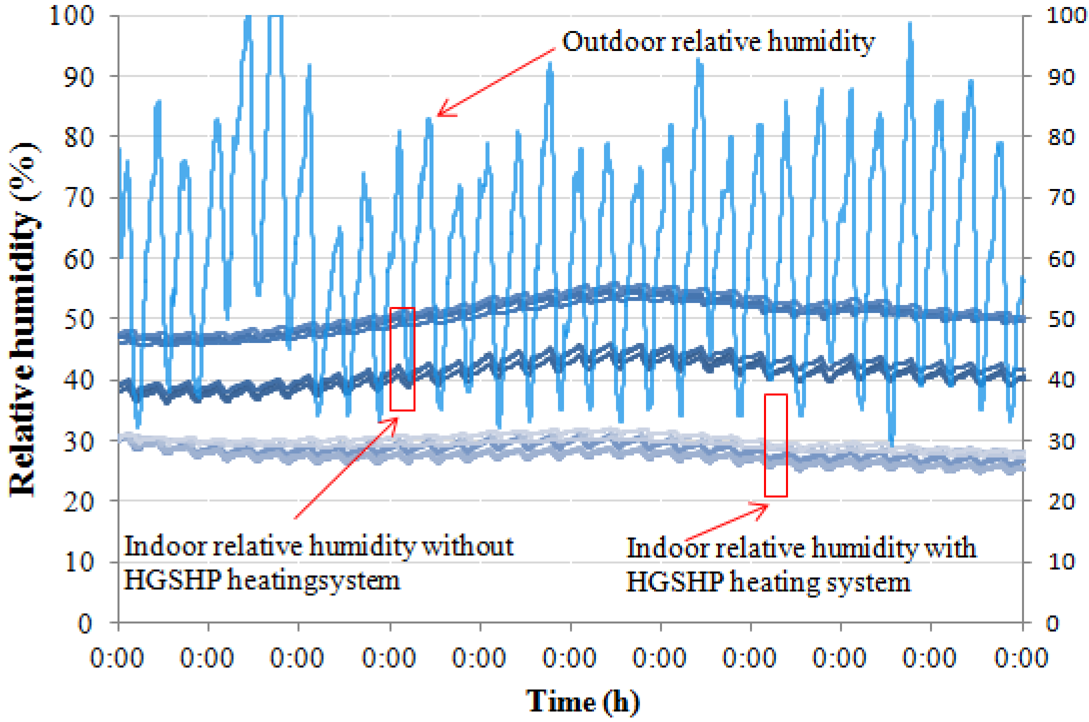

(b)

Fig 7.9 Comparison between indoor and outdoor relative humidity in (a) typical cooling days (July-1 until July-30) and (b) typical heating days (January-1 until January-30)

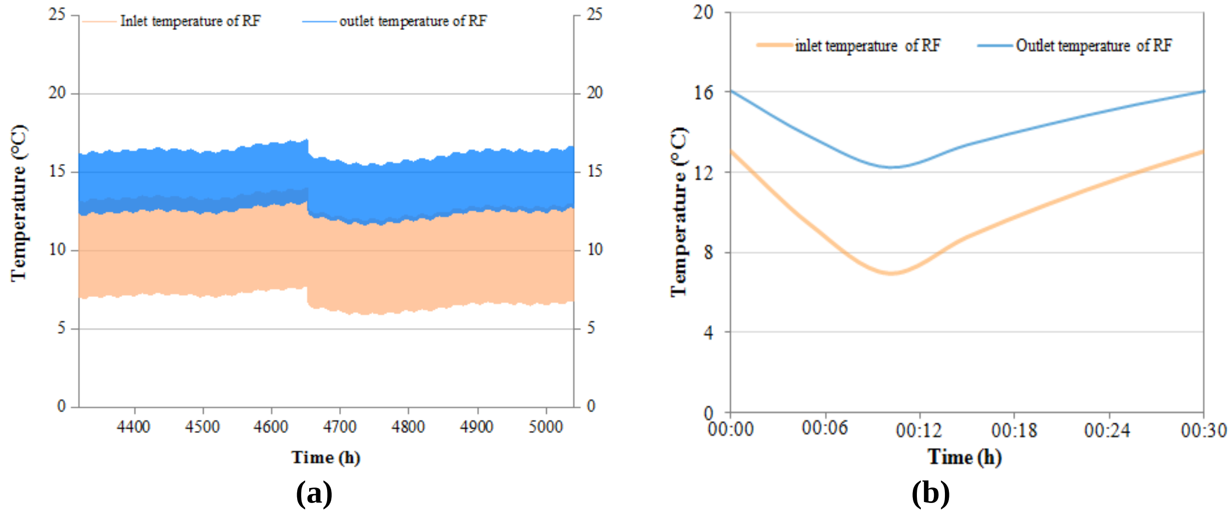

Fig 7.10 Evolution of water temperatures at the internal circuits in (a) the first year of cooling period and (b) typical cooling day for L_{GHX}=500 W/m, $D_{i\text{-}GHX}$ = 0.0363 m and Z = 1 m

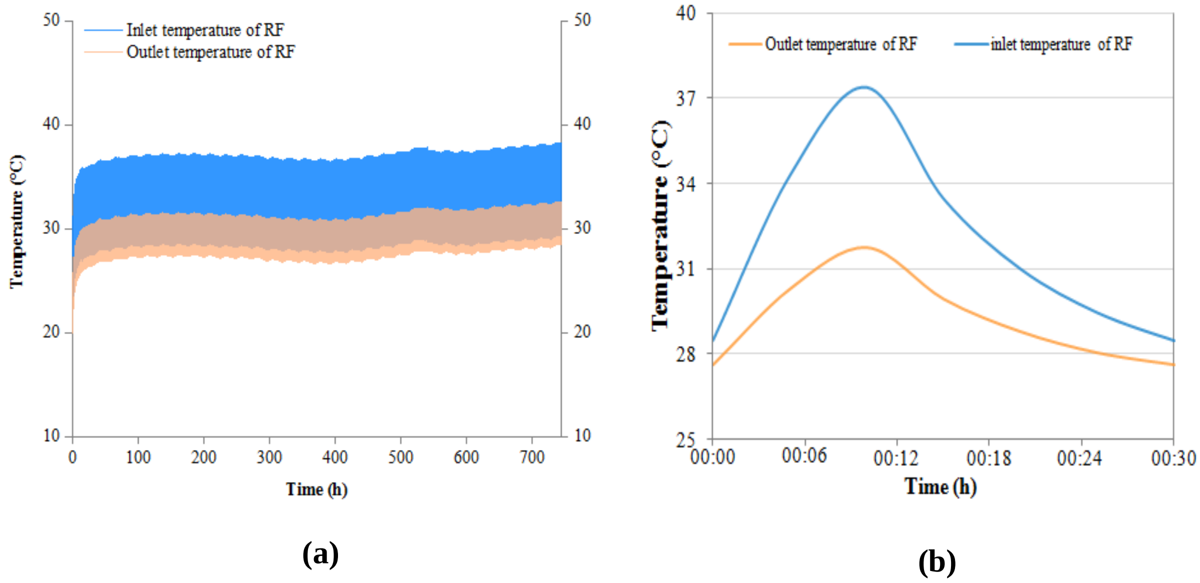

Fig 7.11 Evolution of water temperatures at the internal circuits in (a) the first year of heating period and (b) typical heating day for L_{GHX}=300 W/m, $D_{i\text{-}GHX}$ = 0.029 m and Z = 0.5 m

7.2.2.2 The heat transfer

The simulation of the total heat absorbed from the building in cooling mode and the total heat rejected into the building in heating mode are represented in Fig 7.12 and Fig 7.13. We can note from these figures that the rejected heat in the summer season can reach a maximum and a minimum values of 5.99 kW and 11.49 kW, respectively, corresponding to the compressor on/off operation time. For heating season, the absorbed heat can reach a maximum and a minimum values of 1.5 kW and 10.44 kW, respectively. These considerable values is mainly due to the high thermal loads of the building example in our changeable climate.

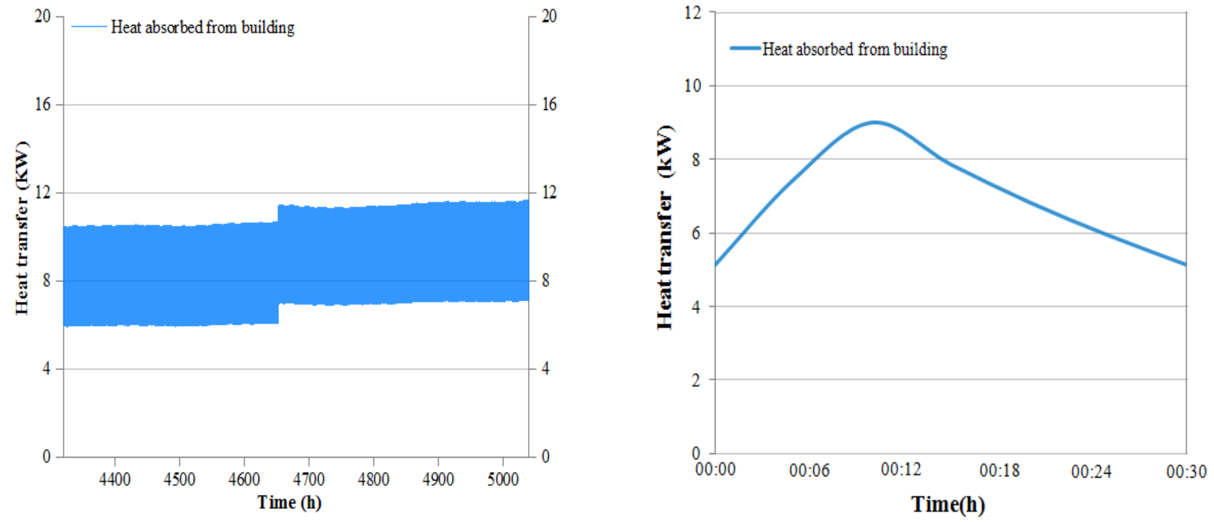

(a) (b)

Fig 7. 12 Evolution of the heat absorbed from the building in (a) the first year of cooling period and (b) typical cooling day for L_{GHX}=500 W/m, $D_{i\text{-}GHX}$ = 0.0363 m and Z = 1 m

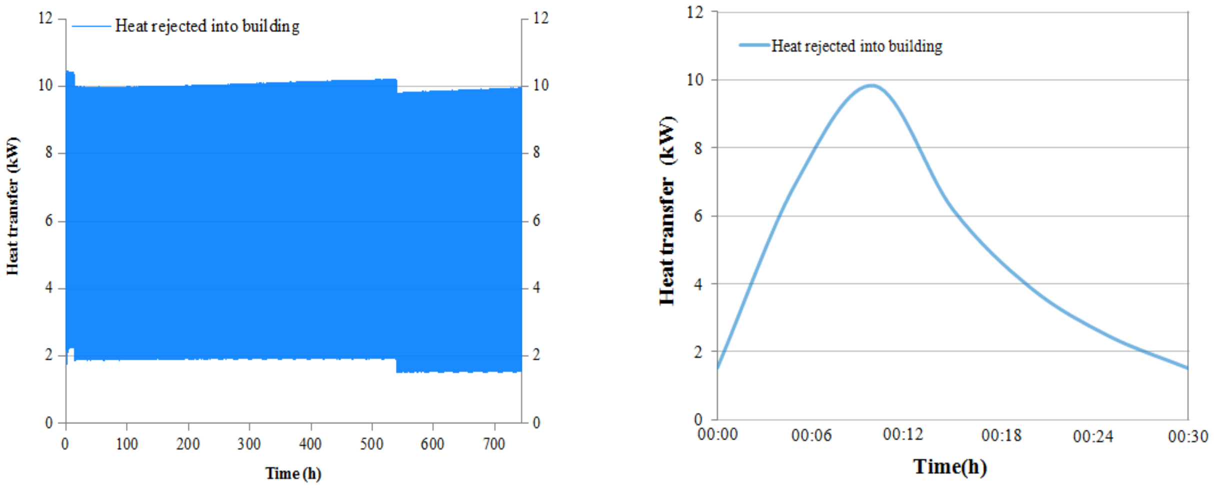

(a) (b)

Fig 7.13 Evolution of the heat injected into the building in (a) the first year of heating period and (b) typical heating day for L_{GHX}=300 W/m, $D_{i\text{-}GHX}$ = 0.029 m and Z = 0.5 m

7.2.3 Energy consumption distribution and COP evaluations

The COP and the operating power consumption of the optimized HGSHP system (including compressor, circulating pump in internal circuit and the circulating pump in external circuit) for the first year of cooling and heating operations were shown in Fig 7.14 and Fig 7.15, respectively. The HGSHP system works splendidly in this building under the selected climate conditions, the average COP in the winter season is about 4.36, and it is about 3.92 in the summer season. Based on this result, the energy efficiency ratio (EER) and seasonal energy efficiency ratio (SEER) of the HGSHPs which are especially important indicators in hot-dry climates can be calculated as 13.44 and 17.42, respectively.

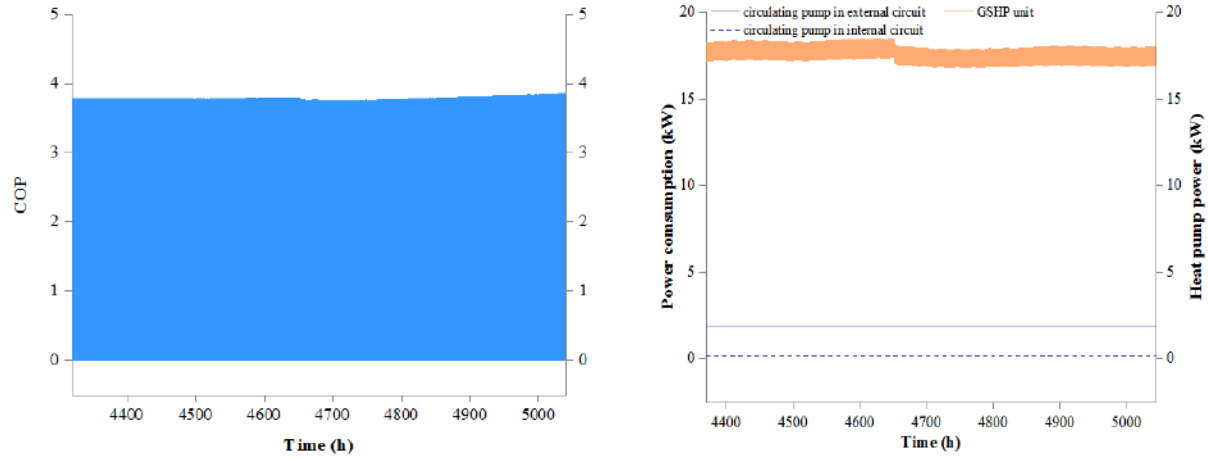

(a) (b)

Fig 7.14 The power analysis of the first year of HGSHPs cooling operation, (a) the COP distribution and (b) the power consumption distribution for L_{GHX}=500 W/m, $D_{i\text{-}GHX}$ = 0.0363 m, $m_{w\text{-}GHX}$ = 1kg/s and Z = 1 m

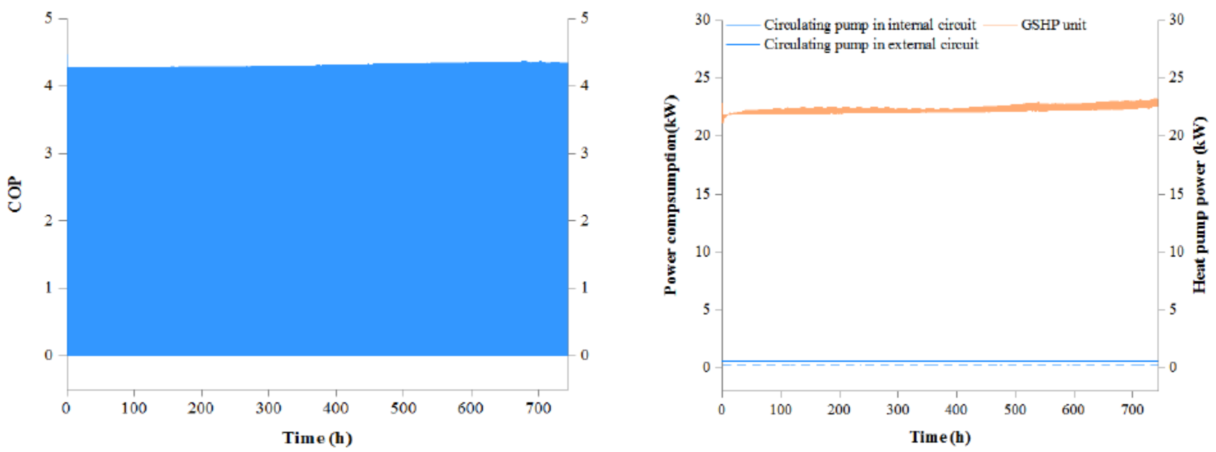

(a) (b)

Fig 7.15 The power analysis of the first year of HGSHPs heating operation, (a) the COP distribution and (b) the power consumption distribution for L_{GHX}=300 W/m, $D_{i\text{-}GHX}$ = 0.029 m, $m_{w\text{-}GHX}$ = 0.5kg/s and Z = 0.5 m

7.3 Conclusion

The chapter mainly introduces the overall performance of HGSHP system in a reference building located under a selected Saharan climate. The operation of the optimized system over first year and ten years is analyzed based on a validated TRNSYS simulation model. Detailed results are listed as follows:

- According to GHX outlet and inlet temperatures and soil temperature for 10 years operation, the HGSHPs showed excellent and stable thermal performance.
- The average values of the COP_c and COP_h for ten years operation were found to be 3.92 and 4.36, respectively. It represents a high system performance when it is compared to other traditional techniques.
- The use of HGHX coupled GSHP as an air conditioning system with improved values of the most-cost effective design parameters lead to diminish the indoor temperature of about 14.96°C in cooling season and increased the indoor temperature by more than 10°C in heating season compared to the case without HGSHP cooling system.
- As an estimation of the geothermal potential of the Saharan territories, the water temperature differences between the inlet and the outlet of the GHX reach a maximum values ranging between 22-22.2°C and 9.19-9.2°C in cooling and heating modes, respectively. These can be translated to an amounts of heat transferred between the GHX and the ground reached 83.6 kW and 15.2 kW in cooling and heating modes, respectively, which reflected the importance of the exploitable shallow geothermal energy in the studied area.

The findings of the present chapter revealed that the horizontal ground source heat pump with radiant floor as heat distribution system is a promising solution to reduce the high energy consumed by the buildings sector in Saharan areas and it could be recommended for heating and cooling applications in the long term.

GENERAL CONCLUSIONS

In this study, the feasibility of improving the performance of a GSHP system coupled with HGHX for the weather conditions of a Saharan environment and more particularly in the southeastern desert of Algeria was evaluated. In order to optimise the system operation, a energy-economic modeling and optimization of the GHXs including GHPs were analyzed for 10 years of operation periodes using both MATLAB code and TRNSYS software which were previously validated. Furthermore, the effects of the optimal system design on the overall performance of the HGSHPs operation for cooling and heating a 95 m^2 surface area was investigated using ASHRAE guidelines constraints. Major findings from this study are summarised as follows.

1 Summary of the main findings

1.1 Dynamic characteristics and model validation

Detailed TRNSYS simulation models were carried out in order to evaluate the energy performance of HGSHP system as well as to analyse its operation conditions.The models were validated using actual data collected from experimental implementation for a HGSHPs conducted in the Research and Technology Center of Energy at Borj Cédria, northern Tunisia. The major findings were as follows:

- The results obtained from the TRNSYS simulation model were confirmed by experimental test and found to be very compatible.
- According to the undisturbed soil temperature before any heat injected or rejected in, the soil thermally stable zone in the selected region corresponds to depths more than 3 m. The ground temperature, at 1 m of depth, is always higher than the average outdoor temperature in heating season and lower than its values in cooling season. This results proves the importance of geothermal energy in the desert environments of our country.

1.2 Feasibility analysis of HGSHPs for Saharan climate

To select an optimal HGSHPs design for Algerien desert climate zones, a feasibility study was carried out in order to evaluate the effects of the local climate on the the overall performance of the GSHPs. The effects of various parameters such as mass flow rate of circulating water, length and burial depth of the GHX on the performance of the GSHPs were analyzed for a ten-year period in order to obtain the most cost-effective design parameters of the HGHX. The main conclusions obtained from this study are presented below:

- High pipe lengths have no significant effect on the energy performance of the HGSHPs and thus not economically. The most-cost effective pipe lengths for both the cooling and the heating are 500 m and 300 m, respectively.
- The thermal performance coefficient decreases and the electric power consumption increases as the pipe diameters decrease. The small pipe diameters are not practical. The most cost-effective design pipe diameters for both the cooling and the heating are 0.036 m and 0.029 m, respectively.
- Increasing the burial depth greatly affects the first investment total cost by increasing the price of earthworks and excavation whereas the system thermal performance was slightly improved. The most-cost effective burial depth of GHX pipe for the cooling and heating modes are 1 m and 0.5 m, respectively.
- The electric power consumption of the well pump increases sharply when the water velocity in the GHX pipe increases. Lower mass flow rates ([0.5-1] kg/s) are more suitable for GSHP operation in this cases.
- For the case of using the HGSHPs in both the cooling and heating seasons, suggested values for pipe length, pipe diameter and burial depth for this case are 500 m, 0.0363 m and 1m respectively.

1.3 Optimal design calibration of HGSHPs

The overall operation of the optimised HGSHPs was calibrated in order in order to further maximize system operating efficiency and thus compensate the high investment costs of GSHP systems without sacrificing internal thermal comfort and violating operating restrictions. The following conclusions are achieved:

- According to the long-term operation analyses of the optimized HGSHPs, the HGHXs showed almost stable thermal performance for both the cooling and heating cases.
- The enhanced HGSHPs can meet the indoors thermal comfort along the cooling and heating seasons of the analyzed climate. It is possible to lower the mean indoor air temperature below 26 °C in summer and raise the mean indoor air temperature to reach 24.5 °C in winter.
- The maximum differences between the GHX inlet and the outlet temperatures can reach 22.2 °C in the cooling mode and 9.2 °C in the heating mode. These can be translated to an amounts of heat transferred between the GHX and the ground reached 83.6 kW and 15.2 kW in cooling and heating modes, respectively, which reflects the importance of the shallow geothermal potential in the studied Saharan territories.
- For ten-year economical operations of HGSHPs, the average values of the COP_c and COP_h were found to be 3.92 and 4.36, respectively. The deviation between the COP_c and COP_h values can be explained by the significantly increase of the outdoor temperature including the soil temperature during the cooling season.

Based on the results obtained in this study, it could be concluded that the development of the GSHP system is promising and profitable solution for providing building sector with energy-efficient cooling and heating in the Saharan climates and arid areas, and we recommend by taking into account all the optimized design criteria which could provide some reference on HGSHPs utilization in like these hot-dray regions.

For future research work, we will focus on using a steady periodic temperatures profile for design a horizontal ground source heat pump system with efficient operation suitable for both heating and cooling modes.

References

[1] Giti N, Younes N, Hossein Y. Designing and optimization of solar assisted ground source heat pump system to supply heating, cooling and hot water demands. Geothermics 2019;82:212–231.

[2] Ghedamsi R, Settou N, Gouareh A, Khamouli A, Saifi N, Recioui B, Dokkar B. Modeling and forecasting energy consumption for residential buildings in Algeria using bottom-up approach. Energy and Buildings 2016;121:309-317.

[3] Amri F. The relationship amongst energy consumption (renewable and non-renewable), and GDP in Algeria. Renewable and Sustainable Energy Reviews 2017;76:62-71.

[4] Kanoglu, M., & Bolatturk, A. "Performance and parametric investigation of a binary geothermal power plant by exergy." Renewable Energy 33.11 (2008): 2366-2374.

[5] The EU Reserch and Innovation Magazine. Available at [accessed 25.02.2021]: https://horizon-magazine.eu

[6] Dye, S. T. "Geoneutrinos and the radioactive power of the Earth." Reviews of Geophysics 50.3 (2012).

[7] Quick, Hubert, et al. "History of international geothermal power plants and geothermal projects in Germany." Proceedings World Geothermal Congress. 2010.

[8] Rybach, Ladislaus, and Mike Mongillo. "Geothermal sustainability-a review with identified research needs." GRC Transactions 30 (2006): 1083-1090.

[9] Limberger, Jon, et al. "Geothermal energy in deep aquifers: A global assessment of the resource base for direct heat utilization." Renewable and Sustainable Energy Reviews 82 (2018): 961-975.

[10] Lund, John W., Derek H. Freeston, and Tonya L. Boyd. "Direct utilization of geothermal energy 2010 worldwide review." Geothermics 40.3 (2011): 159-180.

[11] Sircar, Anirbid, Kriti Yadav, and Shreya Sahajpal. "Overview on Direct Applications of Geothermal Energy." International Advanced Research Journal in Science, Engineering and Technology 3.9 (2016): 128-137.

[12] Chamorro, C. R., Mondéjar, M. E., Ramos, R., Segovia, J. J., Martín, M. C., & Villamañán, M. A. "World geothermal power production status: Energy, environmental and economic study of high enthalpy technologies." Energy 42.1 (2012): 10-18.

[13] Yari, Mortaza. "Exergetic analysis of various types of geothermal power plants." Renewable energy 35.1 (2010): 112-121.

[14] Prananto, L. A., Juangsa, F. B., Iqbal, R. M., Aziz, M., & Soelaiman, T. A. F. "Dry steam cycle application for excess steam utilization: Kamojang geothermal power plant case study." Renewable energy 117 (2018): 157-165.

[15] Zarrouk, Sadiq J., and Hyungsul Moon. "Efficiency of geothermal power plants: A worldwide review." Geothermics 51 (2014): 142-153.

[16] Jalilinasrabady, S., Itoi, R., Valdimarsson, P., Saevarsdottir, G., & Fujii, H. "Flash cycle optimization of Sabalan geothermal power plant employing exergy concept." Geothermics 43 (2012): 75-82.

[17] Aneke, M., Agnew, B., & Underwood, C. "Performance analysis of the Chena binary geothermal power plant." Applied Thermal Engineering 31.10 (2011): 1825-1832.

[18] Franco, A., & Villani, M."Optimal design of binary cycle power plants for water-dominated, medium-temperature geothermal fields." Geothermics 38.4 (2009): 379-391.

[19] Kavanaugh, S. P., & Rafferty, K. D. Geothermal heating and cooling: design of ground-source heat pump systems. ASHRAE, 2014.

[20] Wang, G., Wang, W., Luo, J., & Zhang, Y. "Assessment of three types of shallow geothermal resources and ground-source heat-pump applications in provincial capitals in

the Yangtze River Basin, China." Renewable and Sustainable Energy Reviews 111 (2019): 392-421.

[21] Soltani, M., Kashkooli, F. M., Dehghani-Sanij, A. R., Kazemi, A. R., Bordbar, N., Farshchi, M. J., ... & Dusseault, M. B. "A comprehensive study of geothermal heating and cooling systems." Sustainable Cities and Society 44 (2019): 793-818.

[22] Sarbu, I., & Sebarchievici, C."General review of ground-source heat pump systems for heating and cooling of buildings." Energy and buildings 70 (2014): 441-454.

[23] Kupiec, K., Larwa, B., & Gwadera, M. "Heat transfer in horizontal ground heat exchangers." Applied Thermal Engineering 75 (2015): 270-276.

[24] Sofyan, S. E., Hu, E., & Kotousov, A. "A new approach to modelling of a horizontal geo-heat exchanger with an internal source term." Applied energy 164 (2016): 963-971.

[25] Fujii, H., Nishi, K., Komaniwa, Y., & Chou, N. "Numerical modeling of slinky-coil horizontal ground heat exchangers." Geothermics 41 (2012): 55-62.

[26] Chong, C. S. A., Gan, G., Verhoef, A., Garcia, R. G., & Vidale, P. L. "Simulation of thermal performance of horizontal slinky-loop heat exchangers for ground source heat pumps." Applied Energy 104 (2013): 603-610.

[27] Yang, W., Xu, R., Wang, F., & Chen, S. "Experimental and numerical investigations on the thermal performance of a horizontal spiral-coil ground heat exchanger." Renewable Energy 147 (2020): 979-995.

[28] Rees, Simon, ed. Advances in ground-source heat pump systems. Woodhead Publishing, 2016.

[29] Stober, I., & Bucher, K "History of geothermal energy use." Geothermal Energy. Springer, Berlin, Heidelberg, 2013. 15-24.

[30] Belessiotis, V., & Delyannis, E. "The history of renewable energies for water desalination." Desalination 128.2 (2000): 147-159.

[31] Quick, H., Michael, J., Huber, H., & Arslan, U. "History of international geothermal power plants and geothermal projects in Germany." Proceedings World Geothermal Congress. 2010.

[32] Soltani, M., Moradi Kashkooli, F., Dehghani-Sanij, A. R., Nokhosteen, A., Ahmadi-Joughi, A., Gharali, K., ... & Dusseault, M. B. "A comprehensive review of geothermal energy evolution and development." International Journal of Green Energy 16.13 (2019): 971-1009.

[33] Lund, J. W., & Toth, A. N. "Direct utilization of geothermal energy 2020 worldwide review." Geothermics (2020): 101915.

[34] Michaelides, E. E. S. "Future directions and cycles for electricity production from geothermal resources." Energy Conversion and Management 107 (2016): 3-9.

[35] Huttrer, G. W. "Geothermal power generation in the world 2015-2020 update report." Proceedings World Geothermal Congress. Vol. 2020. 2020

[36] Bertani, R. (2016). "Geothermal power generation in the world 2010–2014 update report." Geothermics 60 (2016): 31-43.

[37] IEA (International Energy Agency). 2011. Technology roadmap: Geothermal heat and power. Paris, Frence. Accessed September 17, 2018. https://www.iea.org/publications/freepublications/publication/ Geothermal_Roadmap.pdf

[38] Saibi, H. "Geothermal resources in Algeria." Renewable and Sustainable Energy Reviews 13.9 (2009): 2544-2552.

[39] Kedaid, F. Z. "Database on the geothermal resources of Algeria." Geothermics 36.3 (2007): 265-275.

[40] Mahmoudi, H., Spahis, N., Goosen, M. F., Ghaffour, N., Drouiche, N., & Ouagued, A. "Application of geothermal energy for heating and fresh water production in a brackish

water greenhouse desalination unit: a case study from Algeria." Renewable and Sustainable Energy Reviews 14.1 (2010): 512-517.

[41] S. Ouali, "Etude Géothermique du Sud de l'Algérie", Mémoire de magister en Géophysique, Université Boumerdés, Mars 2006.

[42] Ouali, S., Chader, S., Belhamel, M., & Benziada, M."The exploitation of hydrogen sulfide for hydrogen production in geothermal areas." International Journal of Hydrogen Energy 36.6 (2011): 4103-4109.

[43] Saibi, H., Ehara, S., Fujimitsu, Y., & Nishijima, J. "Progress of geothermal development in Algeria." Journal of the Geothermal Research Society of Japan 28.4 (2006): 383-397.

[44] Himri, Y., Malik, A. S., Stambouli, A. B., Himri, S., & Draoui, B. "Review and use of the Algerian renewable energy for sustainable development." Renewable and sustainable energy reviews 13.6-7 (2009): 1584-1591.

[45] Fekraoui A. "Geothermal resources in Algeria and their possible use." Geothermics 17.2-3 (1988): 515-519.

[46] Bouraiou, A., Necaibia, A., Boutasseta, N., Mekhilef, S., Dabou, R., Ziane, A., ... & Touaba, O. "Status of renewable energy potential and utilization in Algeria." Journal of Cleaner Production 246 (2020): 119011.

[47] Saiah, S. B. D., & Stambouli, A. B. "Prospective analysis for a long-term optimal energy mix planning in Algeria: Towards high electricity generation security in 2062." Renewable and Sustainable Energy Reviews 73 (2017): 26-43

[48] Deng, Y., & Fedler, C. B. "Multi-layered soil effects on vertical ground coupled heat pump design." Transactions of the ASAE 35.2 (1992): 687-694.

[49] Leong, W. H., Tarnawski, V. R., & Aittomäki, A. "Effect of soil type and moisture content on ground heat pump performance: Effet du type et de l'humidité du sol sur la

performance des pompes à chaleur à capteurs enterrés." International Journal of Refrigeration 21.8 (1998): 595-606.

[50] Radioti, G., Sartor, K., Charlier, R., Dewallef, P., & Nguyen, F. "Effect of undisturbed ground temperature on the design of closed-loop geothermal systems: A case study in a semi-urban environment." Applied energy 200 (2017): 89-105.

[51] Noorollahi, Y., Arjenaki, H. G., & Ghasempour, R. "Thermo-economic modeling and GIS-based spatial data analysis of ground source heat pump systems for regional shallow geothermal mapping." Renewable and Sustainable Energy Reviews 72 (2017): 648-660.

[52] Sanaye, S., & Niroomand, B."Thermal-economic modeling and optimization of vertical ground-coupled heat pump." Energy Conversion and Management 50.4 (2009): 1136-1147.

[53] J. Luo, W. Xue, T. Hu, W. Xiang, J. Rohn, Thermo-economic analysis of borehole heat exchangers (BHE) grouted using drilling cuttings in a dolomite area, Appl. Therm. Eng. 150, 305–315 (2019)

[54] Y. Zhao, Z. Shigang, L. Xun, Cost-effective optimal design of groundwater source heat pumps, Appl. Therm. Eng. 23, 1595–1603 (2003)

[55] S. Sanaye, B. Niroomand, Horizontal ground coupled heat pump: thermal-economic modeling and optimization, Energy Convers. Manag. 51, 2600–2612 (2010)

[56] N. Kayaci, H. Demir, Long time performance analysis of ground source heat pump for space heating and cooling applications based on thermo-economic optimization criteria, Energy Build. 163, 121–139 (2018)

[57] M. Inalli, H. Esen, Experimental thermal performance evaluation of a horizontal ground-source heat pump system, Appl. Therm. Eng. 24, 2219–2232 (2004)

[58] Lamarche, L., & Beauchamp, B. "A fast algorithm for the simulation of GCHP systems." ASHRAE Transactions 113.1 (2007): 470-477.

[59] Kim, M. J., Lee, S. R., Yoon, S., & Jeon, J. S."An applicable design method for horizontal spiral-coil-type ground heat exchangers." Geothermics 72 (2018): 338-347.

[60] Sarbu, I., & Sebarchievici, C."Ground-source heat pumps: Fundamentals, experiments and applications". Academic Press, 2015.

[61] Lyu, C., Leong, W. H., Zheng, M., Chen, G., Ye, S., & Liu, Y. "Verification and analysis of a dynamic simulation model of ground-coupled heat pump with solar seasonal heat storage system." Procedia Engineering 205 (2017): 3154-3161.

[62] De Rosa, M., Ruiz-Calvo, F., Corberán, J. M., Montagud, C., & Tagliafico, L. A "A novel TRNSYS type for short-term borehole heat exchanger simulation: B2G model." Energy Conversion and Management 100 (2015): 347-357.

[63] Dossat, Roy J. Principles of refrigeration. John Wiley & Son, 1961.

[64] Kakac S, Liu H. Heat exchangers: selection, rating and thermal design. CRC Press; 2002.

[65] Kayaci, N., & Demir, H."Comparative performance analysis of building foundation Ground heat exchanger." Geothermics 83 (2020): 101710.

[66] The national society of electricity and gas in Algeria.Sonelgaz of the East.

[67] Shah, R. K., & Sekulic, D. P. Fundamentals of heat exchanger design. John Wiley & Sons, 2003.

[68] Webpage: http://www.algerie.prix-construction.info (accessed June 2019).

[69] A. Abdelali, I.E. Nezli, A.S. Benhamida, Geothermometry application to the Continental Intercalaire geothermal aquifer: a case study of Ouargla region, Energy Procedia 119, 264–269 (2017).

[70] Semahi, S., Zemmouri, N., Singh, M. K., & Attia, S."Comparative bioclimatic approach for comfort and passive heating and cooling strategies in Algeria." Building and Environment 161 (2019): 106271.

[71] Webpage: https://www.bing.com (accessed march 2021).

[72] N. Naili, M. Hazami, I. Attar, A. Farhat, In-field performance analysis of ground source cooling system with horizontal ground heat exchanger in Tunisia, Energy 61, 319–331 (2013)

[73] N. Naili, "Valorisation du potentiel thermique du sol pour la climatisation : utilisation d'une pompe à chaleur géothermale à capteurs horizontaux", Thesis in physics, Faculty of Sciences of Tunis, 2016.

[74] N. Naili, M. Hazami, I. Attar, A. Farhat, Assessment of surface geothermal energy for air conditioning in northern Tunisia: direct test and deployment of ground source heat pump system, Energy Build. 111, 207–217 (2016)

[75] J.P. Holman, Experimental Methods for Engineers, 6th ed., McGraw-Hill Book Co., Singapore, 1994.

Appendix A: Technical potential for all direct heat applications

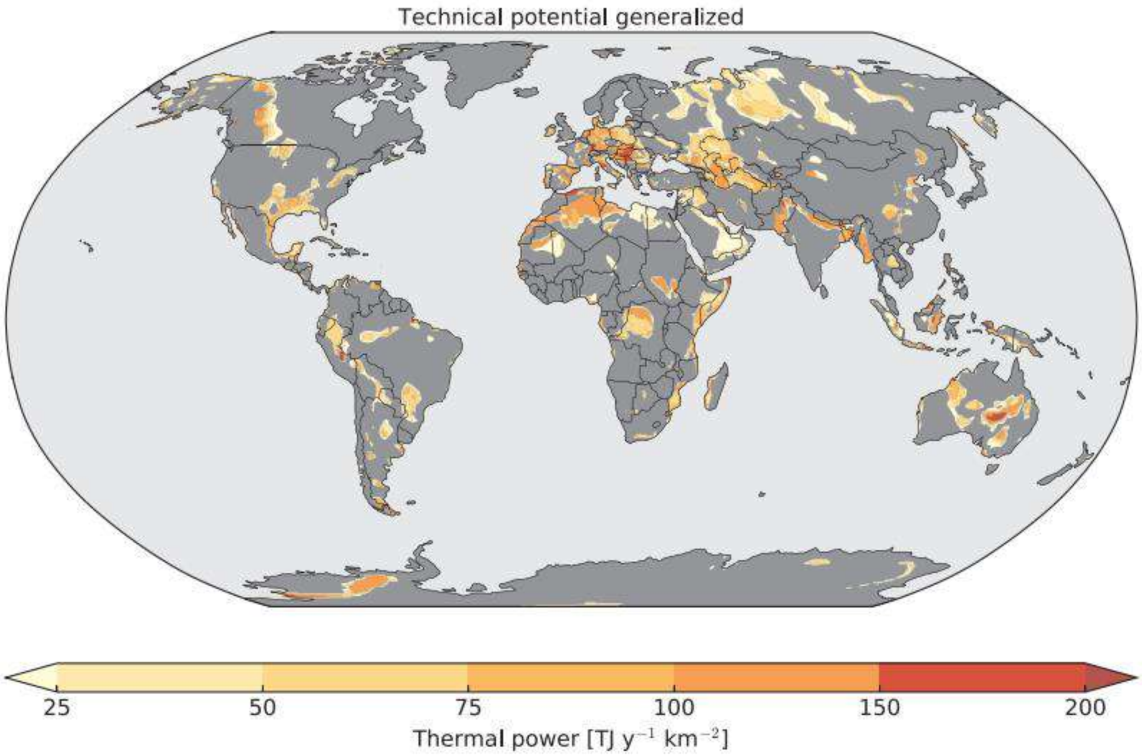

Technical potential map for all direct heat applications combined. The grey color on the land surface indicates regions with an effective aquifer thickness less than 100 m or regions where application-specific (sub) surface temperature requirements are not met [9]

Appendix B : GHX tube configurations

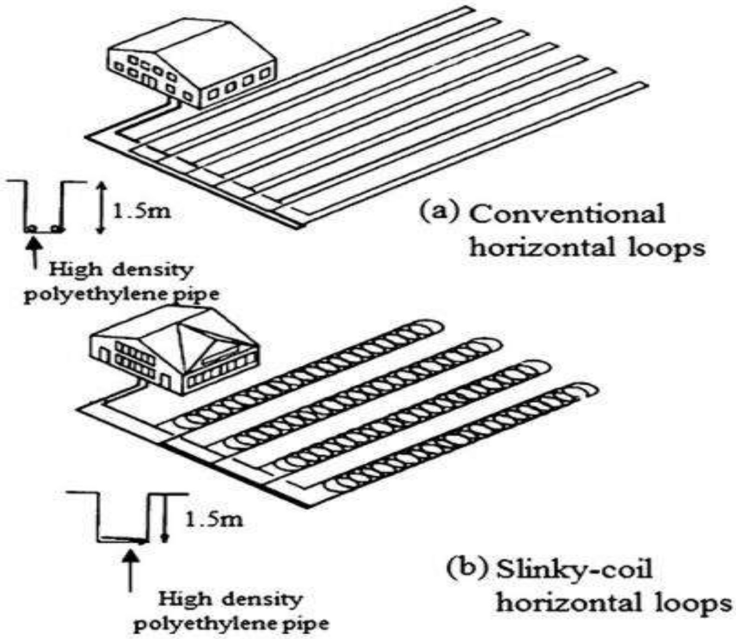

HGHX types, (a) linear and (b) slinky [25]

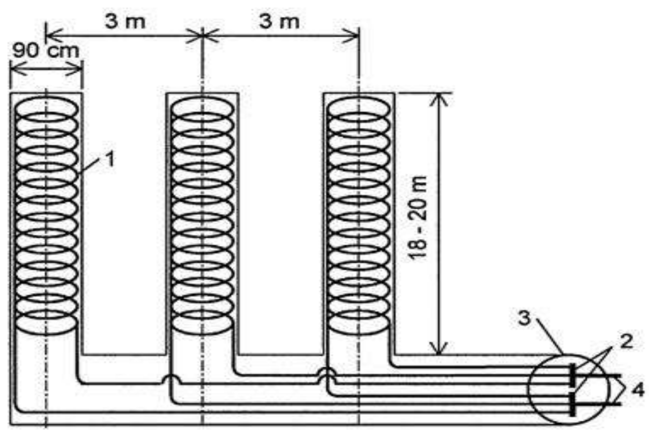

Spiral-coil HGHX [22]

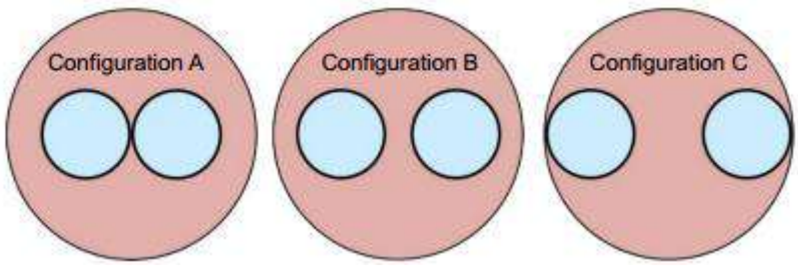

Vertical borehole configurations [28]

Appendix C: The primitive geothermal installations

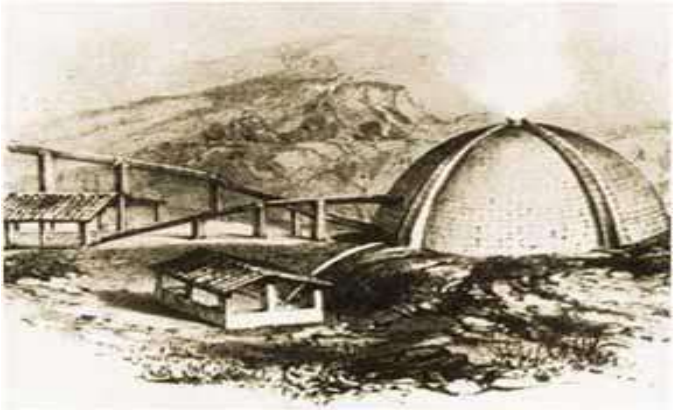

The Covered lagoon of Francesco Larderel, Larderello, Italy, 1827 [21]

The 10 kW experimental power plant of Piero Ginori Conti, Larderello, Italy, 1904 [21]

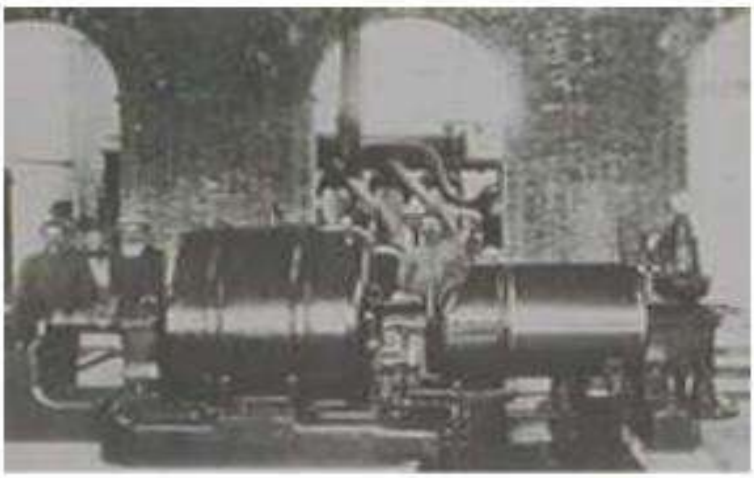

First commercial geothermal power plant, Larderello, Italy 1912 [21]

Appendix D: Statistics of geothermal energy use

Table D.1 Detailed Summary of direct-use data worldwide in 2019 [35]

Region/Continent (#countries/regions)	MWT	TJ/year	GWh/year	Capacity factor
Africa (11)	198	3730	1036	0.597
Americas (17)	23.330	180.414	50.115	0.245
Central America and Caribbean (5)	9	195	54	0.687
North America (4)	22.700	171.510	47.642	0.24
South America (8)	621	8709	2419	0.445
Asia (18)	49.079	545.019	151.394	0.352
Commonwealth of Independent States (5)	2121	15.907	4419	0.238
Europe (34)	32.386	264.843	73.568	0.259
Central and Eastern Europe (17)	3439	28.098	7805	0.259
Western and Northern Europe (17)	28.947	235.745	65.762	0.259
Oceania (3)	613	10.947	3048	0.568
Total (82)	107.727	1.020.887	283.580	0.300

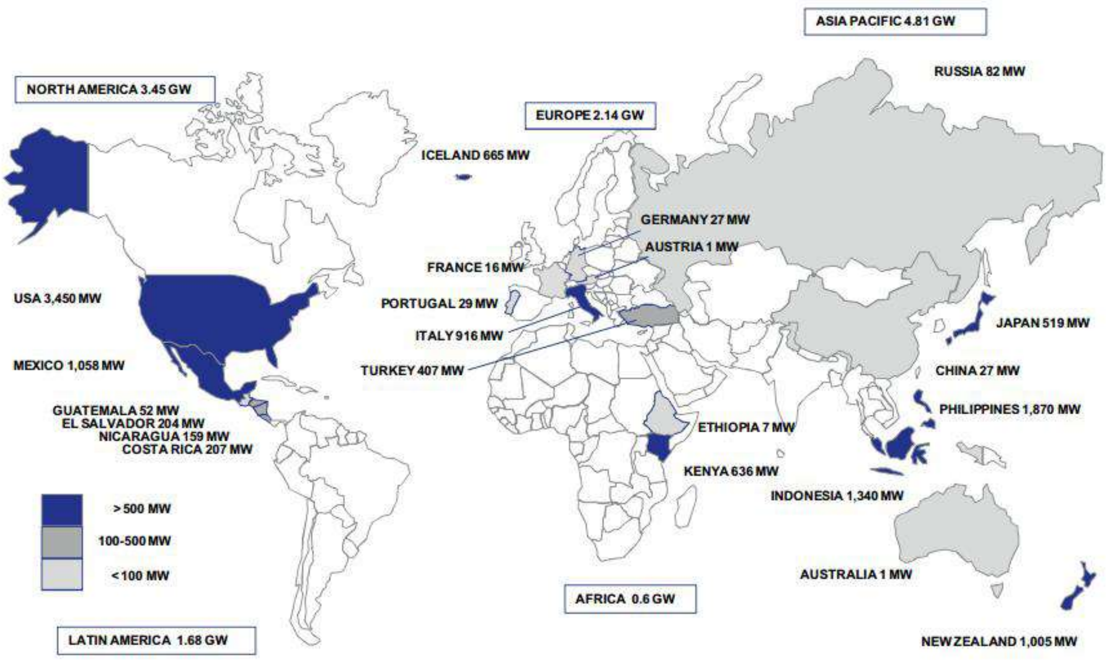

Map of installed geothermal capacity in 2015 worldwide [35]

Appendix E: Thermophysical properties estimation

Table E.1 Thermophysical properties of saturated water [68]

Liquid	T (K)	ρ (kg/m^2)	K (W/mK)	c_p (J/kgK)	**μ** × 10^3(Pa s)	β × 10^6(K^{-1})
Water	273.15	1000	0.569	4217	1.750	-68.05
	280	1000	0.582	4198	1.422	46.04
	290	999.0	0.598	4184	1.080	174.0
	300	997.0	0.613	4179	0.855	276.1
	310	993.0	0.628	4178	0.695	361.9
	320	989.1	0.640	4180	0.577	436.7
	330	984.3	0.650	4184	0.489	504.0
	340	979.4	0.660	4188	0.420	566.0
	350	973.7	0.668	4195	0.365	624.2
	400	937.2	0.688	4256	0.217	896
	500	831.3	0.642	4660	0.118	-
	600	648.9	0.497	7000	0.081	-
	647.3	315.5	0.238	∞	0.045	-

Appendix F: Economic data

Table F.1 Polyethylen**e** pipe (type SDR11) prices [69]

Inner diameter (mm)	Outer diameter (mm)	Thickness (mm)	Price ($/m)
18	20	2	0.81
22.7	25	2.3	1.17
29	32	3	1.179
36.3	40	3.7	2.66

Table F.2 Heat pump (water to water) prices

Cooling capacity (kW)	5.8-9	9-11.3	11.3-15	15-17.5	17.5-22.6
Heating capacity (kW)	7-11	11-14	14-17	17-20	20-28
Heat pump price ($)	998	1057	1198	1129	1926

Appendix G: Uncertainty analysis example

As an example, the uncertainty estimates in the coefficient of performance of the heat pump (COP_{hp}) and in the heat exchange rate at the external circuit of the water-to-water heat pumps (Q_g) can be given as follows:

$$W_{COP_{hp}} = \left[\left(\frac{\partial COP_{hp}}{\partial \dot{m}} W_{\dot{m}} \right)^2 + \left(\frac{\partial COP_{hp}}{\partial C_P} W_{C_P} \right)^2 + \left(\frac{\partial COP_{hp}}{\partial T_O} W_{T_o} \right)^2 + \left(\frac{\partial COP_{hp}}{\partial T_{in}} W_{T_{in}} \right)^2 + \left(\frac{\partial COP_{hp}}{\partial \dot{w}_c} W_{\dot{w}_c} \right)^2 \right]^{1/2} \quad (5.2)$$

$$W_{Q_g} = \left[\left(\frac{\partial Q_g}{\partial \dot{m}} W_{\dot{m}} \right)^2 + \left(\frac{\partial Q_g}{\partial C_P} W_{C_P} \right)^2 + \left(\frac{\partial Q_g}{\partial T_s} W_{T_s} \right)^2 + \left(\frac{\partial Q_g}{\partial T_e} W_{T_e} \right)^2 \right]^{\frac{1}{2}} \quad (5.3)$$

where $W_{\dot{m}}$ and W_{T_i} represent the uncertainty estimates in the measurement of the mass flow rate and the temperature which can be obtained from the Equation (5.4) and the Equation (5.5).

$$W_{\dot{m}} = (W_{ro}^2 + W_{sl}^2)^{1/2} \quad (5.4)$$

$$W_{T_i} = (W_{da}^2 + W_{me}^2 + W_{te}^2)^{1/2} \quad (5.5)$$

where T_i, represents T_o, T_{in} and T_g.